

NASA Contractor Report 172277

(
P
J
D
(

Development of an Advanced Pitch Active Control System for a Wide Body Jet Aircraft

**Wiley A. Guinn, Jerry J. Rising,
and Walt J. Davis**

IN-03

58134

DATE OVERRIDE

P-169

LOCKHEED-CALIFORNIA COMPANY
BURBANK, CALIFORNIA

CONTRACT NO. NAS1-15326

FEBRUARY 1 1984



(NASA-CR-172277) DEVELOPMENT OF AN ADVANCED
PITCH ACTIVE CONTROL SYSTEM FOR A WIDE BODY
JET AIRCRAFT Final Report
(Lockheed-California Co., Burbank.) 169 p

N87-17713

CSCL 01C G3/08 43383
Unclas

general release will be three (3) years from date indicated on this document.



National Aeronautics and
Space Administration

Langley Research Center
Hampton, Virginia 23665

COPY CONTROL NO. 1

FOREWORD

This report documents work accomplished for the NASA Aircraft Energy Efficiency (ACEE) Program by the Lockheed California Company in 1982 toward development of an advanced pitch active control system (PACS) for a commercial wide body jet. The NASA ACEE/EET Program Manager was R.V. Hood Jr. and the NASA Program Monitor was J.R. Gaudy. The Lockheed Program Manager was F.C. English and the Project Engineer was W.A. Guinn. Principal Lockheed and NASA personnel who performed the program were:

W. J. Davis - Control law development
F. Conner
R. H. Rooney
J. J. Rising - Flying qualities analysis
M. G. Chong
K. R. Henke - PACS system architecture
C. D. Siegert
C. S. Willey - Piloted flight simulation test
J. V. Fish
W. D. Grantham (NASA)
W. A. Weaver - Pilots
R. C. Cokeley
L. H. Person Jr. (NASA)
P. W. Brown (NASA)
W. R. Neeley Jr. (NASA)

The program administrator was G. Wiener. The Lockheed and NASA contract administrators were Marie Chainey and J. A. Dorst respectively.

PRECEDING PAGE BLANK NOT FILMED

DEVELOPMENT OF AN ADVANCED PITCH ACTIVE
CONTROL SYSTEM FOR A WIDE BODY
JET AIRCRAFT

Wiley A. Guinn, Jerry J. Rising, and Walt J. Davis

Lockheed-California Company

SUMMARY

Commercial transport aircraft fuel consumption can be significantly reduced by relaxing the longitudinal static stability to reduce trim drag. However, this fuel saving concept usually results in degraded aircraft flying qualities. The flying qualities can be restored by using a highly reliable pitch active control system (PACS) to provide longitudinal stability augmentation.

Work that was accomplished toward development of an advanced PACS is documented in this report. The advanced PACS was designed to provide good flying qualities to a negative 10 percent static stability margin for an advanced transport configuration. Analysis and wind tunnel tests performed during other Lockheed programs indicate that the negative 10 percent stability margin for an advanced wing aircraft provides fuel savings of approximately 4 percent. The PACS described herein was called an advanced PACS to distinguish it from a near-term PACS that was previously developed to provide 2 percent fuel savings for the L-1011 operating at near neutral static stability. (Reference 1).

The L-1011 longitudinal control system is initially described. Then, development of the PACS control law is presented. Analytical simulation and flying qualities analysis methods used for verification of the control law are discussed. Results of piloted flight simulation tests to demonstrate validity of the control law are given. Finally, the architecture of an advanced PACS that is suitable for an L-1011 flight test program is given. This PACS architecture is designed for flight tests to a negative 3 percent static stability margin which is the maximum limit achievable by the L-1011 without extensive structural and c.g. management modifications.

Piloted flight simulation tests on the NASA Langley visual motion simulator demonstrated that the advanced PACS met the design objectives. Test of the baseline aircraft (PACS off) showed the flying qualities for cruise and high-speed flight conditions to be unacceptable at a negative 3 percent static stability margin. When the PACS was engaged the flying qualities were demonstrated to be good for static stability margins to negative 20 percent.

PRECEDING PAGE BLANK NOT FILMED

TABLE OF CONTENTS

Section	Page
SUMMARY	v
LIST OF FIGURES	ix
LIST OF TABLES	xiii
LIST OF SYMBOLS	xv
1. INTRODUCTION	1
1.1 Background	1
1.2 Program Objective	2
1.3 Scope of Program	2
2. L-1011 CONTROL SYSTEM DESCRIPTION	3
3. CONTROL LAW DEVELOPMENT	9
3.1 Advanced PACS Design Objectives	9
3.2 Control Law Synthesis	12
3.2.1 Aero Data	12
3.2.2 Baseline Aircraft Model	12
3.2.3 Feedback Loop Synthesis	12
3.2.4 Feed-Forward Loop Synthesis	23
3.2.5 Primary Gain Scheduling	23
3.2.6 Secondary Gain Scheduling	23
3.3 Control Law Mechanization.	28
3.3.1 Control Column and Actuator System	28
3.3.2 Feedback Loops	28
3.3.3 Feed-Forward Loops	30
3.4 Control Law Analysis	30
3.4.1 Poles and Zeros	30
3.4.2 Nyquist Plots	35
3.4.3 Feel-Force Gradients	37
4. ANALYTIC SIMULATION	45
5. FLYING QUALITIES ANALYSIS	49
5.1 Speed Stability	49
5.2 Maneuver Stability	50

TABLE OF CONTENTS (Continued)

Section	Page
5.2.1	Takeoff Maneuver Stability 56
5.2.2	Cruise Maneuver Stability 59
5.3	Dynamic Stability 61
5.3.1	Linear Analysis 63
5.3.2	Nonlinear Analysis 63
5.4	Trimmability and Stabilizer/Elevator Limits 68
6.	PILOTED FLIGHT SIMULATION TEST 75
6.1	NASA Flight Simulator Center 75
6.2	Simulation Math Model 75
6.3	Flight Conditions 83
6.4	Evaluation Tasks 85
6.5	Evaluation Guidelines 87
6.6	Simulation Test Results 87
6.6.1	Flight Condition 10: Mid Altitude Cruise 89
6.6.2	Flight Condition 15: Maximum Range Cruise 89
6.6.3	Flight Condition 7: High W/ δ Cruise 89
6.6.4	Flight Condition 16: High Speed 100
6.6.5	Flight Condition 18: Landing 100
6.6.6	Flight Condition 17: Holding 100
6.6.7	Flight Condition 19: Takeoff 107
6.6.8	Summary of Simulation Test Results 107
7.	PACS ARCHITECTURE 113
	CONCLUSIONS 117
APPENDIX A	- AERO DATA 119
APPENDIX B	- BASELINE AIRCRAFT MATH MODEL 123
APPENDIX C	- MODAL CONTROL METHOD 127
APPENDIX D	- PITCH ATTITUDE LOOP LAG-LEAD CIRCUIT 136
APPENDIX E	- FEED-FORWARD LOOP CONTROL LAW 139
APPENDIX F	- PRIMARY GAIN SCHEDULING 143
APPENDIX G	- SECONDARY GAIN SCHEDULING 145
APPENDIX H	- PITCH ATTITUDE LOOP SYNCHRONIZER CIRCUIT 147
	REFERENCES 151

LIST OF FIGURES

Figure		Page
1	Longitudinal control system with the advanced PACS	3
2	PACS load path diagram	5
3	Schematic of the L-1011 control system with the advanced PACS series servo	6
4	J curve.	7
5	PACS dynamic stability design objectives	10
6	PACS column force gradient design objective.	11
7	Blended normal-acceleration/pitch-rate response objective.	11
8	Control law synthesis.	13
9	PACS control model	15
10	Flap-up eigenvalues.	18
11	Flap-down eigenvalues.	19
12	Plots of compensated pitch rate feedback gains, flap-up conditions	21
13	Plots of feed-forward gains flaps-up conditions.	24
14	Scheduled feedback gain curves, flap-up conditions	26
15	Scheduled feed-forward gain curves, flap-up conditions	27
16	Advanced PACS block diagram.	29
17	s - plane nomenclature for poles and zeros tables.	34
18	Nyquist plots.	36
19	Open loop column force in turns.	38
20	Full gain PACS, column force gradients	40
21	Partial gain PACS, column force gradients.	40
22	PACS without feed-forward, column force gradients.	42
23	One-g gain PACS, column force gradients.	42
24	Quasi-steady PACS column force gradients	43
25	Time history plots, flight condition 7	46
26	Advanced PACS modified block diagram	51
27	Mach trim compensation	52
28	Mach compensation circuit servo offset schedules	53

LIST OF FIGURES

Figure		Page
29	Mach compensation gain schedule, flaps down.	54
30	PACS configured aircraft speed stability column force characteristics.	55
31	Baseline aircraft takeoff maneuver stability column forces . . .	56
32	Baseline aircraft takeoff pitching moments	57
33	AACS engagement and pitch rate impact on pitching moment \sim takeoff	57
34	Baseline aircraft takeoff maneuver stability stabilizer position characteristics.	58
35	PACS configured aircraft maneuver stability column force characteristics \sim takeoff.	59
36	Baseline aircraft maneuver stability column characteristics \sim cruise	60
37	Aircraft pitching moment versus angle-of-attack characteristics \sim cruise	60
38	AACS engagement and pitch rate impact on pitching moment \sim cruise	61
39	Baseline aircraft cruise maneuver stability stabilizer position characteristics.	62
40	PACS configured aircraft maneuver stability column force gradients \sim cruise	62
41	Baseline aircraft dynamic stability characteristics.	64
42	PACS equipped aircraft stability characteristics	65
43	Flight condition 7: discrete gust model, cruise	66
44	Baseline aircraft response to a moderate vertical gust	67
45	Comparison of aircraft response with and without PACS engaged for a severe vertical gust	69
46	Comparison of aircraft response with and without PACS engaged to various levels of control column step inputs	70
47	Modified elevator versus stabilizer gearing curve.	71
48	Stabilizer deflection trim range for various flight conditions .	73
49	Modified trim stabilizer position versus trim servo displacement characteristics	74

LIST OF FIGURES

Figure		Page
50	Modified pitch feel spring rate schedule	74
51	NASA/Langley transport cab and motion base	76
52	NASA/Langley transport cockpit interior.	77
53	NASA/Langley transport visual display.	78
54	L-1011 S/N 1001 weight/inertia characteristics	79
55	L-1011 S/N 1001 weight/center-of-gravity envelope.	80
56	L-1011-1 S/N 1001 high-speed pitching moment characteristics	81
57	Primary pitch trim system.	82
58	Lateral-directional control system	84
59	Flight simulation test conditions.	85
60	Handling qualities rating scale.	88
61	Cooper-Harper rating for flight condition 10, calm air	90
62	Cooper-Harper rating for flight condition 10, moderate turbulence	91
63	Pilot 5 Cooper-Harper rating for flight condition 15, calm air	93
64	Pilot 5 Cooper-Harper rating for flight condition 15, moderate turbulence	94
65	Cooper-Harper rating for flight condition 7, calm air.	95
66	Cooper-Harper rating for flight condition 7, moderate turbulence	96
67	Flight condition 7 comparison of damping response characteristics with PACS on and off, c.g. at 39 percent mac	97
68	Flight condition 7 comparison of damping response characteristics with PACS on and off, c.g. at 43 percent mac	98
69	Flight condition 7 comparison of damping response characteristics with PACS on and off, c.g. at 50 percent mac	99
70	Cooper-Harper rating for flight condition 16, calm air	101
71	Cooper-Harper rating for flight condition 16, moderate turbulence	102
72	Cooper-Harper rating for flight condition 18, calm air	103
73	Cooper-Harper rating for flight condition 18, moderate turbulence	104

LIST OF FIGURES

Figure		Page
74	Cooper-Harper rating for flight condition 17, calm air. . . .	105
75	Cooper-Harper rating for flight condition 17, moderate turbulence	106
76	Cooper-Harper rating for flight condition 19, calm air. . . .	108
77	Cooper-Harper rating for flight condition 19, moderate turbulence	109
78	Summary of Cooper-Harper ratings for cruise and high speed flight conditions	110
79	Advanced PACS interface block diagram	114
80	Advanced PACS component diagram	115
81	PACS lag-lead circuit block diagram	136
82	PACS feed-forward loop block diagram	139
83	PACS equivalent feedback gain block diagram for N_z signal . .	141
84	PACS secondary gain controller	146
85	PACS pitch synchronizer operation modes	148
86	PACS pitch attitude loop synchronizer circuit	149

LIST OF TABLES

Table		Page
1	PACS CONTROLLER INPUT SIGNALS	4
2	FLIGHT CONDITIONS FOR ADVANCED FLIGHT CONTROL SYSTEM ANALYSIS.	14
3	FEEDBACK GAIN MATRIX (G_1)	17
4	COMPENSATED FEEDBACK GAIN MATRIX (G_2)	20
5	δ_{HT} AND q TRIM CONDITIONS FOR EACH FLIGHT CASE	22
6	PACS GAIN SCHEDULE EQUATION COEFFICIENTS	25
7	SHORT PERIOD FREQUENCY CHARACTERISTICS.	31
8	PHUGOID FREQUENCY CHARACTERISTICS	32
9	CONTROLLER FREQUENCY CHARACTERISTICS.	33
10	OPEN LOOP CASE POLES IN THE RIGHT-HAND SIDE OF THE s PLANE.	35
11	PACS FEEL-FORCE CONFIGURATION EVALUATED	39
12	PILOTED FLIGHT SIMULATION TEST CONDITIONS	49
13	PILOT COMMENTS, FLIGHT CONDITION 10, CALM AIR	92
14	SUMMARY OF COOPER-HARPER RATINGS WITH PACS ON	111
15	LONGITUDINAL AERO DATA, CASE 7b	120
16	DEFINITION OF ELEMENTS FOR MATRICES A AND B	126
17	PACS PITCH SYNCHRONIZER INPUT STATES	150
18	PACS PITCH SYNCHRONIZER SWITCH POSITIONS AND ATTITUDE REFERENCE	150

LIST OF SYMBOLS

A	State-space equation dynamic matrix of aerodynamic data
AACS	Aileron Active Control System
A/C	Aircraft
ACEE	Aircraft energy efficiency
AFCS	Automatic flight control system
B	State-space equation input distribution matrix
C	State-space equation output distribution matrix
C*	Blended normal-acceleration/pitch-rate parameter
C _D	Aircraft drag coefficient
C _F	L-1011 longitudinal control system feel spring
C _L	Aircraft lift coefficient
C _m	Pitching moment coefficient
C _m _{c.g.}	Pitching moment coefficient about a particular aircraft center of gravity
C _m _{.25mac}	Pitching moment coefficient about the wing 25% mac
C _φ	Coefficient of the bank angle term for secondary gain scheduling
C.A.	Calm air atmospheric conditions
c.g.	Aircraft center of gravity
CL	Closed loop (feed-forward or feedback)
Col-in	Control column movement-inches
c.p.	Wing aerodynamic center of pressure
D	State-space equation feed-forward matrix
dB	Decibel
deg	Degrees

$D(s)$	Denominator of transfer function (determinant of baseline aircraft state-space equation in Laplace domain)
F	State-space equation feedback matrix
F_C	Control column force
F_T	Transfer function
FCES	Flight control engineers service panel
FRL	Fuselage reference line
ft	Feet
Fwd	Forward
G	Gain, general representation on Nyquist diagrams
g	Acceleration of gravity
G_1	Computed feedback gains
G_2	J-curve compensated feedback gains
G_3	Computed feed-forward gains
G_4	Computed feedback gains after elimination of velocity sensor signal
G_5	Scheduled gains (Feed-forward and Feedback)
h	Altitude
in.	Inches
I_x	Aircraft inertia about roll axis
I_y	Aircraft inertia about pitch axis
I_z	Aircraft inertia about yaw axis
J	J-curve (relationship between control column displacement and horizontal stabilizer rotation)
j	Unit imaginary number (-1)
J'	Space derivative of J-curve
K_a	Aileron cross feed loop gain
K_c	(1) Coulomb friction; (2) normalizing constant = 2.5

K_d	Detent spring rate
K_{FB}	Feedback gain
K_{FF}	Feed-forward gain
K_L	Total loop gain of closed-loop system
K_M	Mach compensation loop gain
K_{Nz}	Normal acceleration gain
K_R	Yaw rate loop gain
K_S	Spring rate
K_u	Velocity gain
K_V	Viscous friction
K_α	Angle of attack augmented gain
K_θ	Pitch attitude gain
$K_{\dot{\theta}}$	Pitch rate gain
K_ϕ	Bank angle augmented gain
K_3	Combined pitch-attitude/velocity gain
KEAS	Knots equivalent air speed
Kts	Knots
lbs	Pounds
L-1011	Lockheed wide body commercial transport
M	Mach number
M_D	Dive Mach number
M_{mo}	Maximum operation mach number
mac	Mean aerodynamic chord
MCT	Maximum continuous thrust
MTO	Maximum takeoff thrust

n_L	Structural load factor limit
N_Z	Normal acceleration feedback signal
N_{ZF}	Filtered normal acceleration feedback signal
ND	Nose down
$N(s)$	Numerator of transfer function of baseline aircraft in Laplace domain
NU	Nose up
OL	Open loop (PACS not engaged)
PACS	Pitch active control system
PLF	Power for level flight
q	Dynamic pressure
R_G	Yaw rate measured by tilted gyro
rad	Radian
rms	Root mean square of the air turbulence
RSS	Relaxed static stability
RT	Right turn
s	Laplace transform operator
sec	Second
S.L.	Sea Level
slug	English system unit mass equal to 32.2 lb _m
S/N	Serial number
T	Turbulent atmospheric conditions
TE	Trailing edge
TED	Trailing edge down
TEU	Trailing edge up
TR	Stabilizer trim rate
u	State-space equation input vector

V	Aircraft Velocity
V_e	Aircraft equivalent air speed
V_{mo}	Aircraft maximum operating speed
V_s	Aircraft stall speed
V_T	Aircraft velocity at trim
VAC	Alternating current voltage
VDC	Direct current voltage
W	Aircraft weight
w	Input vector from pilot
W_{GUST}	Turbulence gust value
$W_{PEAK GUST}$	Peak turbulence gust value
x	State vector
\dot{x}	Time derivative of state vector
X_A	Electronic input signal to series servo
X_C	Control column displacement
X_C^*	Simulator column reference position
X_S	Output displacement of series servo
X_T	Output displacement of column trim
x_o	Initial dynamic state of aircraft
y	State-space equation feedback signals
z	State-space equation feed-forward signal
α	Angle of attack
α_{FRL}	Angle of attack relative to fuselage reference line
δ	Pressure of air at aircraft altitude/Pressure of air at sea level
δ_{AC}	Symmetric outboard aileron deflection
δ_{AT}	Total differential inboard aileron angle

δ_e	Elevator deflection
δ_F	Wing flap deflection
δ_H	Horizontal stabilizer angle
δ_{Hc}	Signal to power actuator
δ_{HT}	Horizontal stabilizer trim angle
δ_{HT}^*	Modified horizontal stabilizer feedback gain signal for secondary gain scheduling
δ_R	Rudder deflection
δ_{RP}	Control pedal displacement
δ_{SP}	Spoiler deflection
δ_w	Control wheel displacement
δ_α	Secondary scheduling angle-of-attack gain
$\Delta C_{m_{AACS}}$	Incremental pitching moment coefficient due to engagement of the AACS
$\Delta C_{m_{c.g.}}$	Increment in pitching moment coefficient
$\Delta \delta_c$	Mach trim compensation
$\Delta \delta_o$	Mach trim servo offset schedule
ϵ	Principal inertia axis
ζ	Short-period and phugoid mode damping
ζ_{SP}	Short-period mode damping
θ	Pitch attitude feedback signal
$\dot{\theta}$	Pitch rate feedback signal
$\ddot{\theta}$	Time derivative of pitch rate signal
θ_F	Filtered pitch attitude feedback signal
$\dot{\theta}_F$	Filtered pitch rate feedback signal
θ_l	Lagged component of pitch attitude feedback
λ_i	State-space equation eigenvalues
v_i	State-space equation eigenvectors

σ	Turbulence level of wind gust or ω_n
τ	Time constant, general designation
τ_C	Force sensor filter time constant
τ_M	Mach trim compensation filter time constant
τ_P	Power actuator time constant
τ_S	Series servo time constant
τ_Z	Normal acceleration feedback signal filter time constant
$\tau_{\dot{\theta}}$	Pitch rate feedback signal filter time constant
τ_1	Numerator time constant of lag-lead transfer function
τ_2	Denominator time constant of lag-lead transfer function
ϕ	(1) Bank angle, (2) phase angle on Nyquist diagrams
ω	short-period or phugoid mode circular frequency
ω_d	Short-period or phugoid mode damped circular frequency
ω_n	Short-period or phugoid mode natural circular frequency
ω_{SP}	Short-period mode circular frequency
ω_o	Reference short-period mode circular frequency for the specific flight condition

1. INTRODUCTION

1.1 Background

Jet aircraft fuel cost has increased from 12¢ per gallon in 1972 to \$1.00 or more in 1983. As a result, the fuel cost portion of aircraft direct operating cost has increased from 25 percent to nearly 60 percent. This trend was recognized early by aircraft manufacturers and government leaders. Therefore, in 1975 the U.S. Congress requested NASA to establish a program to develop fuel saving technology for commercial transports.

The NASA Aircraft Energy Efficiency (ACEE) program was initiated in 1976. In February 1977 Lockheed received an ACEE program contract for "Development and Flight Evaluation of Active Control Concepts for Subsonic Transport Aircraft" (NASA Contract NAS1-14690). The contract resulted in the development of an aileron active control system (AACS) which provided wing load alleviation. The AACS allowed a 5.8 percent wing span increase for the L-1011-500 (in service date 1980) which decreased fuel consumption by approximately 3 percent (Reference 2). Also, studies were conducted under the contract to evaluate benefits of a pitch active control system (PACS). Piloted flight simulations were conducted on a moving base simulator with an L-1011 cab. These tests showed that with static longitudinal stability relaxed to near neutral and in heavy turbulence a lagged pitch rate damper provided flying qualities which are equivalent to those of the baseline aircraft. The aft c.g. simulation results provided a sufficient basis for proceeding to a flight evaluation of the PACS.

In December 1978 Lockheed was awarded the current contract for "Development and Flight Evaluation of an Augmented Stability Active Control Concept with a Small Tail". A small horizontal tail was to be built and installed on an L-1011; the center of gravity was to be moved aft to provide flight at relaxed longitudinal static stability; and a PACS was to be installed to provide satisfactory flying qualities. As the program progressed wind tunnel tests showed drag reductions of the small tail to be less than were predicted. Also, analyses and wind tunnel tests on other programs had shown that significant fuel savings could be achieved by flying an L-1011 aircraft at near neutral static stability. Therefore, in May 1980 the program was restructured to concentrate on development of near-term, advanced, and future PACS technology for flight at near neutral to negative static stability margins, and to continue small tail drag reduction evaluations by analyses and wind tunnel tests. The near-term and advanced PACS systems were to be developed, installed on a L-1011 and flight tested; and future PACS studies were to include assessment of component technology for future aircraft. The near-term PACS was to provide satisfactory flying qualities at static stability margins near neutral within the linear static stability flight envelope. The advanced PACS was to provide good flying qualities to a negative 10 percent static stability margin and for high-Mach/high-g flight conditions. However, flight tests of the advanced system were to be limited to flight at a negative 3 percent static stability margin because of the L-1011 flight test aircraft structural and c.g. management limitations.

In the fall of 1981 Lockheed decided to phase-out production of the L-1011. Consequently, in December of 1981 the scope of the program was reduced. The near-term PACS development was to be continued as previously planned; the advanced PACS development was to be continued through piloted flight simulation tests; and the future PACS studies were to be stopped. Also, scope of the small tail wind tunnel program was reduced. Tests of future aircraft small tail configurations were deleted from the wind tunnel test program.

The near-term PACS program is reported in Reference 1; the advanced PACS program is reported herein, and the small tail program is reported in Reference 3.

1.2 Program Objective

The advanced PACS program design objective was to develop technology for a PACS which would provide flying qualities at negative static stability margins that were equivalent to those of the baseline aircraft with a mid c.g. position (25 percent mac). Also, the PACS was to compensate for high-Mach/high-g instabilities that degrade flying qualities during upset recoveries and maneuvers.

1.3 Scope of Program

The advanced PACS program consisted of control law development, flying qualities analysis, piloted flight simulation testing on a moving base simulator, and architecture development of a PACS that could be used for a flight test program.

2. L-1011 CONTROL SYSTEM DESCRIPTION

This section describes the longitudinal control system of an L-1011 aircraft equipped with a PACS. A simple block diagram of the longitudinal control system is given in Figure 1. The baseline aircraft control system is represented by the dashed lines and the PACS is represented by solid lines.

The controller is a digital computer with the input signals shown (Table 1). The controller output signal is sent to the two series servos which have a position summed output that is added to the control column displacement. Control authority of the PACS is limited to a stabilizer rotation of ± 1.5 degrees at a cruise trim setting of -1 degree. The control authority varies with trim setting to approximately ± 4 degrees at a trim setting of -10 degrees.

A PACS loads path block diagram is shown in Figure 2. The control system is an irreversible hydro-mechanical system which consists of the following:

- Control column
- Feel and trim system

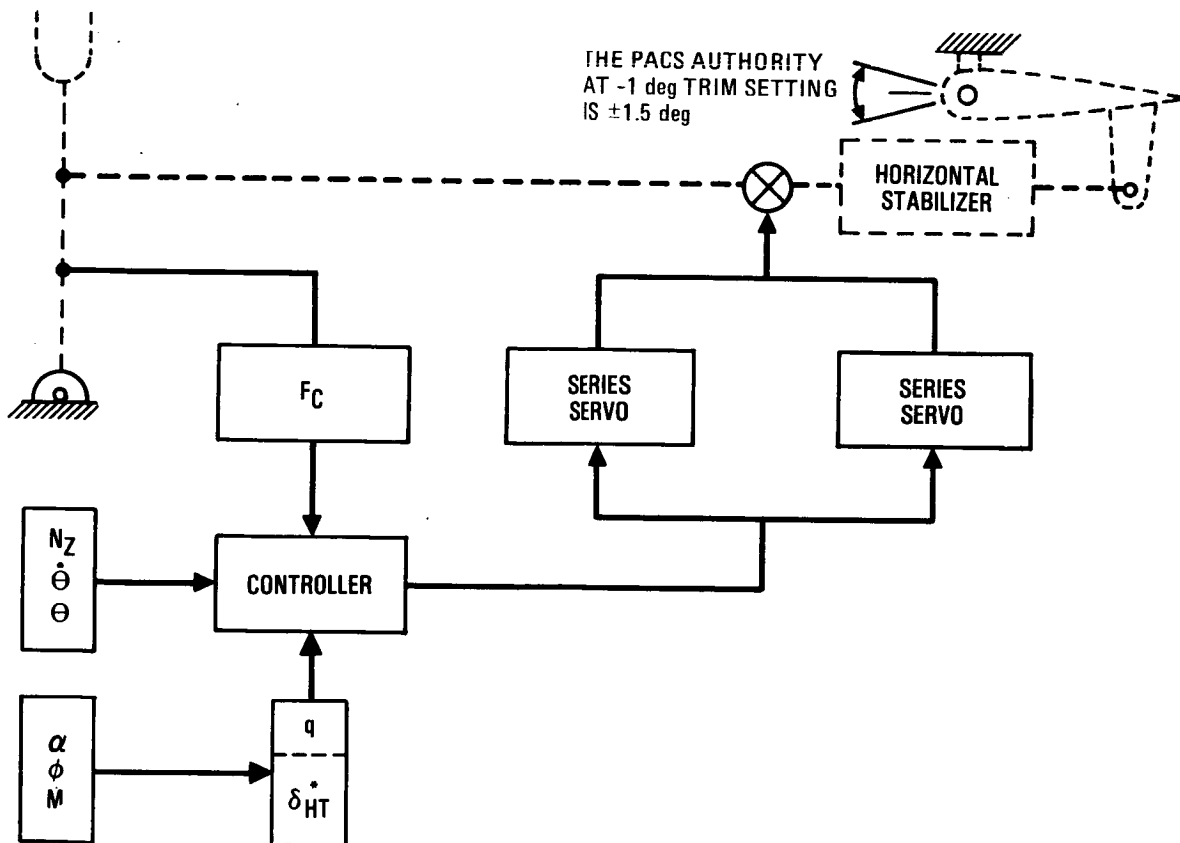


Figure 1. - Longitudinal control system with the advanced PACS.

TABLE 1. - PACS CONTROLLER INPUT SIGNALS

SYMBOL	SIGNAL	TYPE	USE
F_C	Column force	Feed-forward	Column force gradient
N_Z	Normal acceleration	Feedback	Short period mode
$\dot{\theta}$	Pitch rate		Phugoid mode
θ	Pitch attitude		
q	Dynamic pressure	Primary gain scheduling	Compensation for flight condition changes
δ_{HT}^*	Horizontal stabilizer trim		
α	Angle of attack	Secondary gain scheduling	Compensation for pitch-up and AACS outboard aileron operation
ϕ	Bank angle		
M	Mach number		

- Autopilot
- Stabilizer power servo system

A schematic diagram of the control system is shown in Figure 3. The solid black linkage system shown in the figure represents the PACS series servo tie-in mechanism. This tie-in arrangement allows the series servo output to provide input to the stabilizer actuators via a nonlinear mechanical linkage and hydraulic servo valve without moving the control column.

The nonlinearizer in the mechanical linkage consists of four bars: the three indicated in Figure 3 and the airframe structure. This nonlinearizer changes the stabilizer rotation (δ_H) sensitivity with relation to control column displacement (X_C) as shown in Figure 4. This relationship is called the J curve. Two δ_H versus X_C curves are shown in the figure: the curve on the right for a stabilizer trim setting (δ_{HT}) of zero and the curve on the left for a trim setting of -10 degrees. The dashed line provides a locus of trim points. Thus, a family of J curves exists over the range of trim settings, and every trim setting has a different column to stabilizer gain about trim which must be considered in computing the PACS feedback gains.

ORIGINAL PAGE 19
OF POOR QUALITY

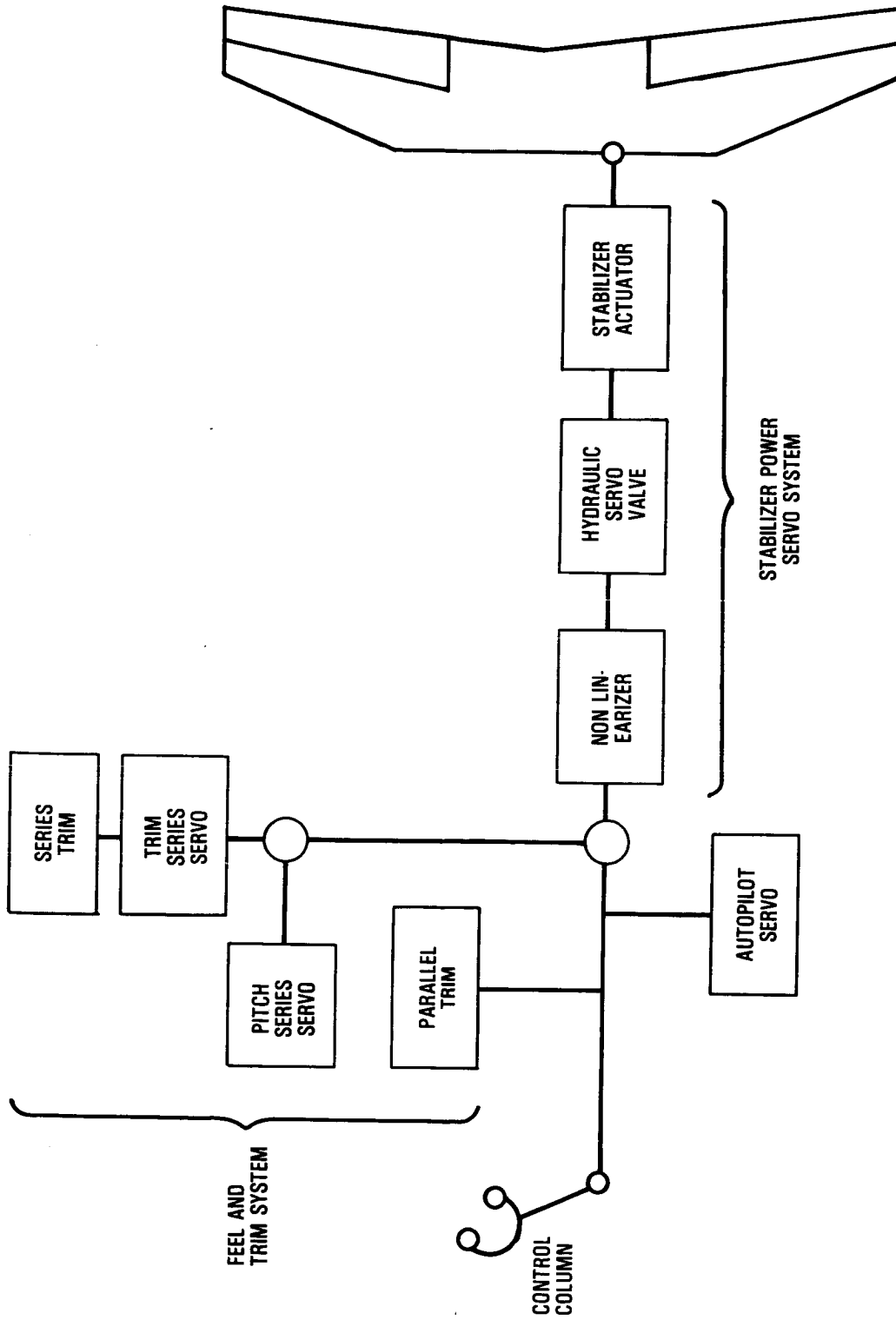


Figure 2. - PACS load path diagram.

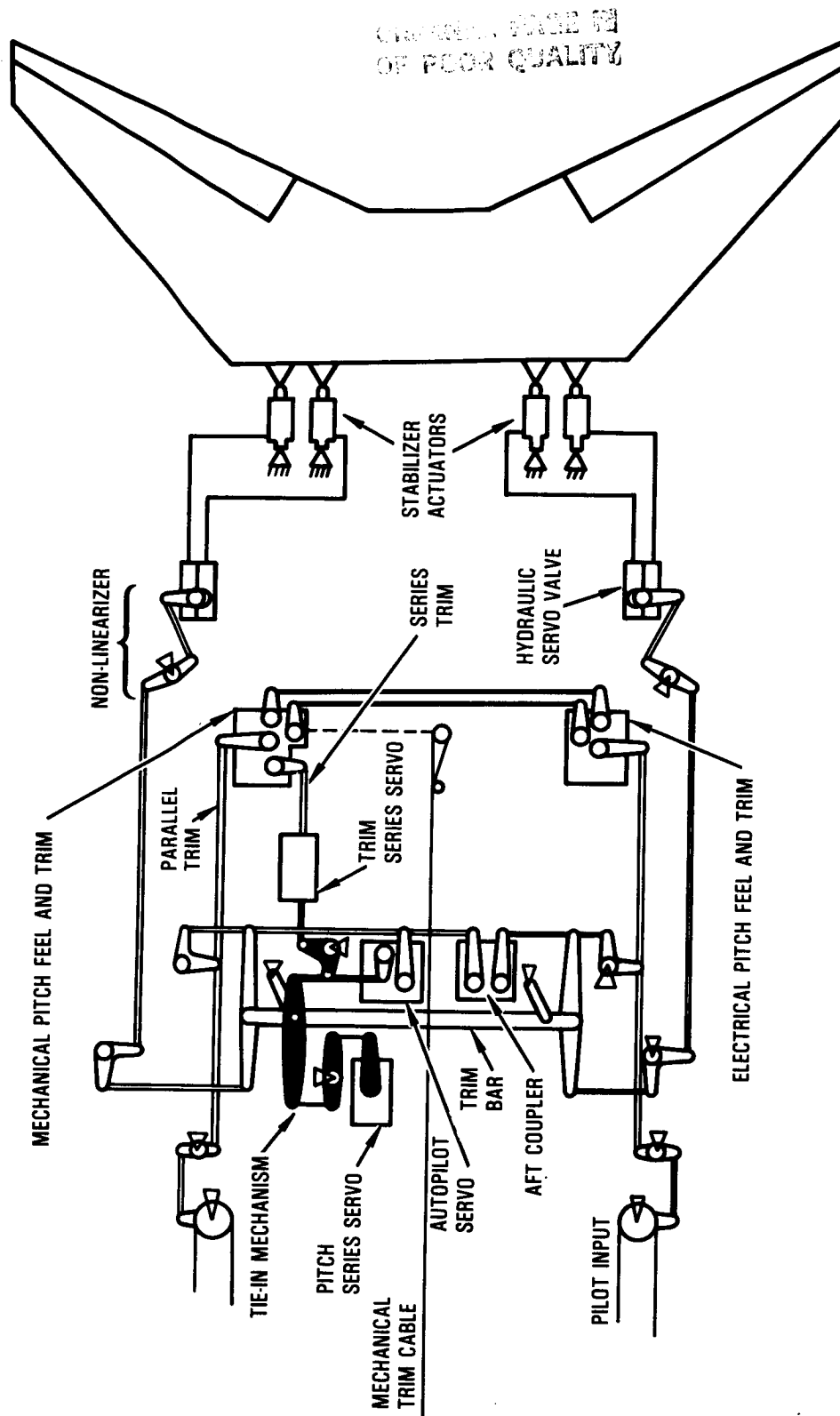


Figure 3. - Schematic of the L-1011 control system with the advanced PACS series servo.

ORIGINAL PAGE IS
OF POOR QUALITY

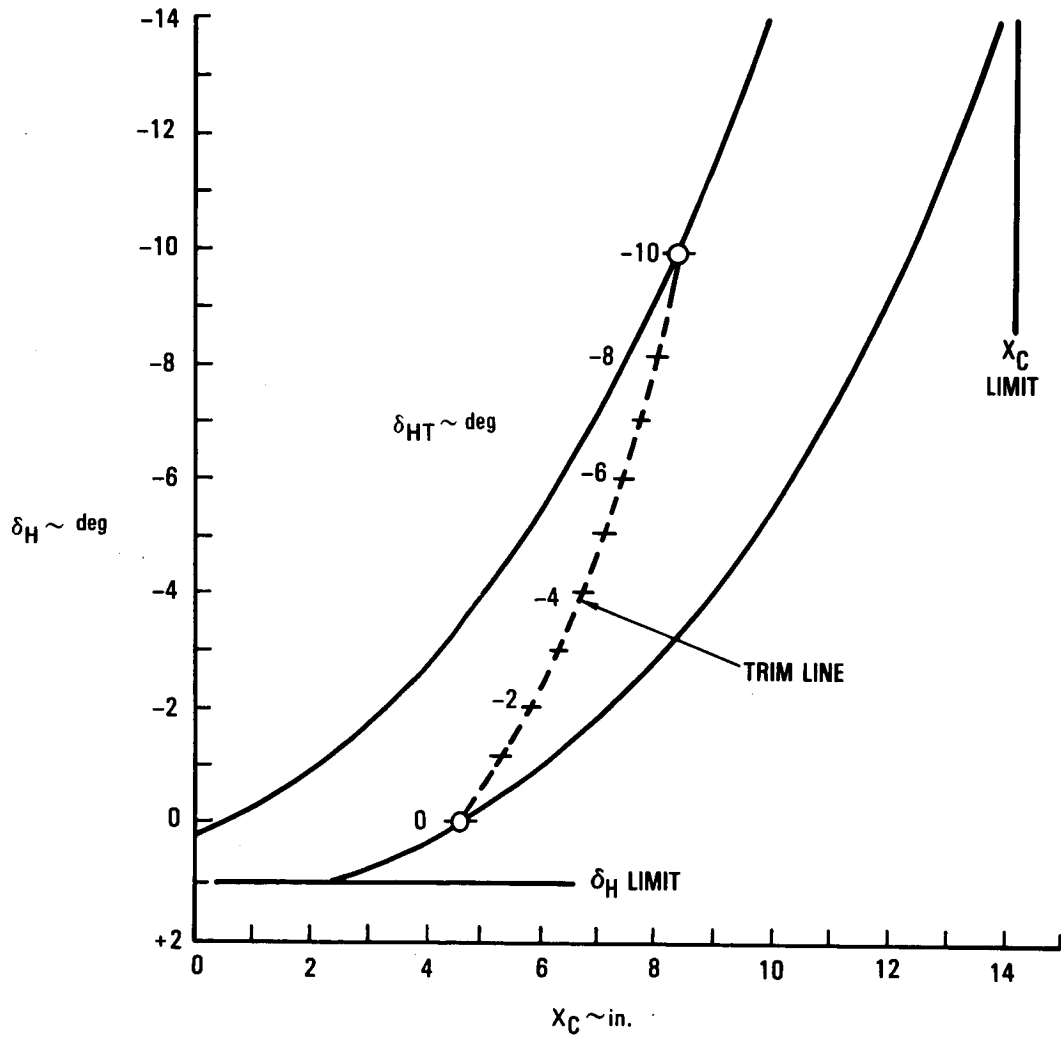


Figure 4. - J curve.

3. CONTROL LAW DEVELOPMENT

Design criteria were developed for the short period mode and phugoid mode frequency and damping, for the blended normal-acceleration/pitch rate (C*) time history, and for the column force gradient.

The control law synthesis procedure utilized the modal control method of modern control theory to determine feedback gains which satisfied the prescribed stability criteria for the complete envelope of L-1011 flight conditions. Matrix algebra was applied to the state-space equations to determine the corresponding set of feed-forward gains. Primary gain scheduling was accomplished by expressing the feedback and feed-forward gains as second-degree polynomials in terms of the dynamic pressure (q) and the horizontal stabilizer trim angle (δ_{HT}). Secondary gain scheduling was provided by a modified stabilizer trim signal (δ_{HT}^*) for pitch-up and AACS operating conditions.

Mechanization of the control laws included the specification of signal filter requirements, defined lag-lead and pitch synchronizer circuits, and designated values for bias switches.

Closed-loop poles were evaluated for 56 selected cases. Nyquist plots were used in 13 selected cases to determine the phase and gain margins.

Details of the control law development are given in the following sections.

3.1 Advanced PACS Design Objectives

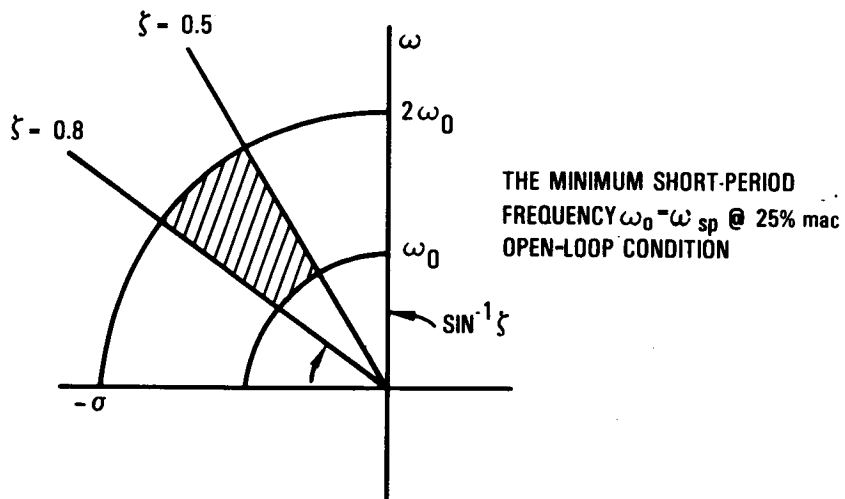
The PACS configured aircraft was designed to have the capability to operate over the full flight envelope with static stability margins to -10 percent (c.g. at 50% mac) and to have flying qualities equivalent to those of the baseline aircraft with the c.g. at 25% mac. The 25% mac c.g. location represents the existing L-1011 baseline configuration which is considered to have excellent flying qualities.

The PACS design objectives were as follows:

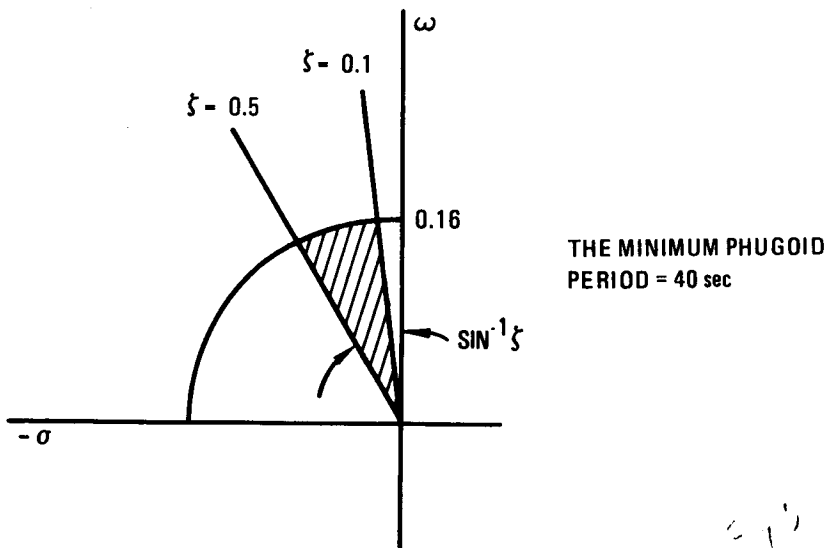
- The short-period and phugoid modes frequency and damping characteristics should fall within the shaded s-plane areas given in Figure 5.
- The column-force gradients should fall within the column-force versus load-factor boundaries designated in Figure 6 and have nearly constant slope.
- The blended normal-acceleration/pitch-rate (C*) time history response to a step command should fall within the limits designated in Figure 7.

PRECEDING PAGE BLANK NOT FILMED

ORIGINAL PAGE IS
OF POOR QUALITY



A. SHORT PERIOD MODE



B. PHUGOID MODE

Figure 5. - PACS dynamic stability design objectives.

ORIGINAL PAGE IS
OF POOR QUALITY

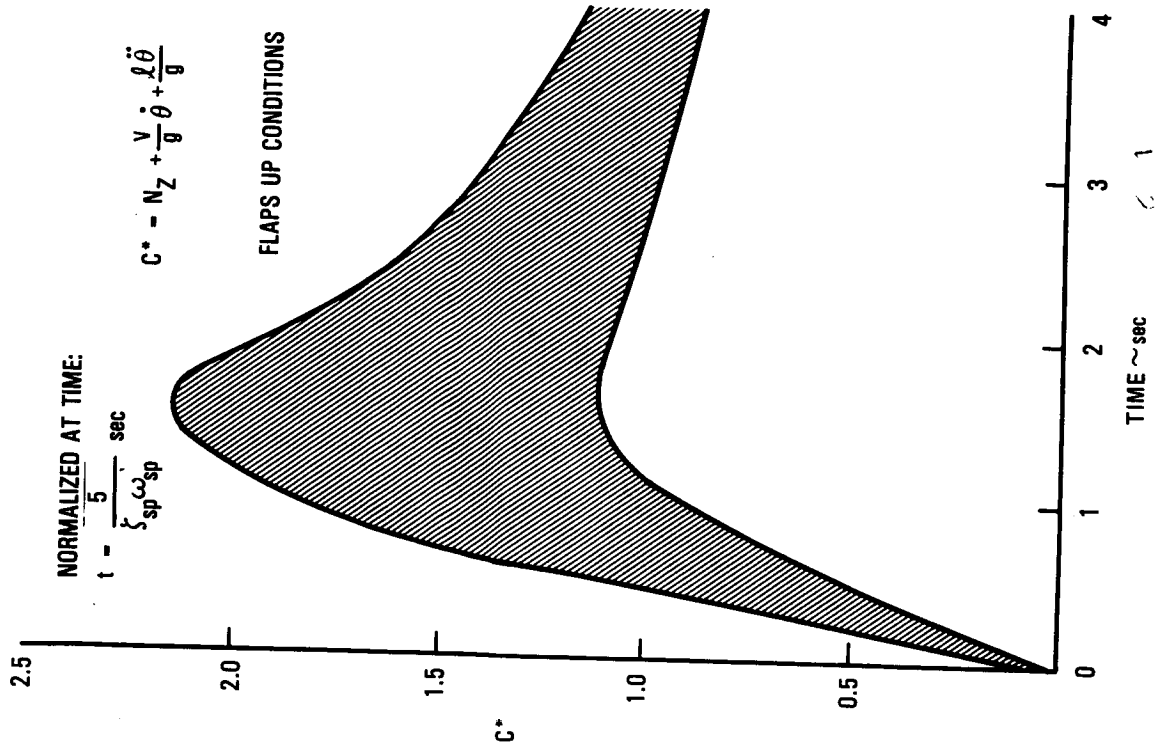


Figure 7. - Blended normal-acceleration/pitch-rate response objective.

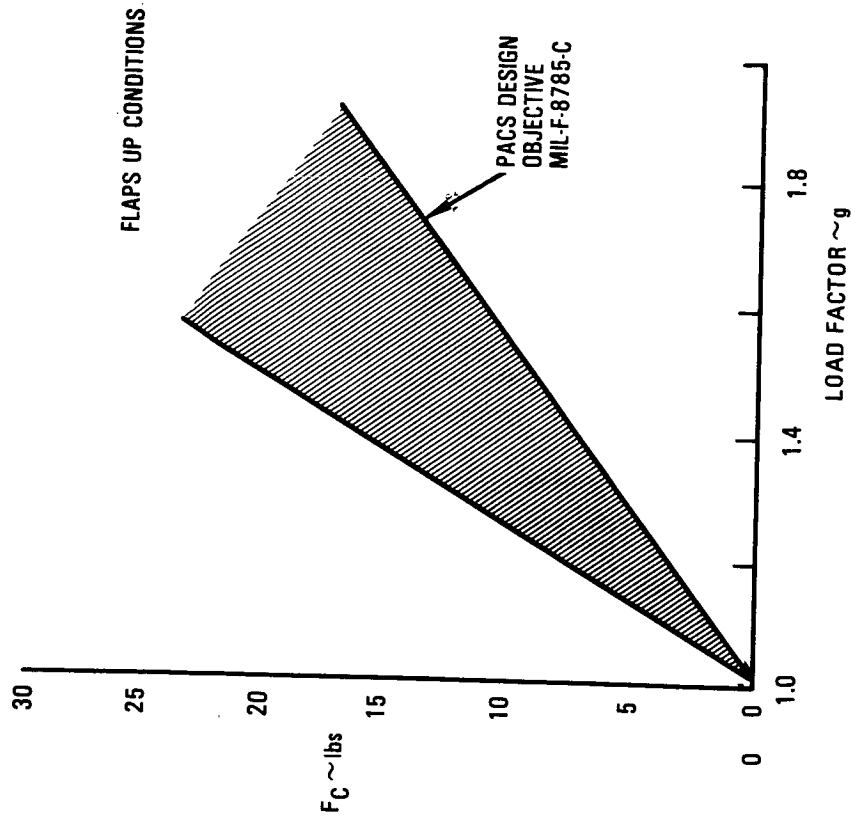


Figure 6. - PACS column force gradient design objective.

3.2 Control Law Synthesis

The control law synthesis process was accomplished as shown in Figure 8. Each block in the synthesis process is described briefly in the following paragraphs.

3.2.1 Aero Data. - The synthesis process started with a separate set of aero data for each of the flight cases listed in Table 2. Each case is defined by the flight condition number shown in the first column of the table and a letter (a through e) representing one of the c.g. locations in the next five columns. Thus, the case numbers are 1a, 1b, ..., 1e, 2a, 2b, ..., 2e, etc. The aero data consist of the trim condition parameters and the derivatives at trim given in Appendix A.

3.2.2 Baseline Aircraft Model. - The PACS control math model in state-space form is shown in Figure 9. The baseline math model (Appendix B) was the state-space equation of the system with the control loops open (Eq. 1).

$$\{\dot{x}\} = [A] \{x\} + [B] \{u\} \quad (\text{Eq. 1})$$

Equation 1 was used to obtain a set of eigenvalues $(\lambda_i)_j$ and eigenvectors $(v_i)_j$ for each of the 14 flight conditions with c.g. location at 25% mac. These 14 sets ($j = 1, 2, \dots, 14$) of eigenvalues and eigenvectors are called the reference eigenstructure $(\lambda_i, v_i)_j$ for the respective flight conditions. Each set of the eigenstructure complies with the design objectives given in Figures 5 and 7.

3.2.3 Feedback Loop Synthesis. - The feedback loop synthesis for each flight condition was accomplished in three steps:

- Modal control synthesis (computation of feedback gains)
- J curve compensation
- Deletion of velocity signal

With the feedback loop in Figure 9 closed, the modal control synthesis method (see Appendix C) yields the set of feedback gains represented by G_1 in Figure 8. The closed-loop state-space equation of the system in Figure 9 is:

$$\{\dot{x}\} = ([A] + [B][F][C])\{x\} \quad (\text{Eq. 2})$$

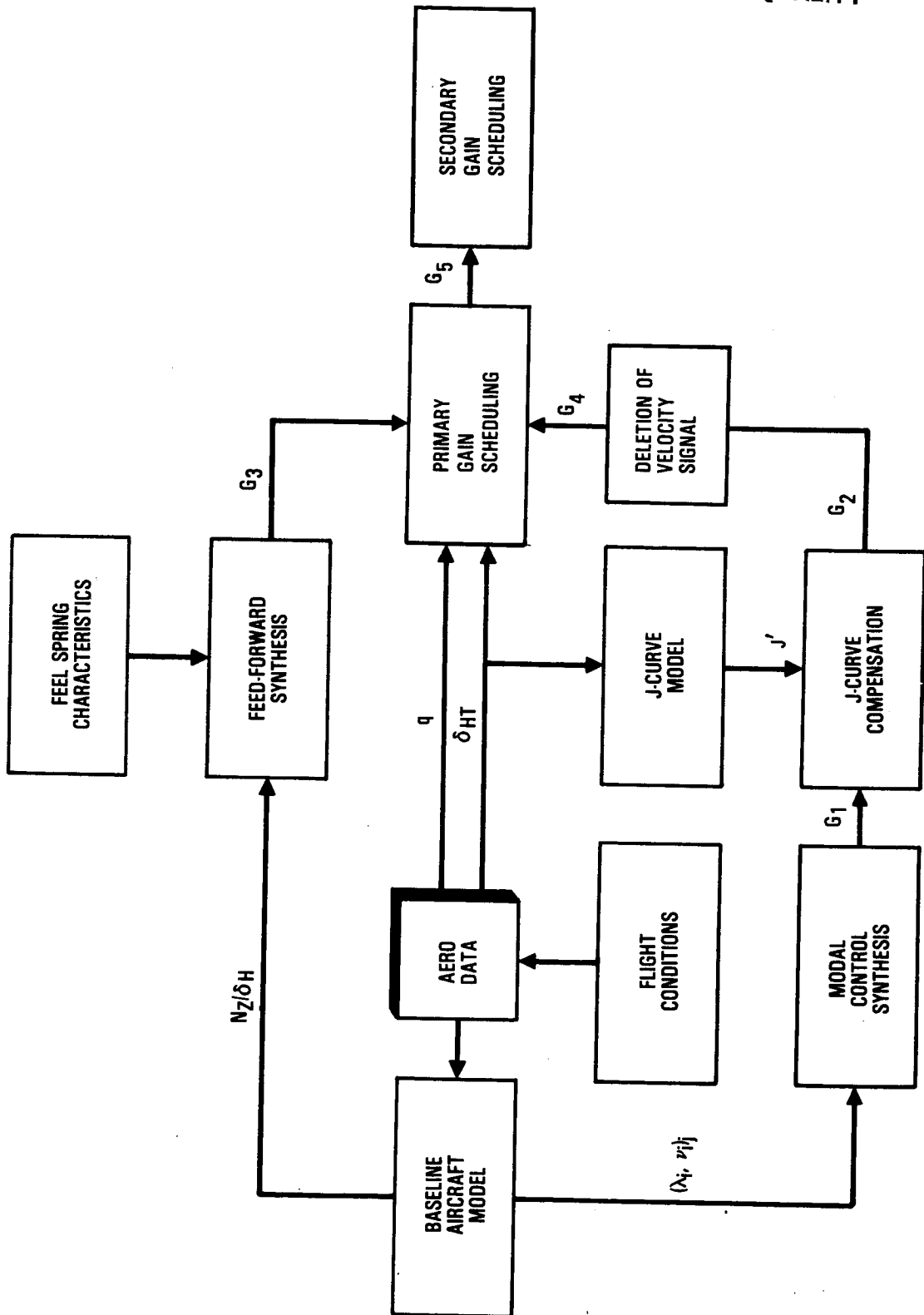


Figure 8. - Control law synthesis.

TABLE 2. - FLIGHT CONDITIONS FOR ADVANCED FLIGHT CONTROL SYSTEM ANALYSIS

FLIGHT CONDITION	c.g. ~ % mac							WEIGHT lbs	δ_F deg	h ft	V (KEAS/M)	ENGINE POWER	GEAR POSITION
	FORWARD c.g. POSITION a	MID-c.g. POSITION b	AFT c.g. POSITION c	NEUTRAL STABILITY c.g. POSITION d	NEGATIVE STABILITY c.g. POSITION e								
1. TAKEOFF	19.6	25	32.2	37	-	422,000	26	S.L.	145/0.22	MTO	DOWN		
2. TAKEOFF	13.8	25	35	42	-	305,000	26	S.L.	123/0.19	MTO	DOWN		
3. CLIMB	-	25	32.2	37	50	422,000	0	10,000	274/0.5	MCT	UP		
4. CLIMB	-	25	34.5	40.2	50	360,000	0	10,000	369/0.67	MCT	UP		
5. CLIMB	-	25	35	42	50	305,000	0	10,000	369/0.67	MCT	UP		
6. CRUISE	-	25	33.1	37.7	50	408,000	0	37,000	245/0.8	PLF	UP		
7. CRUISE	-	25	33.1	37.7	50	408,000	0	37,000	254/0.83	PLF	UP		
8. CRUISE	-	25	33.1	37.7	50	408,000	0	37,000	263/0.86	PLF	UP		
9. CRUISE	-	25	33.1	37.7	50	408,000	0	37,000	276/0.9	PLF	IP		
10. CRUISE	-	25	34.5	40.2	50	360,000	0	33,000	280/0.83	PLF	UP		
11. CRUISE	-	25	35	42	50	285,000	0	33,000	290/0.86	PLF	UP		
12. LANDING	16.4	25	34.5	40.3	-	358,000	42	S.L.	149/0.23	PLF	DOWN		
13. LANDING	14.8	25	35	42	-	325,000	42	S.L.	142/0.21	PLF	DOWN		
14. LANDING	12.0	25	35	42	-	265,000	42	S.L.	128/0.19	PLF	DOWN		

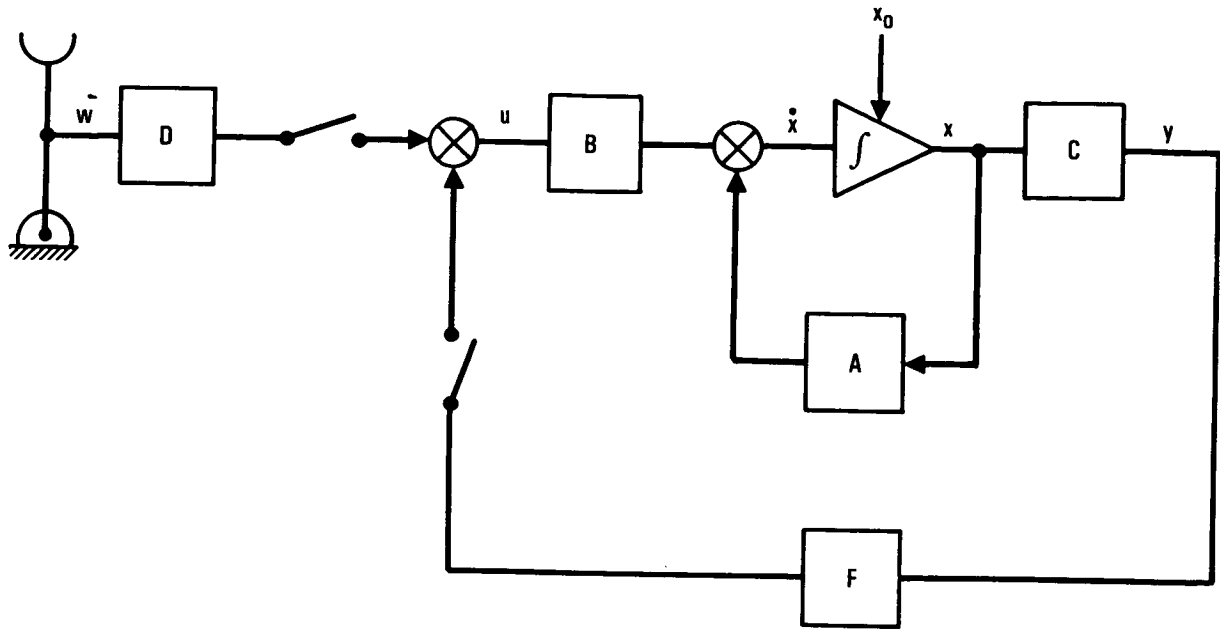


Figure 9. - PACS control model.

The reference eigenstructure for each flight condition was assigned to the matrix $([A] + [B][F][C])$ for each of the corresponding c.g. locations in accordance with the standard eigenvector equation:

$$([A] + [B][F][C])\{v_i\}_j = (\lambda_i)_j\{v_i\}_j \quad (\text{Eq. 3})$$

Each element of Equation 3 is known except the gain matrix F. Values of the matrix elements for matrices A, B, and C are different for each c.g. location, whereas the desired values of $(\lambda_i)_j$ and $(v_i)_j$ remain unchanged over the c.g. range for each specific flight condition.

Steps performed for computing the feedback gains from Equation 3 are:

- Insert a set of eigenvalues and truncated eigenvectors for a specific flight condition.
- Insert a corresponding set of aero data for a specific c.g. location.
- Partition the matrices (Appendix C).
- Solve the partitioned equation explicitly for matrix F.

This process was performed for each flight case to produce the 56 x 4 feedback matrix (G_1) in Table 3.

The table headings consist of velocity gain (K_u), pitch attitude gain (K_θ), normal acceleration gain (K_{N_z}), and pitch rate gain ($K_{\dot{\theta}}$). The table shows gains for only four c.g. locations for each flight condition. For the flap-down flight conditions (numbers 1, 2, 12, 13, and 14), gains for c.g. locations a through d of Table 2 are given; and for the flap-up flight conditions, gains for c.g. locations b through e are given. The discarded gain values were least important for the respective flight conditions. Eliminating one c.g. position reduced the number of points to be used for gain scheduling and permitted a more accurate curve fit of the remaining four points.

An evaluation of the feedback equation pole placement was made by comparing the closed loop poles with the design objectives given in Figure 5 and with the poles of the open loop cases. Figures 10 and 11 show the dominant pole placements for 36 flap-up and 20 flap-down flight cases, respectively. These cases are the 56 that were selected for gain scheduling. Open and closed-loop poles in the short-period mode frequency range are shown at the top of the figures and those in the phugoid frequency range are shown at the bottom. The closed-loop damping scatter is due to gain scheduling tradeoffs. A few of the closed-loop, short-period, flap-up eigenvalues slightly missed the corresponding boundaries in Figure 10. However, they were considered acceptable because the criteria were objectives and not rigid requirements.

The feedback gains were adjusted to compensate for the nonlinearizer (J curve) in the L-1011 control system. Figure 8 shows the δ_{HT} input to the J-curve model from the aero data. The J-curve model is a set of equations that was curve fitted to the family of curves shown in Figure 4. The output of the J-curve model was the J-curve derivative (J') corresponding to δ_{HT} for the specific flight condition being evaluated. The slope of all members of the J-curve family is the same for any specified value of δ_{HT} . The compensated feedback gain matrix (G_2) given in Table 4 was determined by application of Equation 4.

$$[G_2] = [J']^{-1} [G_1] \quad (\text{Eq. 4})$$

J' is a diagonal matrix of 56 J-curve derivatives. A plot of the compensated pitch rate gain ($K_{\dot{\theta}}$) is shown in Figure 12 for the flap-up flight conditions to illustrate the compensated gain values. This figure is a plot of the $K_{\dot{\theta}}$ flap-up values in Table 4 as a function of the corresponding δ_{HT} values of Table 5 for each dynamic pressure, q .

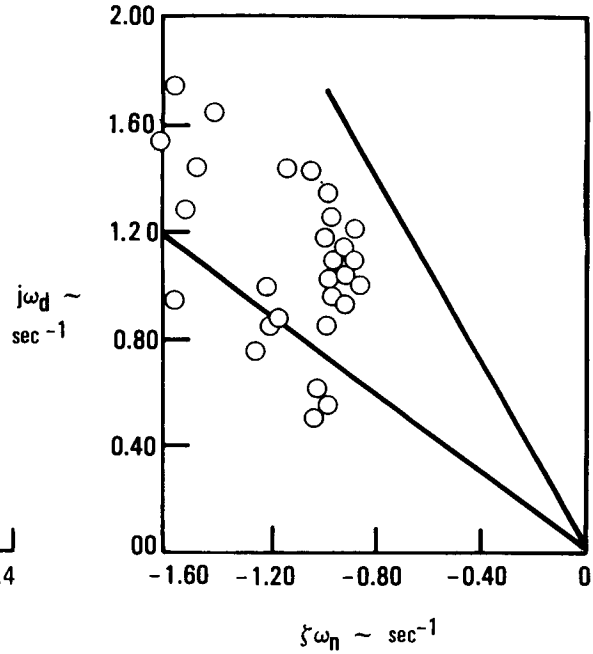
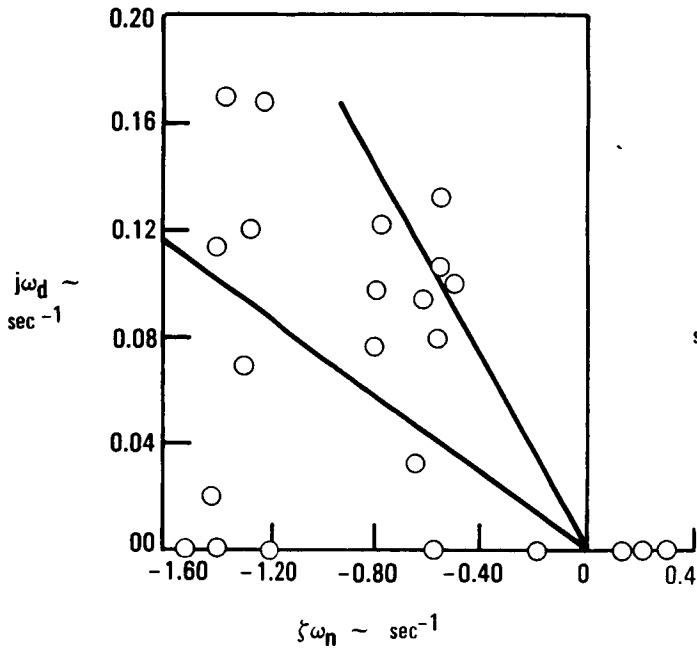
Control of the phugoid mode requires a velocity gain component. Because of frequent velocity changes associated with changing trim conditions, use of a velocity signal is undesirable. Consequently a method was devised (Appendix D) where the velocity gain (K_u), and the pitch attitude gain (K_θ) could be combined to eliminate the need for a velocity signal. Thus, instead

TABLE 3. - FEEDBACK GAIN MATRIX (G_1)

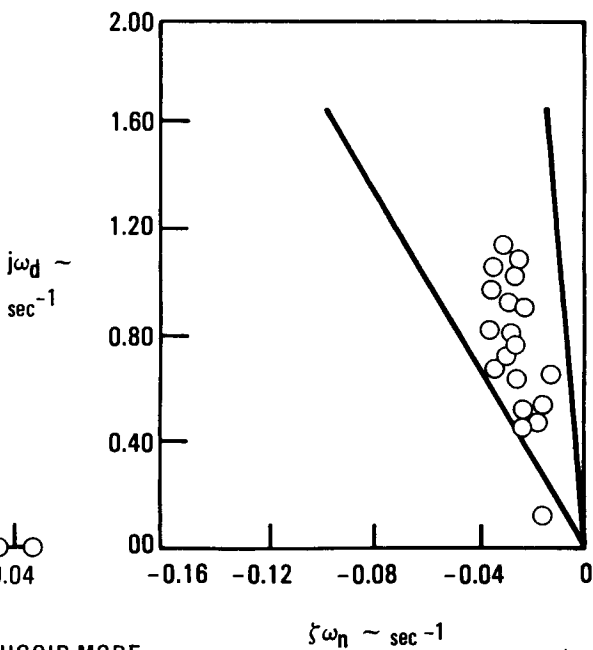
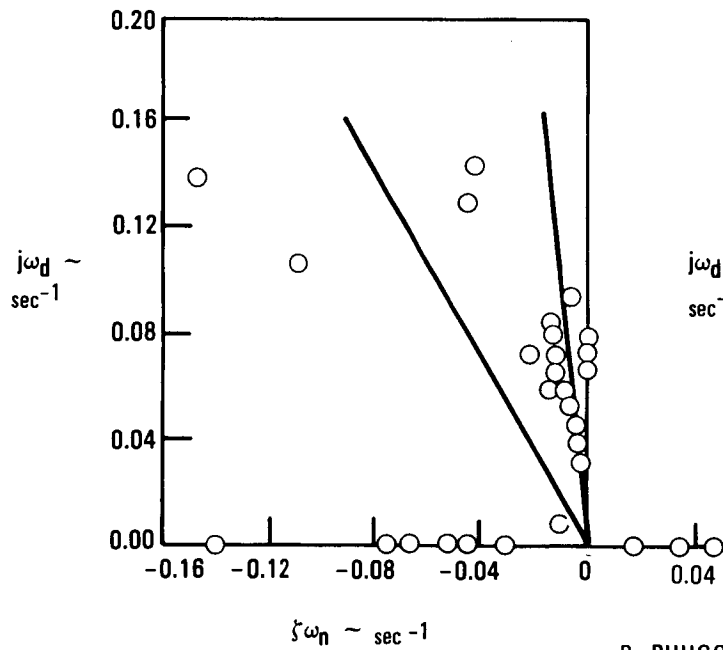
CASE	K_u	K_θ	K_{Nz} deg/g	$K_{\dot{\theta}}$ -sec
1A	0.0692	-0.116	-0.9855	-0.434
1B	0.104	-0.119	-1.8850	-0.444
1C	0.172	-0.134	-3.6039	-0.524
1D	0.227	-0.144	-5.0420	-0.584
2A	0.0718	-0.138	-1.4782	-0.595
2B	0.140	-0.144	-3.2143	-0.628
2C	0.257	-0.175	-6.3025	-0.796
2D	0.391	-0.209	-9.7403	-0.994
3B	0.0541	-0.0397	-0.1988	-0.130
3C	0.0747	-0.041	-0.2830	-0.155
3D	0.0863	-0.0402	-0.6188	-0.167
3E	0.142	-0.0446	-1.7991	-0.242
4B	0.00534	-0.011	0.1450	-0.0484
4C	0.0189	-0.0104	-0.1381	-0.0733
4D	0.0269	-0.00996	-0.3088	-0.0894
4E	0.043	-0.00962	-0.6303	-0.126
5B	0.00719	-0.0091	-0.1083	-0.0279
5C	0.0187	-0.00827	-0.1306	-0.0510
5D	0.0271	-0.00777	-0.2956	-0.0697
5E	0.0381	-0.00754	-0.5025	-0.0974
6B	0.0247	-0.0129	-0.04927	-0.162
6C	0.0126	-0.0127	0.09397	-0.154
6D	0.0241	-0.0125	-0.27674	-0.170
6E	0.0659	-0.0136	-1.4954	-0.252
7B	0.0612	-0.0144	2.1830	-0.118
7C	0.0873	-0.164	0.09397	-0.145
7D	0.0987	-0.0175	-0.25382	-0.159
7E	0.148	-0.024	-1.3997	-0.240
8B	-0.0037	-0.00949	0.43831	-0.108
8C	0.0180	-0.0104	0.01415	-0.125
8D	0.0351	-0.0112	-0.32429	-0.150
8E	0.0849	-0.0124	-1.3407	-0.217
9B	0.0356	-0.000699	-0.04956	-0.108
9C	0.0536	-0.00115	-0.50764	-0.141
9D	0.0674	-0.00146	-0.77922	-0.163
9E	0.101	-0.00205	-1.5871	-0.221
10B	-0.0378	-0.00881	0.28533	-0.130
10C	-0.0178	-0.00858	-0.20168	-0.158
10D	-0.00551	-0.00891	-0.52426	-0.136
10E	0.0201	-0.00906	-1.1345	-0.237
11B	0.0358	-0.00817	0.19022	-0.0769
11C	0.0548	-0.00843	-0.16902	-0.110
11D	0.0665	-0.00816	-0.43201	-0.133
11E	0.0834	-0.8821	-0.76203	-0.169
12A	0.0496	-0.0876	-0.64744	-0.393
12B	0.0957	-0.0938	-1.7704	-0.424
12C	0.170	-0.108	-3.5351	-0.501
12D	0.238	-0.124	-51.4516	-0.588
13A	0.0363	-0.0876	-0.82506	-0.420
13B	0.0876	-0.0945	-2.0798	-0.453
13C	0.162	-0.108	-3.8847	-0.528
13D	0.239	-0.124	-5.7869	-0.629
14A	0.0985	-0.114	-1.1860	-0.459
14B	0.157	-0.120	-25.9550	-0.478
14C	0.234	-0.136	-43.2583	-0.543
14D	0.319	-0.156	-6.1879	-0.634

OPENED LOOP

CLOSED LOOP



A. SHORT PERIOD MODE

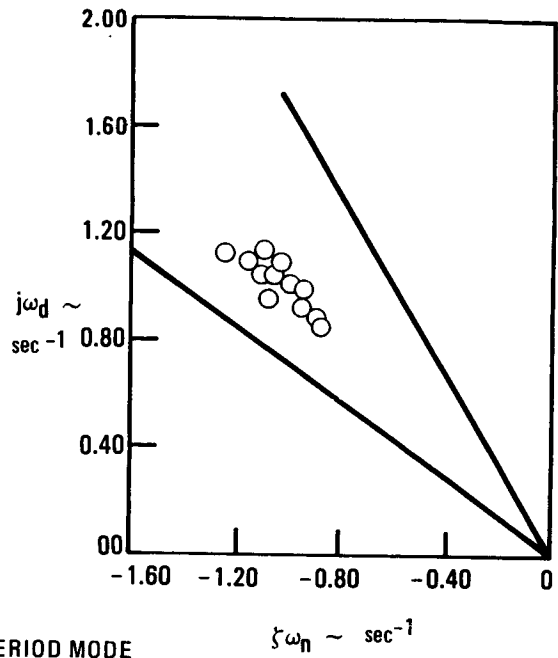
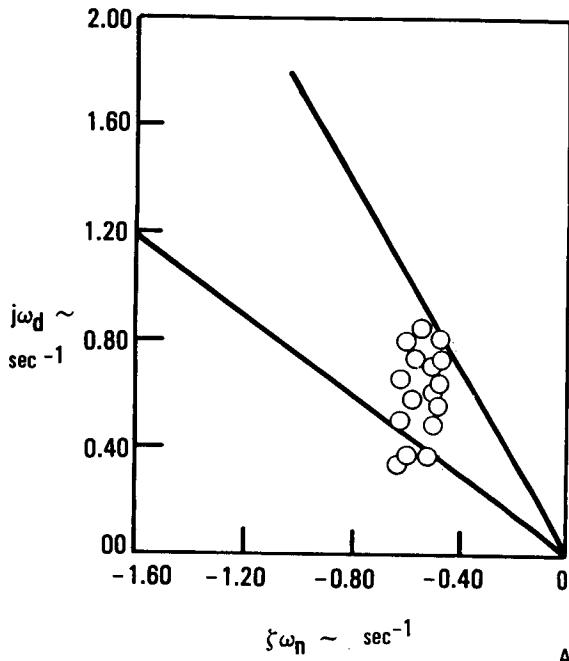


B. PHUGOID MODE

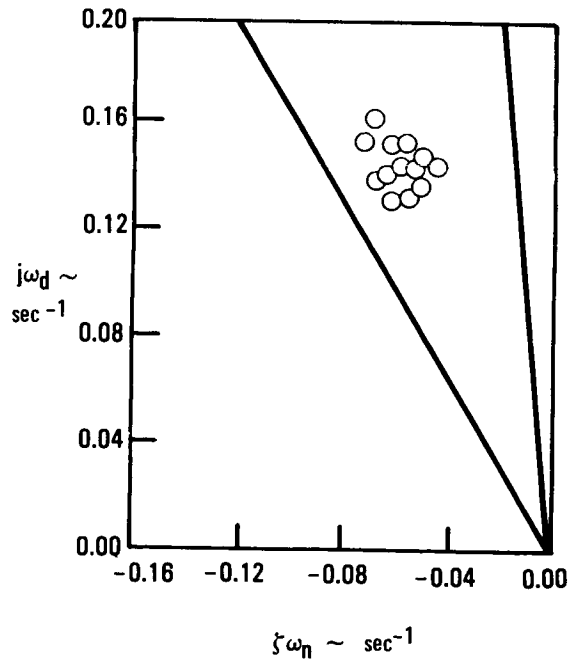
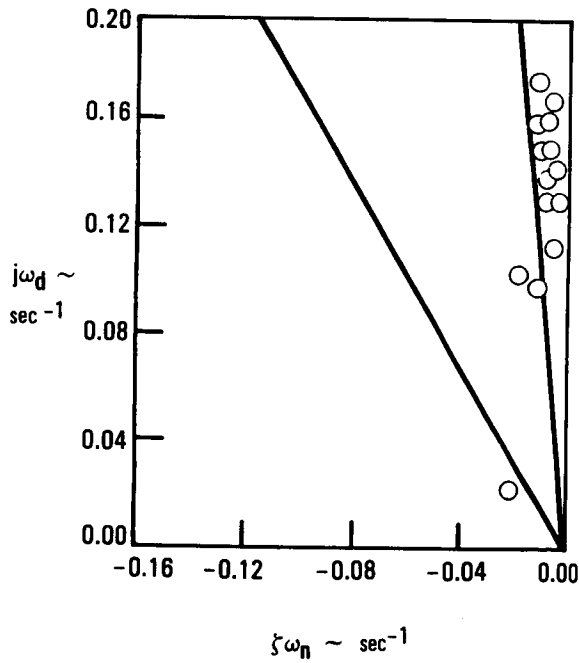
Figure 10. - Flap-up eigenvalues.

OPENED LOOP

CLOSED LOOP



A. SHORT PERIOD MODE



B. PHUGOID MODE

Figure 11. - Flap-down eigenvalues.

ORIGINAL QUALITY
OF POOR QUALITY

TABLE 4. - COMPENSATED FEEDBACK GAIN MATRIX (G_2)

CASE	K_u	K_θ	K_{N_z} deg/g	$K_{\dot{\theta}}$ - sec
1A	0.079861	-0.133871	-1.1373	-0.500861
1B	0.130845	-0.149717	-2.37159	-0.558608
1C	0.253478	-0.197477	-5.31109	-0.772224
1D	0.389597	-0.247145	-8.65355	-1.002310
2A	0.080263	-0.154267	-1.65247	-0.665136
2B	0.187112	-0.192458	-4.29592	-0.0839331
2C	0.454108	-0.309218	-11.1363	-1.406497
2D	1.013633	-0.541814	-25.2508	-2.576858
3B	0.104016	-0.076330	0.38228	-0.249947
3C	0.159097	-0.087322	-0.60281	-0.330121
3D	0.199221	-0.092800	-1.42844	-0.385515
3E	0.428737	-0.137800	-5.55861	-0.747706
4B	0.012824	-0.026417	-0.34813	-0.116235
4C	0.049774	-0.027389	-0.36366	-0.193039
4D	0.075318	-0.027887	-0.86471	-0.250313
4E	0.135468	-0.030307	-1.98559	-0.396952
5B	0.017773	-0.022495	0.26769	-0.068967
5C	0.050394	-0.022287	-0.35203	-0.137439
5D	0.077784	-0.022302	-0.84861	-0.200058
5E	-0.119027	-0.023556	-1.56979	-0.304285
6B	0.046369	-0.024217	0.09402	-0.304118
6C	0.026743	-0.026955	0.19945	-0.326855
6D	0.055634	-0.028856	-0.63885	-0.392440
6E	0.206452	-0.042606	-4.68485	-0.789466
7B	0.117311	-0.027603	1.31792	-0.226188
7C	0.188561	-0.035423	0.20294	-0.313189
7D	0.228629	-0.040952	-0.59399	-0.372078
7E	0.462363	-0.074978	-4.34960	-0.749778
8B	-0.007373	-0.018910	0.87342	-0.207237
8C	0.040389	-0.023336	0.03174	-0.280478
8D	0.085334	-0.027229	-0.78839	-0.364675
8E	0.273638	-0.039966	-4.32125	-0.699404
9B	0.072922	-0.001432	-0.10153	-0.241709
9C	0.122554	-0.002629	-1.16070	-0.322390
9D	0.165566	-0.003586	-1.91414	-0.400405
9E	0.318192	-0.006458	-4.99997	-0.696241
10B	-0.079541	-0.018538	0.60040	-0.273552
10C	-0.042236	-0.020358	-0.47853	-0.374895
10D	-0.014284	-0.023098	-1.35911	-0.482189
10E	0.062620	-0.028226	-3.53429	-0.738350
11B	0.081237	-0.018539	0.43167	-0.174500
11C	0.138079	-0.021241	-0.42588	-0.277165
11D	0.182629	-0.022410	-1.18642	-0.365258
11E	0.256272	-0.025228	-2.34156	-0.519305
12A	0.058653	-0.103589	-0.76559	-0.464730
12B	0.128241	-0.125695	-2.37245	-0.568174
12C	0.281634	-0.178920	-5.85655	-0.829992
12D	0.481169	-0.250693	-10.40205	-1.88770
13A	0.042143	-0.101701	-0.95787	-0.487609
13B	0.117594	-0.126856	-2.79197	-0.608104
13C	0.272417	-0.181611	-6.43241	-0.887878
13D	0.523655	-0.271687	-12.67921	-1.378156
14A	0.110854	-0.128310	-1.33488	-0.516615
14B	0.210756	-0.161087	-3.48416	-0.641664
14C	0.393492	-0.228696	-7.27427	-0.913102
14D	0.698938	-0.341800	-13.55980	-1.389111

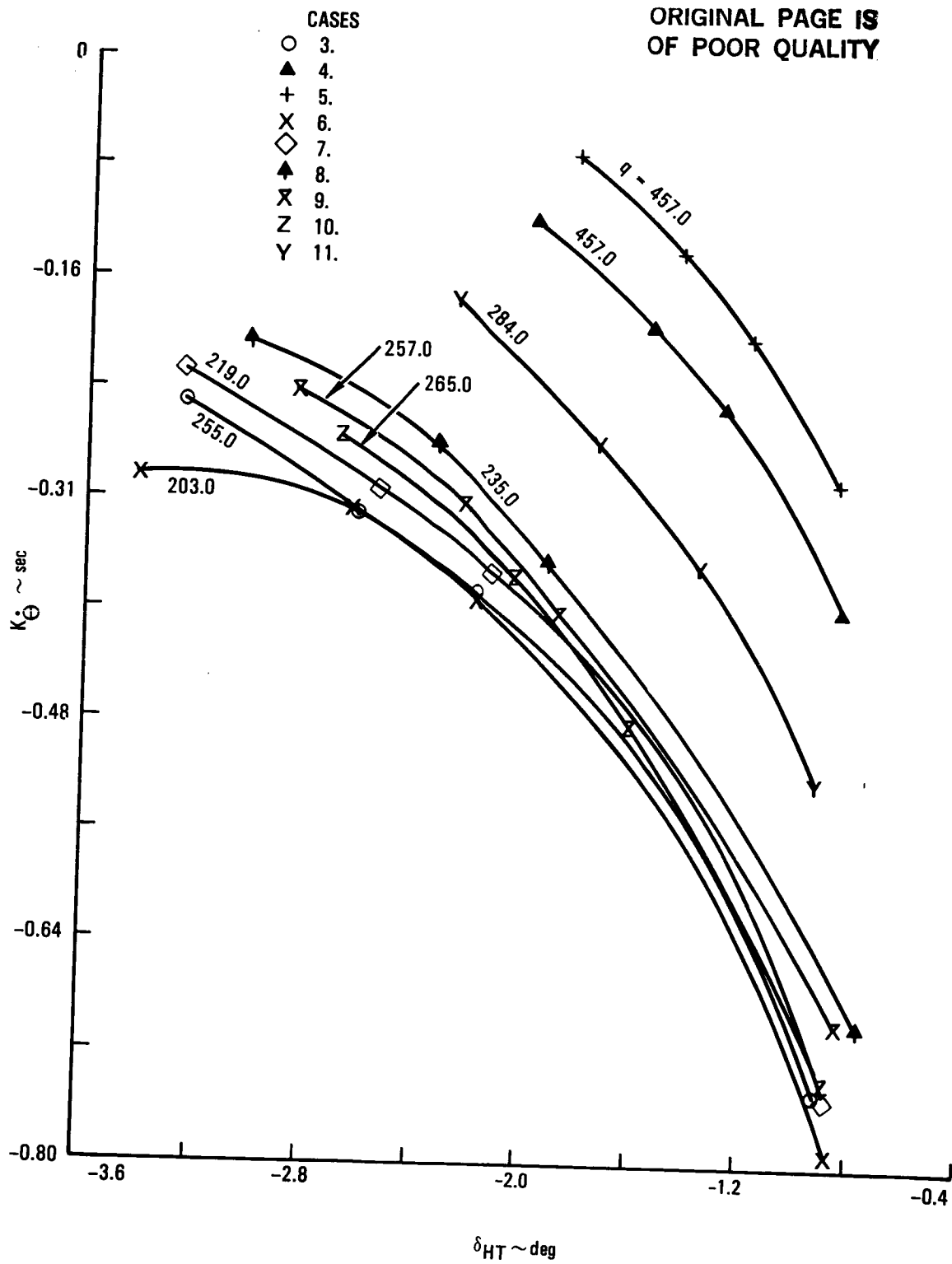


Figure 12. - Plots of compensated pitch rate feedback gains, flap-up conditions.

ORIGINAL PAGE IS
OF POOR QUALITY

TABLE 5. - δ_{HT} and q TRIM CONDITIONS FOR EACH FLIGHT CASE

FLIGHT CASE NUMBER	$\delta_{HT} \sim \text{deg}$	q $\sim \text{lbs/ft}^2$
1A	-8.35	71.2
1B	-7.15	
1C	-5.39	
1D	-4.07	
2A	-8.85	51.2
2B	-6.42	
2C	-3.85	
2D	-1.63	
3B	-3.26	255.0
3C	-2.63	
3D	-2.19	
3E	-0.92	
4B	-1.99	457.0
4C	-1.56	
4D	-1.30	
4E	-0.85	
5B	-1.85	457.0
5C	-1.46	
5D	-1.20	
5E	-0.88	
6B	-3.42	203.0
6C	-2.65	
6D	-2.19	
6E	-0.87	
7B	-3.28	219.0
7C	-2.55	
7D	-2.12	
7E	-0.88	
8B	-3.03	235.0
8C	-2.34	
8D	-1.93	
8E	-0.77	
9B	-2.86	257.0
9C	-2.24	
9D	-1.88	
9E	-0.85	
10B	-2.70	265.0
10C	-2.05	
10D	-1.63	
10E	-0.89	
11B	-2.28	284.0
11C	-1.76	
11D	-1.38	
11E	-0.94	
12A	-7.99	75.2
12B	-6.39	
12C	-4.35	
12D	-2.94	
13A	-8.26	68.3
13B	-6.37	
13C	-4.23	
13D	-2.47	
14A	-8.74	55.5
14B	-6.37	
14C	-4.23	
14D	-2.47	

of scheduling K_u and K_θ a new set of gains in terms of K_3 , τ_1 , and τ_2 (see Appendix D) were selected for scheduling. Thus the revised set of compensated feedback gains to be scheduled was

$$K_\theta, K_{Nz}, 1/\tau_2, \frac{\tau_2}{\tau_1} - 1, \text{ and } K_3 \frac{\tau_1}{\tau_2} .$$

3.2.4 Feed-Forward Loop Synthesis. - The feed-forward loop synthesis considered the feedback and feed-forward loops (Figure 9) to be closed. The control equation is now written as:

$$\{\dot{x}\} = ([A] + [B][F][C])\{x\} + [B][D]\{w\} \quad (\text{Eq. 5})$$

This equation was solved by the method given in Appendix E to obtain a transfer function of Nz/δ_H which was combined with the feel spring characteristics shown in Figure 8. The resulting feed-forward gains (K_{FF}) are plotted in Figure 13.

3.2.5 Primary Gain Scheduling. - The primary gain scheduling was accomplished in the same way for the feedback and feed-forward gains. A curve fitting procedure (Appendix F) was used to express the gain curves (e.g. Figures 12 and 13) in terms of a second degree polynomial as given by equation 6.

$$K = a + bq + cq^2 + d\delta_{HT} + e\delta_{HT}^2 \quad (\text{Eq. 6})$$

A least squares curve fit computer program used the q and δ_{HT} values in Table 5 to determine the equation coefficients which are given in Table 6. The q and δ_{HT} values are provided by the aero data as shown in Figure 8. Plots of the feedback pitch rate and the feed-forward scheduled gains for the flap-up conditions are shown in Figures 14 and 15, respectively. These gains are applicable to the complete flap-up flight envelope.

3.2.6 Secondary Gain Scheduling. - Secondary gain scheduling is required to compensate for:

- Pitch up at high-Mach/high-g flight conditions
- Outboard aileron symmetric activity when the AACS is activated.

ORIGINAL PAGE IS
OF POOR QUALITY

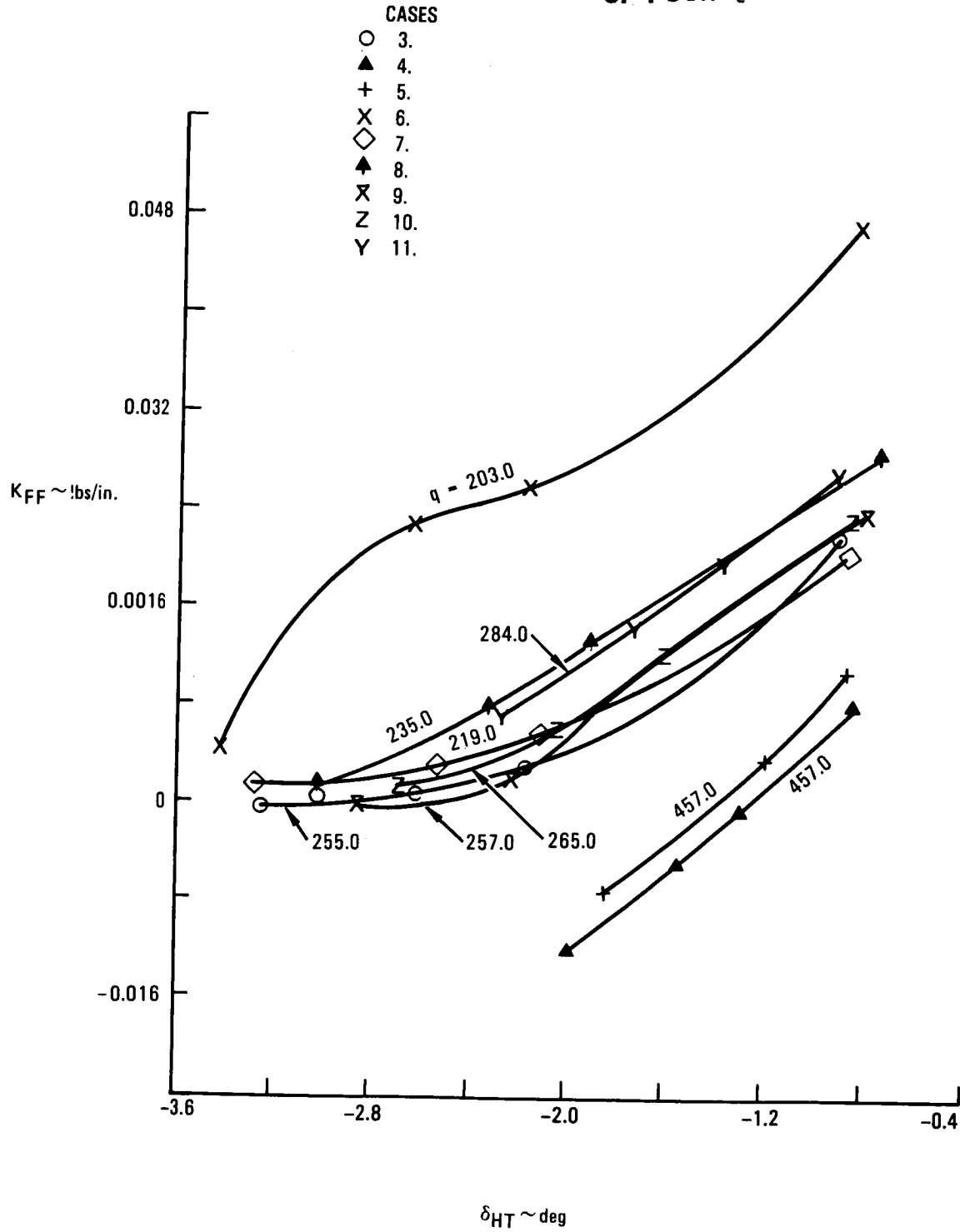


Figure 13. - Plots of feed-forward gains flaps-up conditions.

TABLE 6. - PACS GAIN SCHEDULE EQUATION COEFFICIENTS

FLAP SETTING	COEF.	$K_{\dot{\theta}} \sim \text{sec}$	$K_{N_Z} \sim \text{deg/g}$	$1/\tau_2 \cdot \text{sec}^{-1}$	$\tau_2/\tau_1 - 1$	$K_3 \tau_1/\tau_2$	$K_{FF} \sim \text{in/lb}$
FLAPS-UP	a	-1.4295	9.7718	2.2322×10^{-2}	-2.9433×10	-1.4028×10^{-1}	2.1328×10^{-2}
	b	1.5023×10^{-3}	8.96×10^{-3}	-2.8474×10^{-5}	2.9511×10^{-1}	1.5431×10^{-4}	2.0571×10^{-4}
	c	0	0	0	-4.1698×10^{-4}	0	-4.0915×10^{-7}
	d	-5.0386×10^{-1}	4.5098	0	4.2547	-4.2834×10^{-2}	2.6975×10^{-2}
	e	-7.6620×10^{-2}	6.0459×10^{-1}	0	0	-7.4588×10^{-3}	3.8428×10^{-3}
FLAPS DOWN	a	-3.6149	36.2224	8.7222×10^{-2}	-1.5771	-1.0483	3.2829×10^{-1}
	b	1.1658×10^{-2}	9.9013×10^{-2}	-4.7143×10^{-4}	1.8067×10^{-1}	4.0909×10^{-3}	2.4014×10^{-3}
	c	0	0	0	-1.4232×10^{-3}	0	-3.5719×10^{-5}
	d	-6.0629×10^{-1}	7.0302	0	3.4827×10^{-1}	-1.5772×10^{-1}	6.8201×10^{-2}
	e	-3.9313×10^{-2}	4.3358×10^{-1}	0	0	-9.7027×10^{-3}	4.0296×10^{-3}

$$K = a + bq + cq^2 + d \delta_{HT} + e \delta_{HT}^2$$

The pitch-up phenomena is caused by a loss of lift at the wing tips during high-Mach/high-g flight conditions which causes the aerodynamic center of pressure (c.p.) to shift forward. Thus, the distance between the c.g. and the c.p. is shortened, and the static stability margin is reduced in a manner similar to when the c.g. is moved aft relative to a fixed c.p. Consequently, the scheduled gain curves already developed can be used to stabilize the pitch-up conditions. The feedback and feed-forward gain values are changed by augmenting the gain scheduling δ_{HT} value by a required increment to provide a δ_{HT}^* value (Appendix G). The modified value δ_{HT}^* changes the feedback gains to provide the increased control command for the horizontal stabilizer, and changes the feed-forward gains to provide the desired column force gradients. If the feed-forward gains were not provided, the column force gradients would be incorrect and might encounter severe reversals.

The AACS operates the outboard ailerons in a symmetric mode in response to normal acceleration of the aircraft c.g. and wing tips. This symmetric mode produces a c.p. shift that is equivalent to an aft c.g. shift of about 5 percent mac. The change in pitching moment can be corrected in the same manner as for the pitch-up by providing the primary gain-scheduling signal δ_{HT} with an augmented increment.

ORIGINAL PAGE IS
OF POOR QUALITY

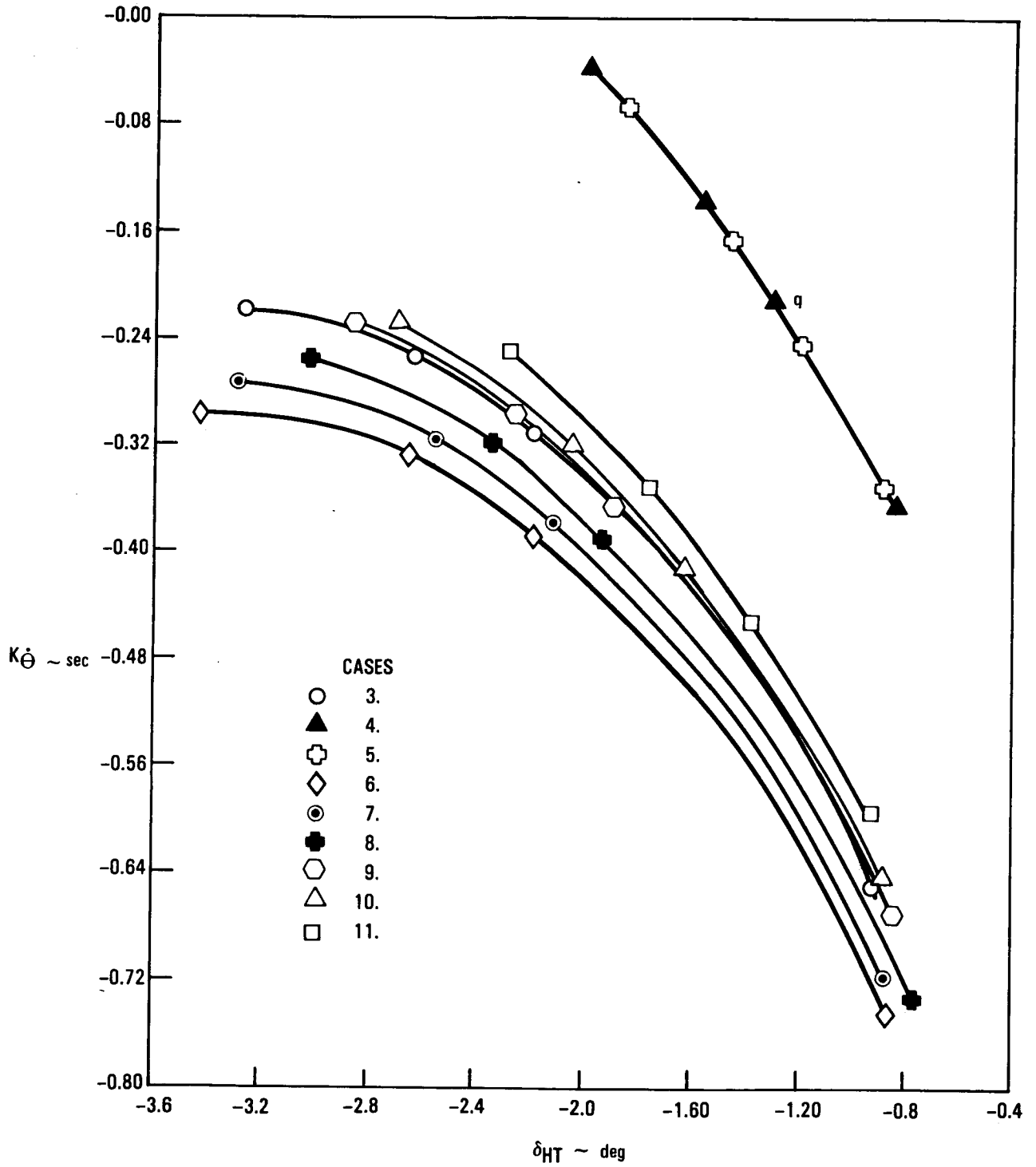


Figure 14. - Scheduled feedback gain curves, flap-up conditions.

ORIGINAL PAGE IS
OF POOR QUALITY

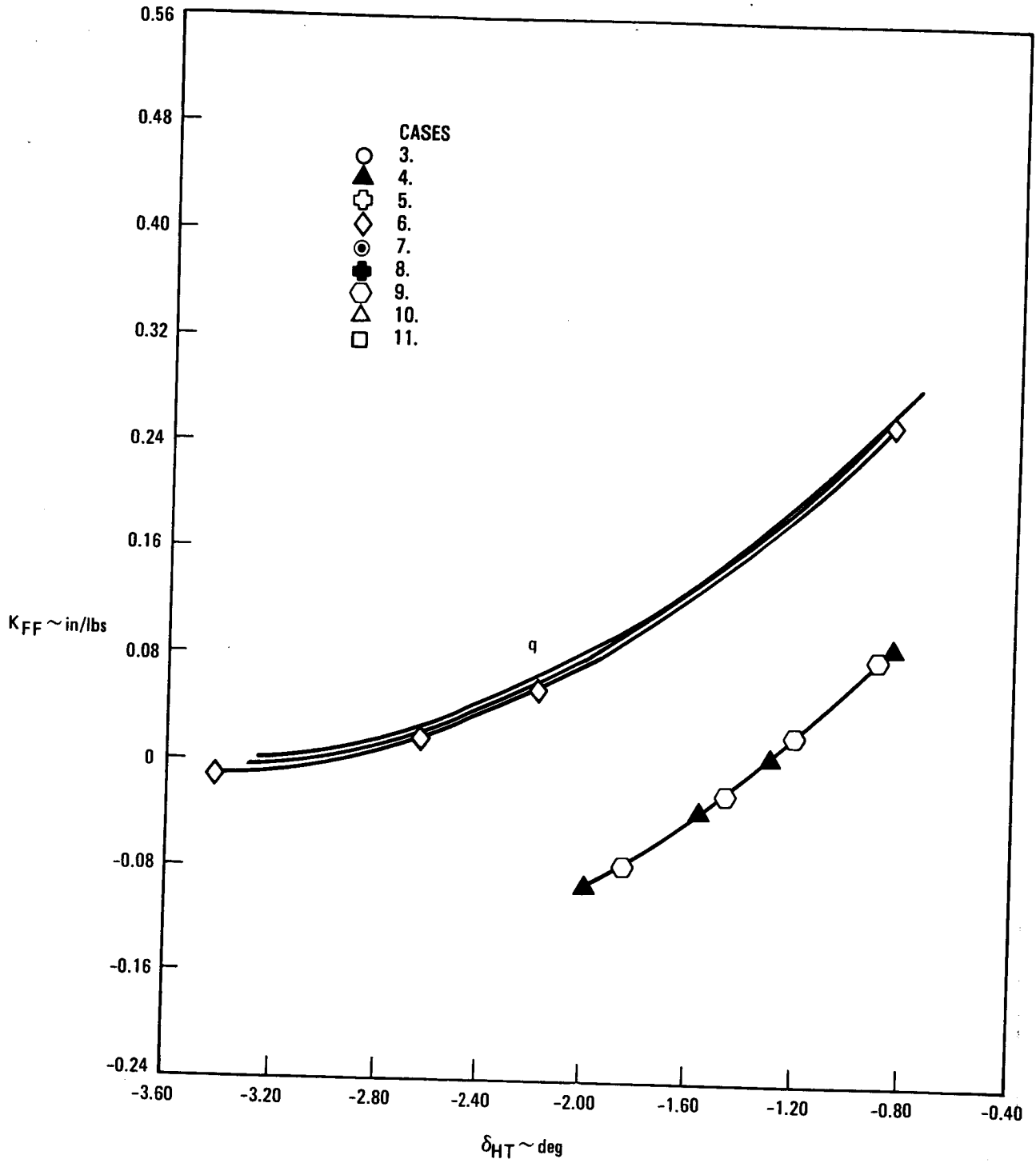


Figure 15. - Scheduled feed-forward gain curves, flap-up conditions.

The secondary gain scheduling method is discussed in Appendix G. The sensor signals required for secondary gain scheduling are angle of attack (α), aircraft bank angle (ϕ), and Mach number (M), as shown in Figure 1.

3.3 Control Law Mechanization

The advanced PACS block diagram is shown in Figure 16. This diagram is considered to be divided into three parts for discussion:

- Control Column and actuator system: control column, column trim, series servos, J curve, stabilizer trim, and power actuator.
- Feedback loops: pitch rate ($\dot{\theta}$), normal acceleration (N_Z), and pitch attitude (θ).
- Feed-forward loop: column force (F_C).

3.3.1 Control Column and Actuator System. - The control column displacement (X_C) and column trim (X_T) are summed along with the series servo outputs (X_S). The nonlinearizer represented by the J curve (J) changes the linear displacements into stabilizer rotations which are dependent upon the trim condition. In the model (Figure 16) stabilizer trim (δ_{HT}) is subtracted and leaves the linear signal (δ_{HC}) to command the power actuator which rotates the horizontal stabilizer.

The column trim consists of the parallel trim which relieves the force on the control column and the series trim which places the control column at the desired location. The parallel trim and series trim are set simultaneously by a trim wheel (mechanical trim cable) as shown in Figure 3 or by a motor controlled by an electrical pitch feel and trim switch located on the control column.

The input to the series servos is an electric signal (X_A) from the summed feed-forward and feedback loops. The transfer function $1/(\tau_S s + 1)$ in each servo block represents the servo lag characteristics. The output of the series servos are position summed so that the control authority of each series servo is 0.75 degree at the cruise trim setting of -1 degree. This provides a maximum position summed output of 1.5 degree at the cruise trim setting. The series servos were position summed so that failure of one servo would not provide a stabilizer hardover which results in loads greater than the aircraft limit loads.

The power actuator lag characteristics are presented by $1/(\tau_P s + 1)$ as shown in the figure.

3.3.2 Feedback Loops. - The $\dot{\theta}$ and N_Z feedback signals are used for control of the short-period modes. These signals are filtered through the first-order low-pass filters shown in Figure 16. The filter time constants $\tau_{\dot{\theta}}$ and τ_Z are equal to 0.03 seconds. The filter time constants $\tau_{\dot{\theta}}$ and τ_Z are equal to .03 seconds. The filtered signals $\dot{\theta}_F$ and N_{ZF} are subject to gains of $K_{\dot{\theta}}$ and K_{N_Z}

respectively. The gain scheduling parameters q and δ_{HT}^* are provided to set the desired gain values. A normalizing constant $1/K_C$ is used in each feedback loop so that the gain from the gain schedules through the J curves for a δ_{HT} setting of -10 degrees is equal to 1. The value of K_C is 2.5 degrees stabilizer per inch of column.

The θ feedback signal is used to control the phugoid mode. This signal is processed through a pitch synchronizer, a lag-lead circuit, and a gain amplifier. The pitch synchronizer suppresses the attitude hold during maneuvers and sets a new attitude reference at the synchronizer output when a control column force is applied (see Appendix H). The lag-lead circuit eliminates the need for a velocity gain sensor (Appendix D) that would be required for phugoid mode control. The gains to be scheduled are (see Table 6):

$$\frac{1}{\tau_2}, \left(\frac{\tau_2}{\tau_1} - 1 \right), \text{ and } K_3 \frac{\tau_1}{\tau_2}$$

3.3.3 Feed-Forward Loop. - The feed-forward loop is used to provide the desired control column feed-forward gradients. The feel spring converts the column displacement (X_C) to pounds (F_C). The force sensor converts F_C to an electric voltage. A flaps-up/flaps-down bias signal switches the time constant of the feed-forward low pass filter which is related to the reference baseline aircraft short-period mode. It provides the frequency variant part of the feed-forward transfer function (see Appendix E). The feed-forward signal is then passed through the gain amplifier (K_{FF}) and summed with the feedback signals to provide the series servo input signal (X_A).

3.4 Control Law Analysis

Thirteen of the flight cases that were used for control law synthesis were selected for stability margin analysis. These were representative of all of the cases and included those that were expected to have the least gain or phase margins. All closed loop poles of fifty six flight cases were checked.

3.4.1 Poles and Zeros. - The short period mode, phugoid mode, and controller characteristics for each of the 13 selected cases are shown in Tables 7, 8, and 9 respectively. The nomenclature for the Tables are shown in Figure 17. Each Table shows the flight case number, specifies the control condition as open loop (OL) or closed loop (CL), and gives the poles and zeros. Table 9 also lists the open loop gain factor (K).

TABLE 7. - SHORT PERIOD FREQUENCY CHARACTERISTICS

Flight Case Number	Control Cond.	Poles			Zeros		
		ω_n	ζ	$1/\tau$	ω_n	ζ	$1/\tau$
1b	OL	0.853	0.538				0.615
	CL	1.18	0.695				
1d	OL	0.719	0.655				1.06
	CL	1.27	0.700				
4b	OL	2.03	0.589		7.76	-0.198	2.99
	CL	1.84	0.847				
4d	OL	1.41	0.881				
	CL	2.09	0.705				
4e	OL			2.51 -0.134			
	CL	2.18	0.641				
7b	OL	1.40	0.37		0.296	0.482	1.17
	CL	1.64	0.682				
7d	OL	0.960	0.571				
	CL	1.48	0.641				
7e	OL			1.44 0.0515			
	CL	1.40	0.691				
10b	OL	1.57	0.454		.337	.354	2.09
	CL	1.80	0.626				
10d	OL	0.972	0.764				
	CL	1.79	0.616				
10e	OL			1.73 0.0760			
	CL	1.78	0.613				
13b	OL	0.901	0.613				0.973
	CL	1.30	0.679				
13d	OL	0.687	0.828				1.54
	CL	1.49	0.684				

TABLE 8. - PHUGOID FREQUENCY CHARACTERISTICS

Flight Case Number	Control Cond.	Poles			Zeros		
		ω_n	ζ	$1/\tau$	ω_n	ζ	$1/\tau$
1b	OL	0.143	0.040		0.155	0.716	
	CL	0.148	0.303				
1d	OL	0.113	0.054		0.149	0.514	
	CL	0.141	0.368				
4b	OL	0.0416	0.066				-0.0873 +0.0466
	CL	0.0648	0.176				
4d	OL			-0.0328 0.0414	0.0774	0.377	
	CL	0.0483	0.336				
4e	OL	0.182	0.604		0.0652	0.300	
	CL	0.0415	0.476				
7b	OL	0.0679	0.188				0.0221 0.0330
	CL	0.0734	0.358				
7d	OL	0.0771	0.156		0.0819	0.455	
	CL	0.0801	0.308				
7e	OL			-0.0731 -0.233	0.0748	0.284	
	CL	0.0881	0.289				
10b	OL	0.0668	0.136				0.0206 0.136
	CL	0.0877	0.245				
10d	OL	0.0839	0.090		0.0916	0.315	
	CL	0.0898	0.240				
10e	OL	0.146	-0.876		0.0830	0.257	
	CL	0.0942	0.246				
13b	OL	0.150	0.060		0.161	0.650	
	CL	0.153	0.344				
13d	OL	0.0990	0.123		0.161	0.480	
	CL	0.153	0.405				

TABLE 9. - CONTROLLER FREQUENCY CHARACTERISTICS

Flight Case Number	Control Cond.	Gain	Poles 1/τ				Zeros 1/τ		
			Power Servo	Series Servo	Sensors	Compensator Poles	Power Servo	Series Servo/Sensor	Compensator Zeros
1b	OL	49.7	6.23	20.1	33.0	0.0537		55.9	0.0611
	CL		5.04	20.5	32.9	0.0556			
1d	OL	287	6.23	20.1	33.0	0.0537	12.3		0.0635
	CL		5.39	19.5	33.5	0.0602			
4b	OL	-82.0	6.23	20.1	33.0	0.00920			0.00830
	CL		5.11	20.7	32.7	0.00886			
4d	OL	95.1	6.23	20.1	33.0	0.00920		28.5	0.00826
	CL		5.50	20.3	33.0	0.00795			
4e	OL	300	6.23	20.1	33.0	0.00920	5.30	11.5	0.00848
	CL		6.07	19.5	33.5	0.00726			
7b	OL	-35.6	6.23	20.1	33.0	0.0161		-77.1	
	CL		4.68	21.0	32.6	0.0167			
7d	OL	80.2	6.23	20.1	33.0	0.0161		39.6	0.0205
	CL		5.01	20.5	33.0	0.0183			
7e	OL	313	6.23	20.1	33.0	0.0161	12.3		0.0217
	CL		5.50	19.5	33.5	0.0212			
10b	OL	-24.2	6.23	20.1	33.0	0.0148		-97.3	
	CL		4.86	20.9	32.7	0.0171			
10d	OL	131	6.23	20.1	33.0	0.0148		26.9	0.0196
	CL		5.18	20.3	33.1	0.0180			
10e	OL	317	6.23	20.1	33.0	0.0148	3.15	13.2	0.0192
	CL		5.57	19.5	33.5	0.0187			
13b	OL	61.8	6.23	20.1	33.0	0.0550		48.0	0.0605
	CL		5.07	20.4	33.0	0.0550			
13d	OL	335	6.23	20.1	33.0	0.0550		11.9	0.0583
	CL		5.35	19.4	33.6	0.0579			

CHARACTERISTICS OF
OF POOR QUALITY

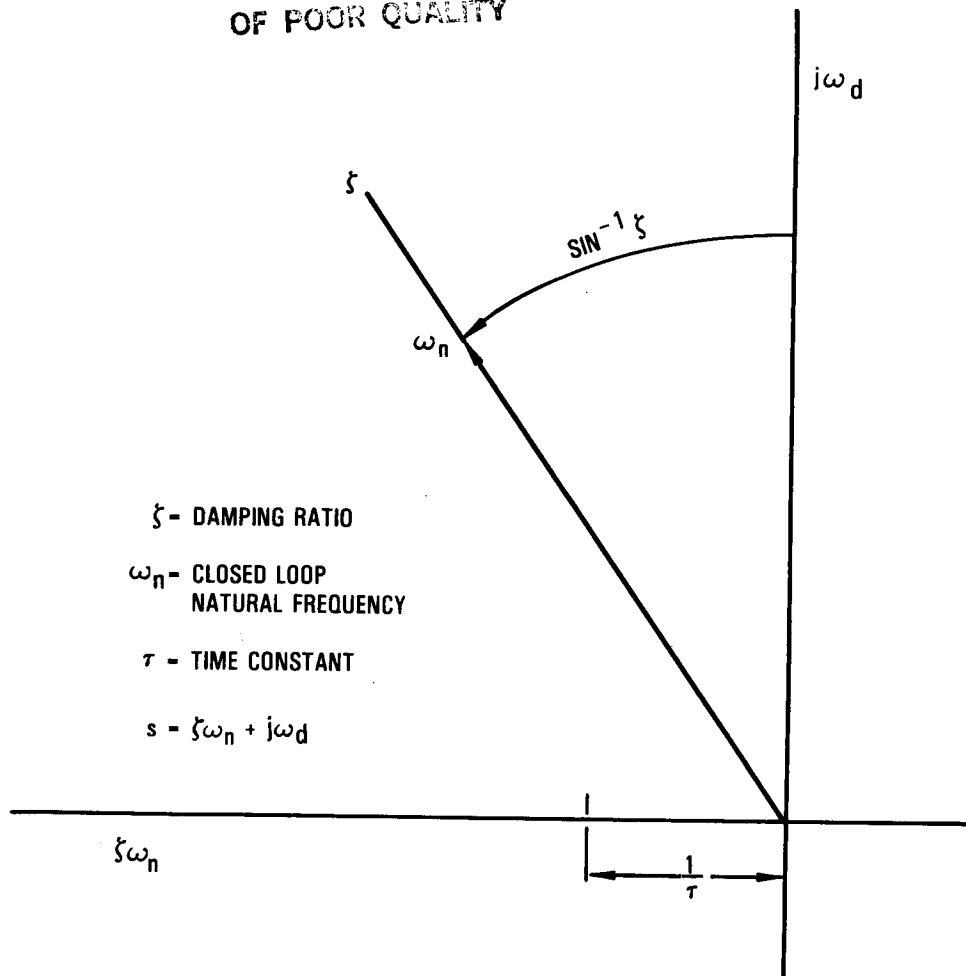


Figure 17. - s - plane nomenclature for poles and zeros tables.

The open loop transfer function is:

$$(F_T)_{OL} = K \frac{N(s)}{D(s)} \quad (\text{Eq. 7})$$

The value of the numerator $N(s)$ for each case is the product of terms corresponding to the zero values in the frequency ranges of the short period mode, phugoid mode, and controller as given in Tables 7, 8, and 9 respectively. The value of the denominator $D(s)$ is the product of terms corresponding to the pole values.

Any pole on the positive real axis or complex pair of poles that fall in the right-hand side of the s plane (Figure 17) represents an unstable mode. Poles shown in Tables 7, 8, and 9 that fall in the right-hand plane represent the open loop cases listed in Table 10. Identification of these poles is necessary for evaluation of the Nyquist plots which will be subsequently discussed.

All of the closed-loop poles are in the left-hand plane. Most of the poles comply with the design objectives of Figure 5. The few closed-loop poles that fall outside the prescribed boundaries (see Figure 10) were judged to be acceptable for continuing with piloted flight simulation tests.

3.4.2 Nyquist Plots. - Nyquist plots were used to evaluate the gain and phase margins of the PACS. The plots that were selected for illustration are shown in Figure 18. These plots represent a locus of gain-phase points (G, ϕ) as the circular frequency (ω) varies from negative to positive infinity. Only the half of the locus from zero to infinity is shown. Since the points are complex conjugate pairs, the other half of the locus is the mirror image with respect to the horizontal axis. The closed loop system is stable if and only if the number of counterclockwise encirclements of the locus about the -1 point of the plot is equal to the number of open loop poles in the right-hand plane.

Plots a and b in Figure 18 for flight cases 1d and 4b, respectively, represent stable closed-loop systems where there are no open-loop poles in the right-hand plane and no encirclements of the -1 point. If the gain in plot b were increased by a factor of 3 (9.5 dB) or if the phase had an additional lag greater than 22 degrees there would be a clockwise encirclement of the -1 point. This means that for this system the gain margin is 9.5 dB and the phase margin is 22 degrees.

In plots c and d for flight cases 4d and 4e, respectively, the locus makes one counterclockwise encirclement of the -1 point. Consequently, these closed-loop systems are stable because the open-loop systems have a

TABLE 10. - OPEN LOOP CASE POLES IN THE RIGHT-HAND SIDE OF THE s PLANE

FLIGHT CASE	SHORT-PERIOD MODE ~ sec ⁻¹	PHUGOID MODE ~ sec ⁻¹
4e	- 0.134	- 0.0328 - 0.0731, -0.233 0.146 / sin ⁻¹ (-0.876)*
4d		
7e		
10e		

*TWO COMPLEX POLES SYMMETRIC WITH RESPECT TO REAL AXIS.

CRITICAL POINTS OF POOR QUALITY

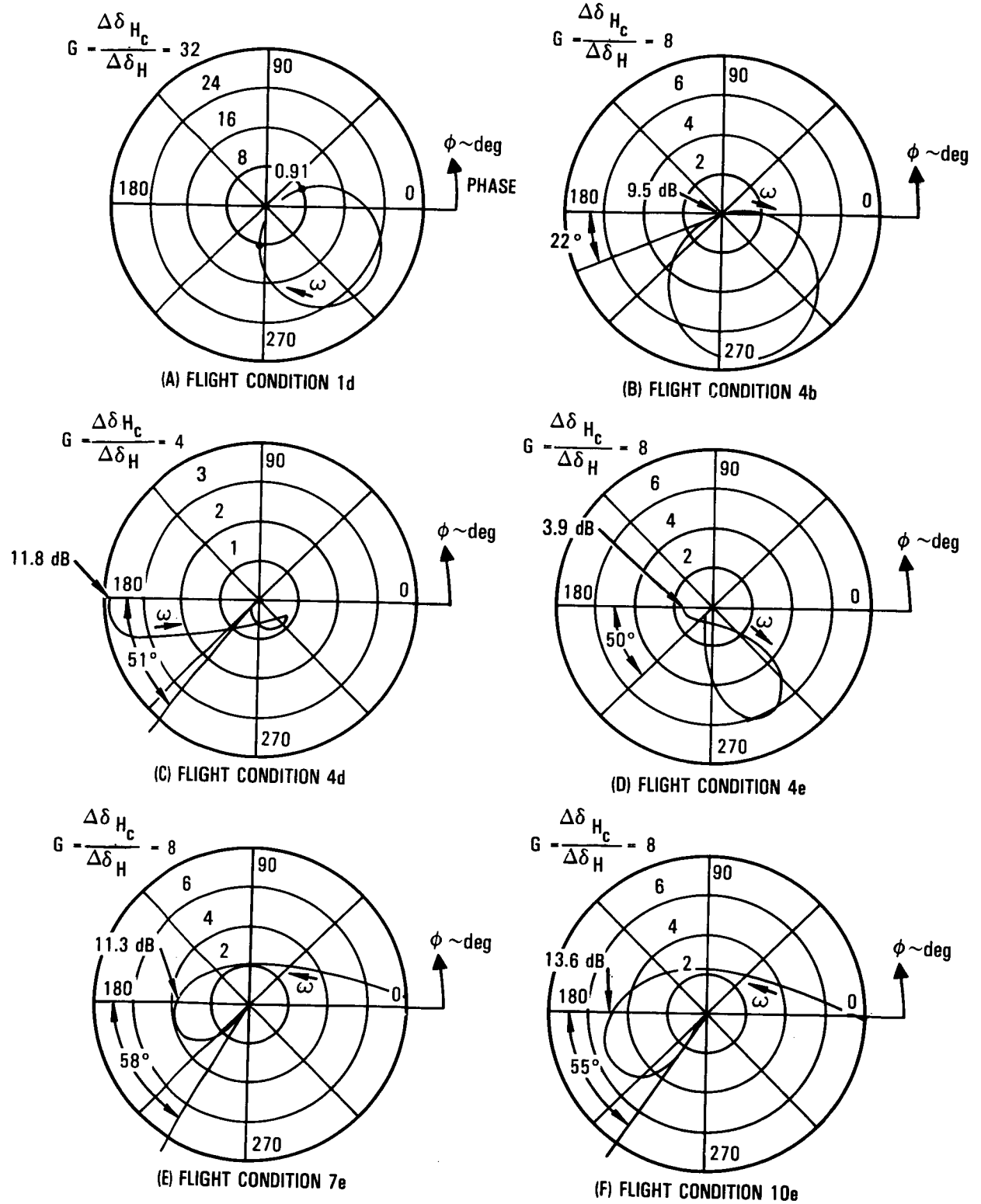


Figure 18. - Nyquist plots.

**ORIGINAL PAGE IS
OF POOR QUALITY**

pole in the right-hand plane as listed in Table 10. The phase and gain margins for these cases were determined to be:

	<u>Gain Margin</u>	<u>Phase Margin</u>
Case 4d	-11.8 dB	51 deg
Case 4e	-3.9 dB	50 deg

Plots e and f for flight cases 7e and 10e, respectively, have two counter-clock encirclements of the -1 point (the one shown and one for the mirror image). This closed-loop system is stable because there are two open-loop poles in the right-hand s plane as listed in Table 10. The phase and gain margins for these cases were determined to be:

	<u>Gain Margin</u>	<u>Phase Margin</u>
Case 7e	-11.3 dB	58 deg
Case 10e	-13.6 dB	55 deg

3.4.3 Feel-Force Gradients. - The baseline aircraft configuration maneuver (wind-up turn) column-force gradients are shown for flight conditions 6, 7, 9, and 11 in Figure 19a through d respectively. These curves are typical of the column-force gradients for the other flight conditions and show how the gradients change significantly with c.g. location and are highly dependent on load factor. The force gradients decrease as the c.g. moves aft because of increased control sensitivity. The gradient for each flight condition is shown to be negative for the 50% mac c.g. location. This negative gradient is unacceptable and indicates the need for a PACS. Flight condition 7 was selected to illustrate comparison of six experimental PACS configurations that are listed in Table 11. Figure 19b represents the PACS configuration 1, flight condition 7, column forces.

The full gain PACS (configuration 2) provides a maneuver (wind-up turn) column-force gradient that is nearly independent of the c.g. location and load factor. The column gradients for this configuration are shown in Figure 20. The curves shown in the figure satisfy the column-force gradient objectives and are representative of the other flight conditions.

The partial gain PACS (configuration 3) demonstrates the importance of bank angle gains on column-force gradients. The bank angle gain scheduling component is shown in Appendix G to be $C_{\delta} \delta_{HT}^2 (1 - \cos \theta)$. The optimum C_{δ} was determined to be 0.05 and this value was used for the full gain PACS. The partial gain case has no bank angle gain ($C_{\delta} = 0$). The force gradients for this configuration are shown in Figure 21. A comparison of the curves in Figure 21 with the desired force gradient curves in Figure 20 show the effect of deleting the bank angle from the secondary gain scheduling.

ORIGINAL PAPER
OF POOR QUALITY

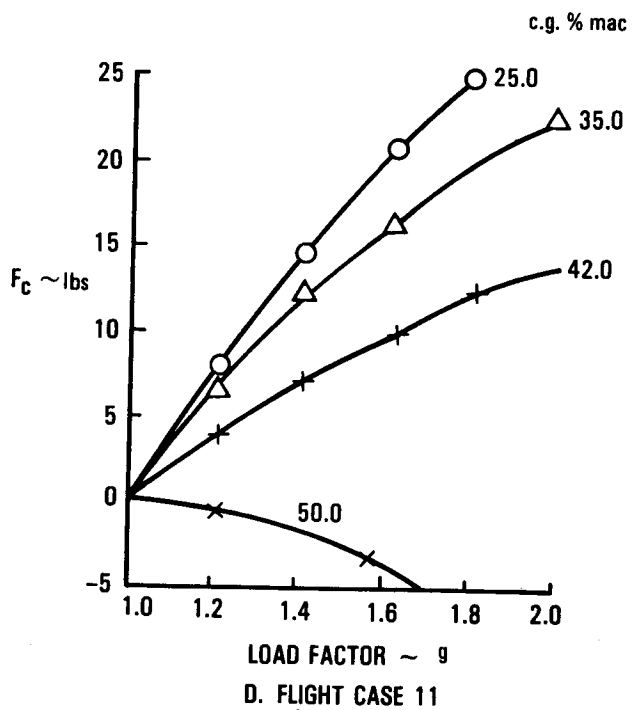
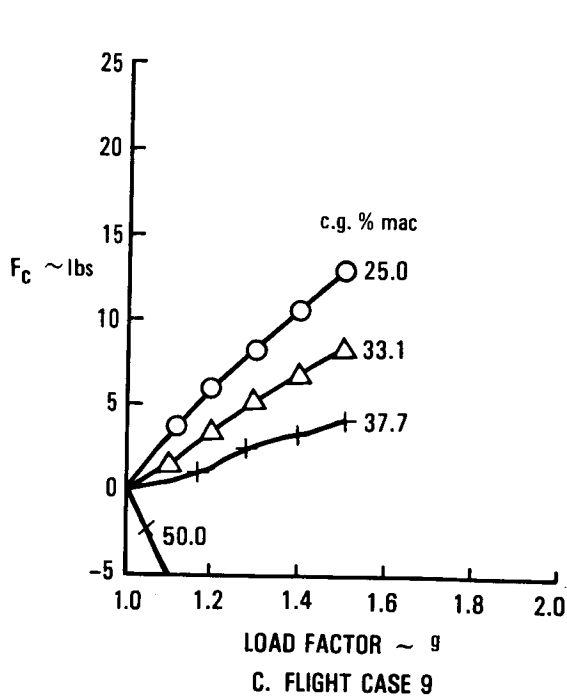
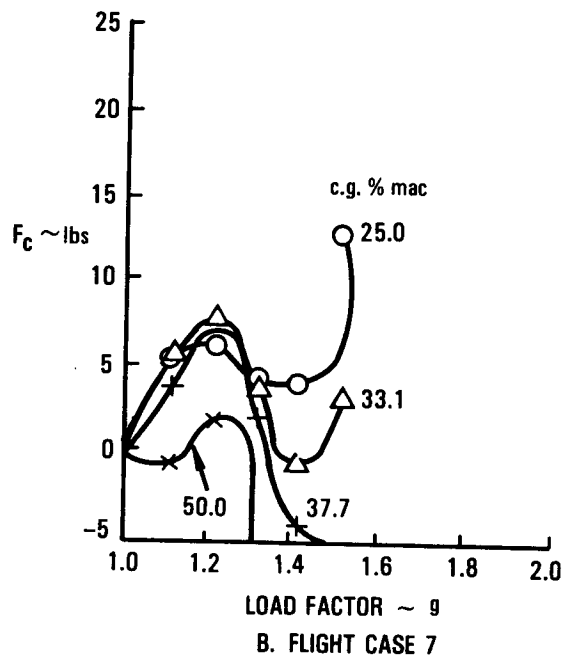
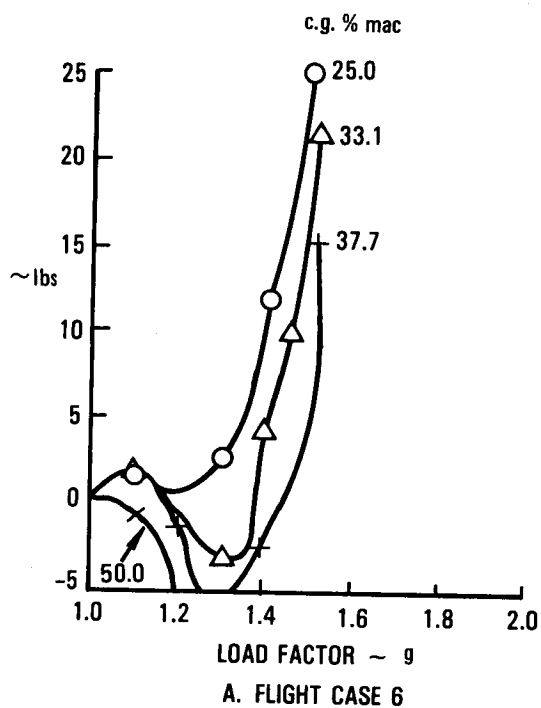


Figure 19. - Open loop column force in turns.

TABLE 11. - PACS FEEL-FORCE CONFIGURATION EVALUATED

PACS CONFIGURATION	GAINS	FEEDBACK	FEED-FORWARD	AUGMENTED GAIN SCHEDULE	
				BANK ANGLE	ANGLE OF ATTACK
1. BASELINE AIRCRAFT		$K_{\dot{\theta}}, K_{\theta}, K_u, K_{Nz}$	-	-	-
2. PACS/FULL GAIN		$K_{\dot{\theta}}, K_{\theta}, K_{Nz}$	K_{FF}	K_{ϕ}	K_{α}
3. PACS/PARTIAL GAIN		$K_{\dot{\theta}}, K_{\theta}, K_{Nz}$	K_{FF}	-	K_{α}
4. PACS/NO FEED-FORWARD		$K_{\dot{\theta}}, K_{\theta}, K_{Nz}$	-	-	K_{α}
5. PACS/ONE-g GAIN		$K_{\dot{\theta}}, K_{\theta}, K_{Nz} = \text{CONST}$	$K_{FF} = \text{CONST}$	$K_{\phi} = \text{CONST}$	$K_{\alpha} = \text{CONST}$
6. PACS/QUASI-STEADY GAIN		$K_{\dot{\theta}}, K_{\theta}, K_{Nz} = \text{CONST}$	$K_{FF} = \text{CONST}$	$K_{\phi} = \text{CONST}$	K_{α}

ORIGINAL PAGE IS
OF POOR QUALITY

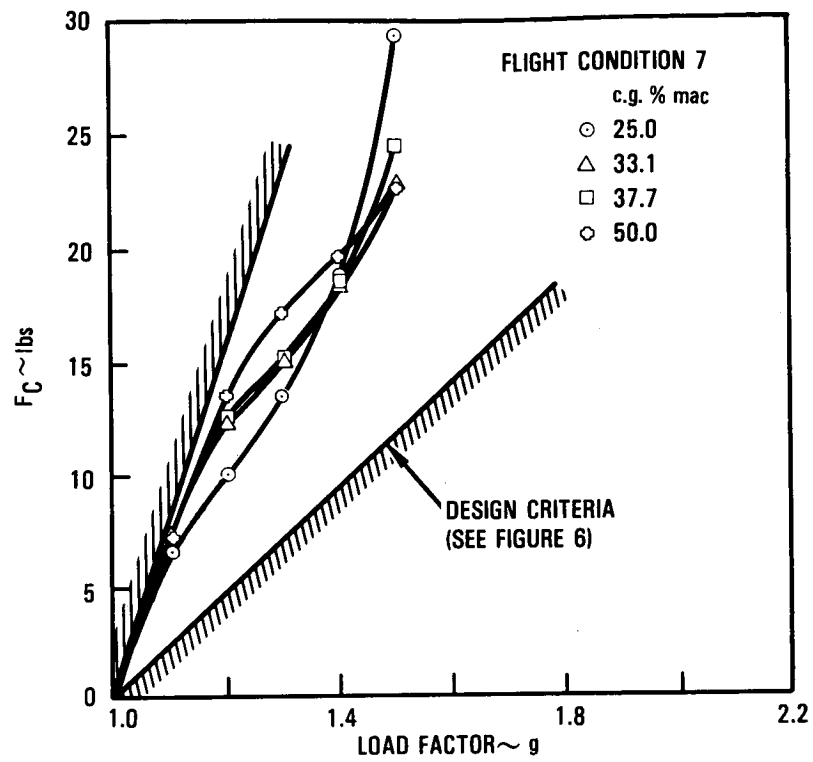


Figure 20. - Full gain PACS, column force gradients.

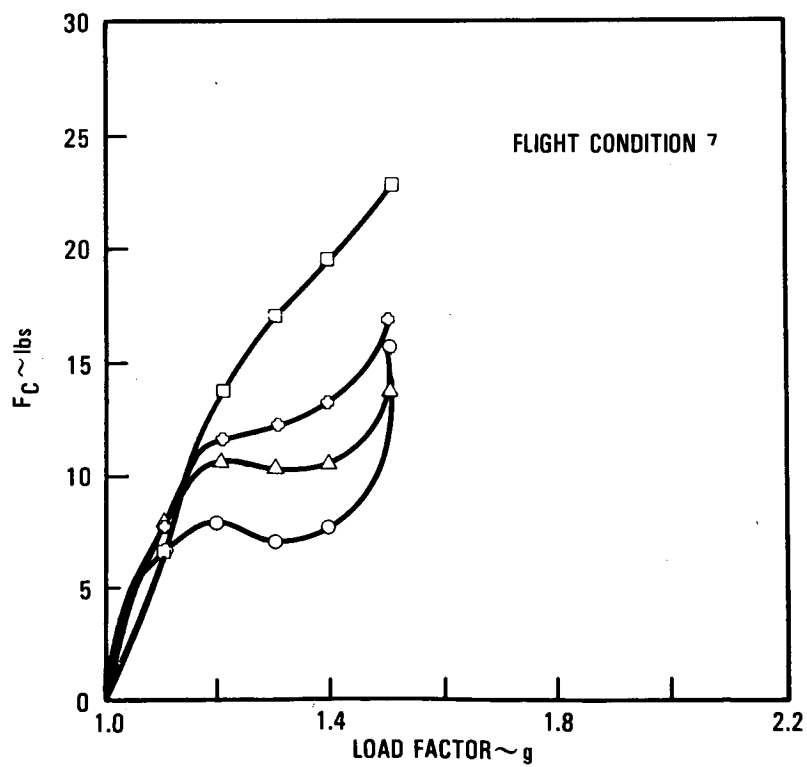


Figure 21. - Partial gain PACS, column force gradients.

For the PACS with feedback but without feed-forward (configuration 4), the column-force gradient increases as the c.g. location is moved aft as shown in Figure 22. This increase is due to excessive cancellation of the stabilizing feedback loop gain signals. A comparison of Figures 22 and 20 show that for the 25% mac c.g. location the PACS without feed-forward provides a column force gradient that is less than desirable. As the c.g. is moved to 38 and 50% mac, the force gradients are greater than desirable.

The one-g gain PACS (configuration 5) has all gains frozen at the maneuver threshold value. This configuration permits undesirable column-force reversals as shown in Figure 23. Comparison of Figures 21 and 23 illustrates a natural benefit that results (with gains not frozen) from the stabilizer deflection commanding nose-up attitude during a turn.

The quasi-steady gain PACS (configuration 6) freezes all gains at the maneuver threshold values except the increment due to the angle-of-attack signal. The column forces for this configuration are shown in Figure 24. There is only a slight improvement over the configuration 5 force gradients and demonstrates that the α signal does not have much effect on column forces. It would have a significant effect if it were added to the $(1-\cos \phi)$ term in the bank angle mechanization.

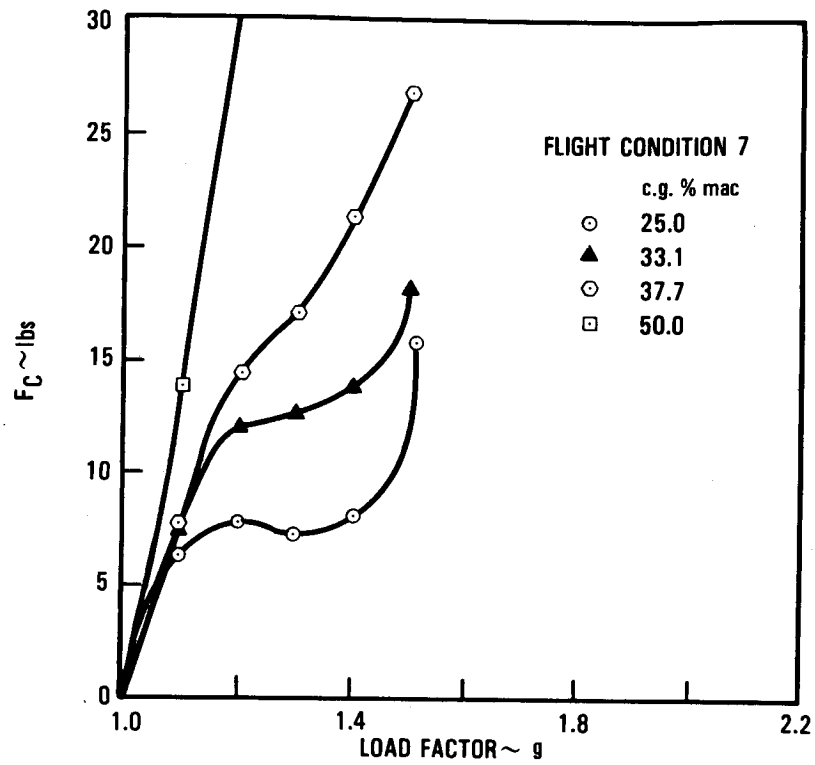


Figure 22. - PACS without feed-forward, column force gradients.

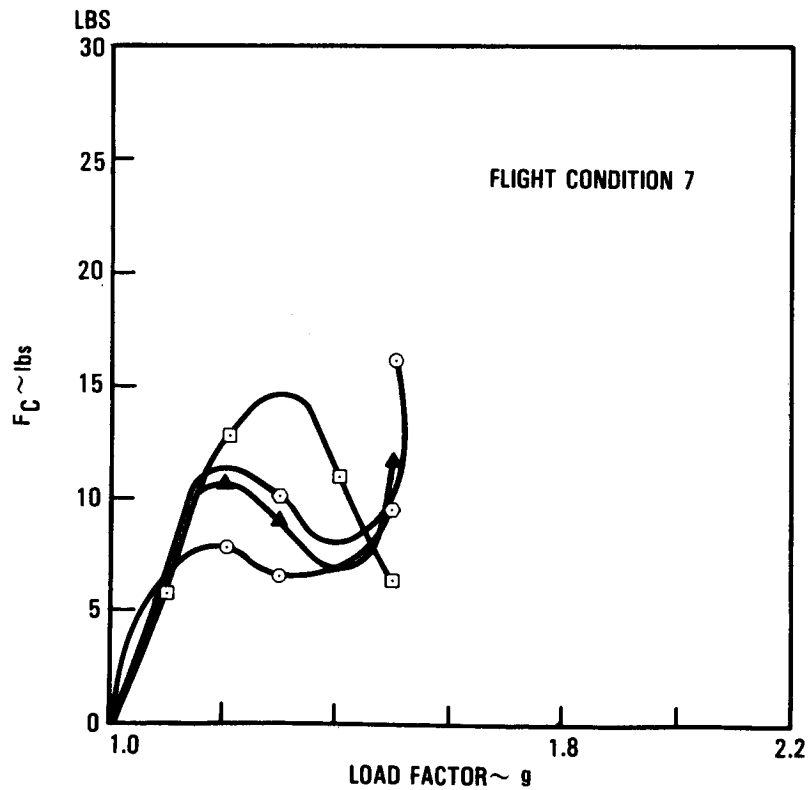


Figure 23. - One-g gain PACS, column force gradients.

ORIGINAL PAGE IS
OF POOR QUALITY

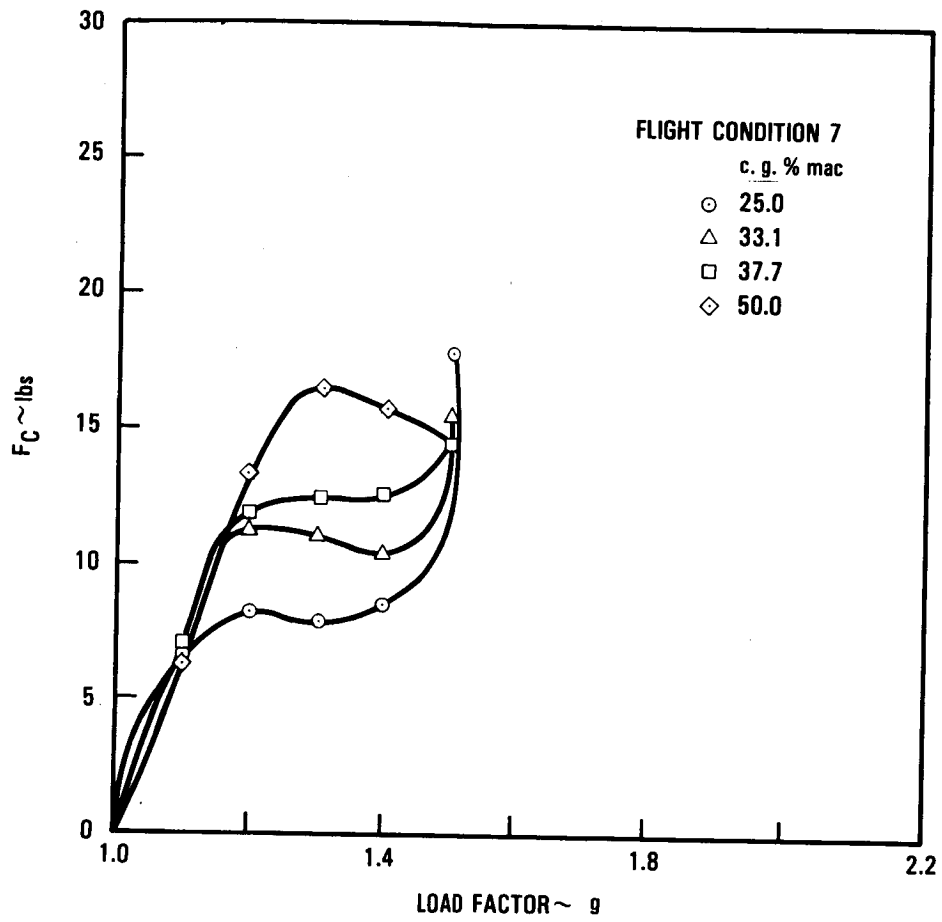


Figure 24. - Quasi-steady PACS column force gradients.

4. ANALYTICAL SIMULATION

Analytical simulation was performed by using a computer program that has been developed over a period of several years. The program is called PICSS (Program for Interactive Continuous System Simulation). Drag, lift, and moment coefficients are input to the program for the clean aircraft configuration as functions of angle of attack and Mach number. These coefficients are incremented by pitch rate and angle-of-attack rate in maneuvering flight, by deflections of the ailerons and stabilizer, and by trim variations due to center of gravity travel. Also, ground effects, gear and flaps, direct lift control, and aerodynamic effects due to structural deflections are included in the program.

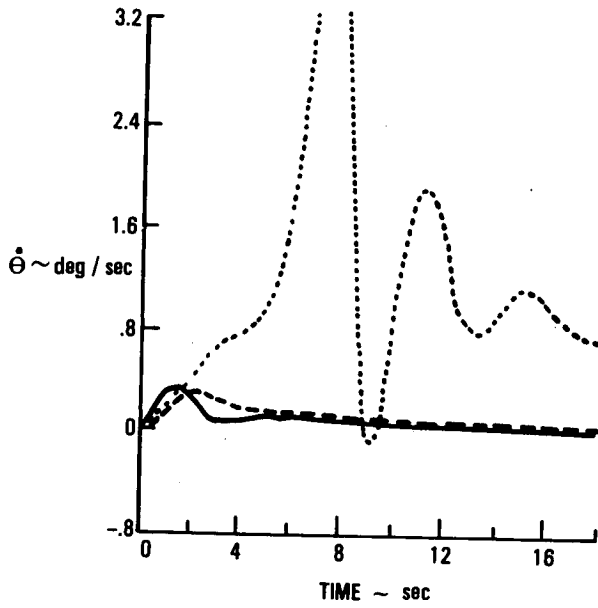
Time history outputs of the program include:

- N_z - Normal acceleration
- M - Mach number
- h - Altitude
- $\Delta\delta_{HT}$ - Incremental trim position of horizontal stabilizer
- δ_H - Horizontal stabilizer position
- α - Angle of attack
- θ - Pitch attitude
- $\dot{\theta}$ - Pitch rate
- θ_ℓ - Lagged component of pitch attitude feedback
- C_m - Pitching moment coefficient
- C_D - Drag coefficient
- C_L - Lift coefficient
- $\Delta C_{L_{AACS}}$ - Incremental lift coefficient due to active AACS
- $\Delta C_{m_{AACS}}$ - Incremental pitching moment coefficient due to active AACS

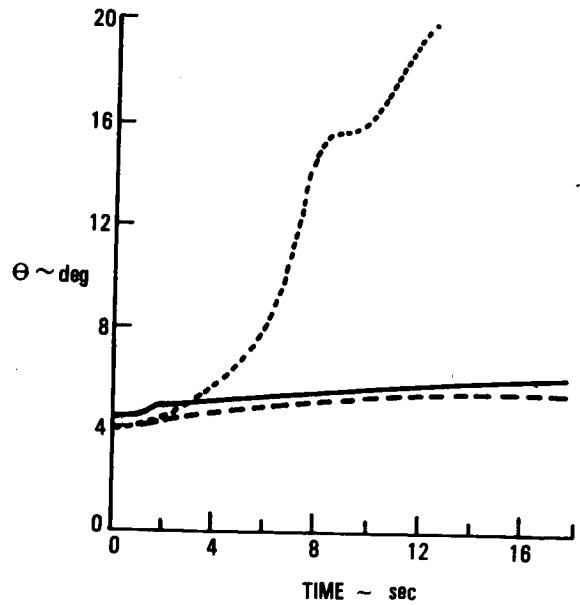
The most significant time history parameters for flight condition 7 are plotted in Figure 25. Pitch rate is shown in part a. The solid line represents the open loop condition with c.g. at 25% mac (case 7b OL). This is the reference case which represents the desired pitch-rate response. The dotted line represents the open loop condition with c.g. at 50% mac (case 7e OL). The pitch-rate amplitude response for this case is unacceptable. The dashed line represents the PACS-on condition with c.g. at 50% mac (case 7e CL). As shown in the figure the closed loop pitch-rate response with c.g. at 50% mac compares

ORIGINAL PAGE IS
OF POOR QUALITY

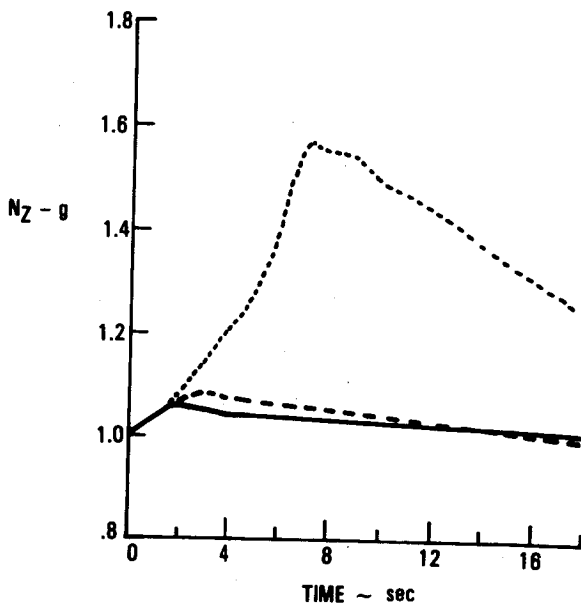
CASE
 — 7b OL
 - - - 7e OL
 - - - 7e CL



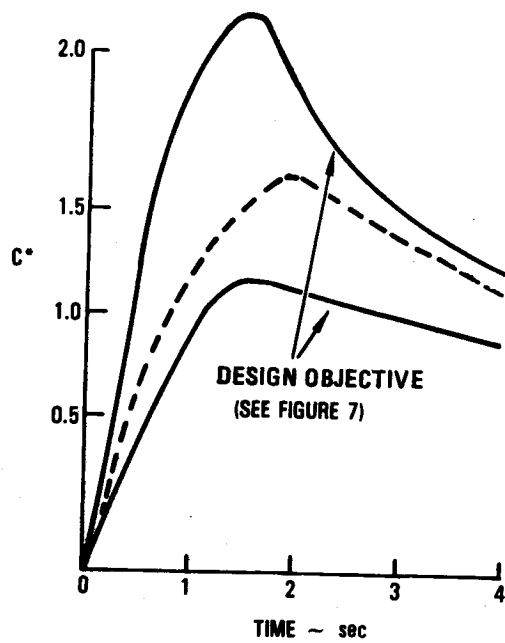
A. PITCH RATE



B. PITCH ATTITUDE



C. NORMAL ACCELERATION



D. $C^* \sim \text{BLENDED } N_z/\Theta$

Figure 25. - Time history plots, flight condition 7.

favorably with the open loop pitch-rate response with c.g. at 25% mac. Parts b and c of Figure 25 show the pitch attitude and normal acceleration responses respectively. Part d of the figure shows how the blended normal-acceleration/pitch-rate response (C*) compares with the design objective defined in Figure 7.

Similar responses were obtained for the other flight conditions. Consequently, the control law was considered to be valid.

5. FLYING QUALITIES ANALYSIS

Speed stability, maneuver stability, dynamic stability, and controllability flying qualities were performed for the flight conditions listed in Table 12, as described in the following sections, to determine conformance of the PACS configured aircraft with FAR Part 25 and MIL-F-8785C criteria.

5.1 Speed Stability

The speed stability analysis determines the column force required to maintain the aircraft at a speed other than trim speed. FAR Part 25 defines satisfactory column force characteristics as follows:

- A pull force shall be required to maintain speed below trim speed and a push force shall be required to maintain speed above trim speed.
- Stick forces shall vary monotonically with speed.
- The average stick force gradient shall be at least -1 lb per 6 KEAS increase throughout the speed range.

Speed stability analysis of the PACS configuration (Figure 16) showed an abrupt column force reversal for the takeoff condition with the c.g. at 25% mac and unstable column force gradients for the 50% c.g. position. Also, unsatisfactory force gradients were shown to exist for the hold condition aft c.g. positions.

TABLE 12. - PILOTED FLIGHT SIMULATION TEST CONDITIONS

Flight Condition	Weight 1000 lbs	c.g. % mac	Altitude 1000 ft	V _e KEAS
7. Cruise W/δ = 1.9 x 10 ⁶ lbs	408	25 to 50	37	254 (M = 0.83)
10. Cruise W/δ = 1.4 x 10 ⁶ lbs)	360	25 to 50	33	260 (M = 0.83)
15. Cruise W/δ = 1.6 x 10 ⁶ lbs	360	25 to 50	36	280 (M = 0.83)
16. M _{mo} /V _{mo}	350	25 to 50	25	357
17. Holding	335	25 to 50	10	250
18. Landing (δ _F = 33 deg)	330	25 to 50	2	135 (1.3 V _s)
19. Takeoff (δ _F = 26 deg)	380	25 to 50	2	137 (1.2V _s)

The column force reversal for the takeoff condition is a result of the feed-forward gain schedule being a function of dynamic pressure and stabilizer deflection angle (Figure 13). Dynamic pressure increases with speed and decreases the feed-forward gain from positive to negative values. Negative gain causes the PACS series servo to oppose control column input and to reverse abruptly the column force at 50 knots above the trim speed. This problem was remedied by restricting the lower bound of the feed-forward gain (K_{FF}) to zero.

The unstable column force gradients for the takeoff condition are associated with the feed-forward loop that reduces the force needed to trim the aircraft and the small stabilizer deflection gradient that is required to trim the aircraft throughout the speed range. The unsatisfactory column force gradients for the hold condition were due to inadequate or contrary stabilizer gradients throughout the speed range. These problems were solved by adding a Mach compensation circuit that operates through the Mach trim system as shown by the dashed lines in Figure 26. The feed-forward gain restriction is also shown in the figure. Mach trim compensation ($\Delta\delta_c$) shown in Figure 27 was available as part of the baseline aircraft pitch and trim system.

The Mach compensation circuit consists of two elements: Mach trim servo offset schedule, and loop gain schedule. The Mach trim servo offset schedule ($\Delta\delta_o$) is different for the flap-down and flap-up flight conditions as shown in Figure 28. The Loop gain (K_M) given in Figure 29 is scheduled with Mach number and stabilizer angle to provide the desired speed stability column force gradient throughout the c.g. range. The stabilizer gain schedule input has a 20 second filter and the Mach trim offset schedule input has a 10 second filter to limit servo offset gain overshoot.

Speed stability column force characteristics for the reconfigured PACS (Figure 26) are shown in Figure 30 for the hold and cruise conditions. FAR Part 25 design criteria is shown for comparison. The hold condition column force gradients comply with the design criteria in all respects, whereas the cruise condition criteria does not vary monotonically with speed as desired. However, the column forces were considered satisfactory to continue with piloted flight simulation tests.

5.2 Maneuver Stability

The maneuver stability analysis determined the column forces required to maintain the airplane in steady wind-up turns or quasi-steady pushovers. Satisfactory maneuver stability column forces according to the MIL-F-8785C are a steadily increasing pull to maintain positive load factors and a steadily increasing push to maintain negative load factors.

The upper and lower column force maneuver criteria boundaries for takeoff are:

- Upper boundary = 120 lbs/g
- Lower boundary = $\frac{35}{n_L - 1}$ lbs/g

ORIGINAL PAGE IS
OF POOR QUALITY

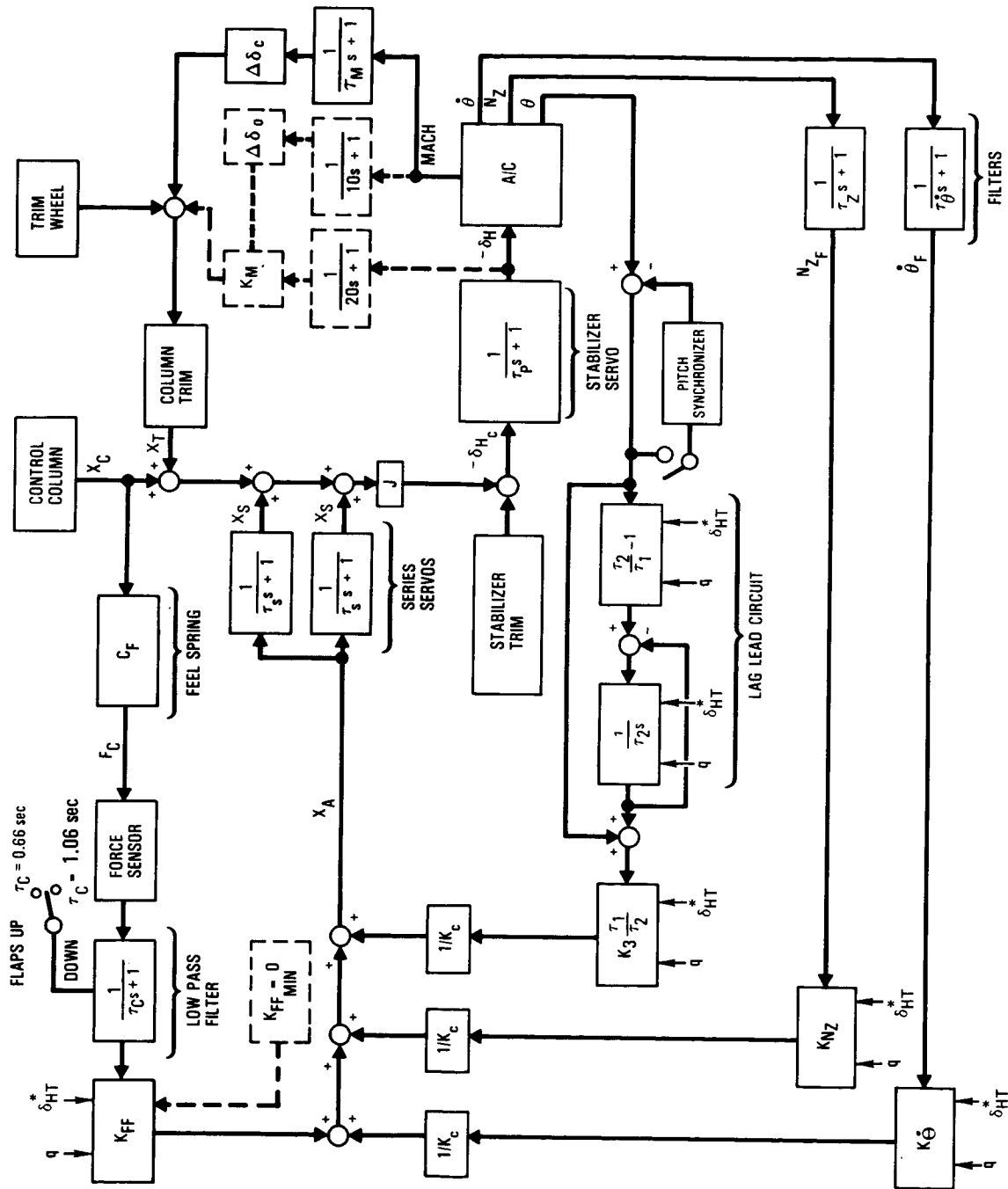


Figure 26. - Advanced PACS modified block diagram.

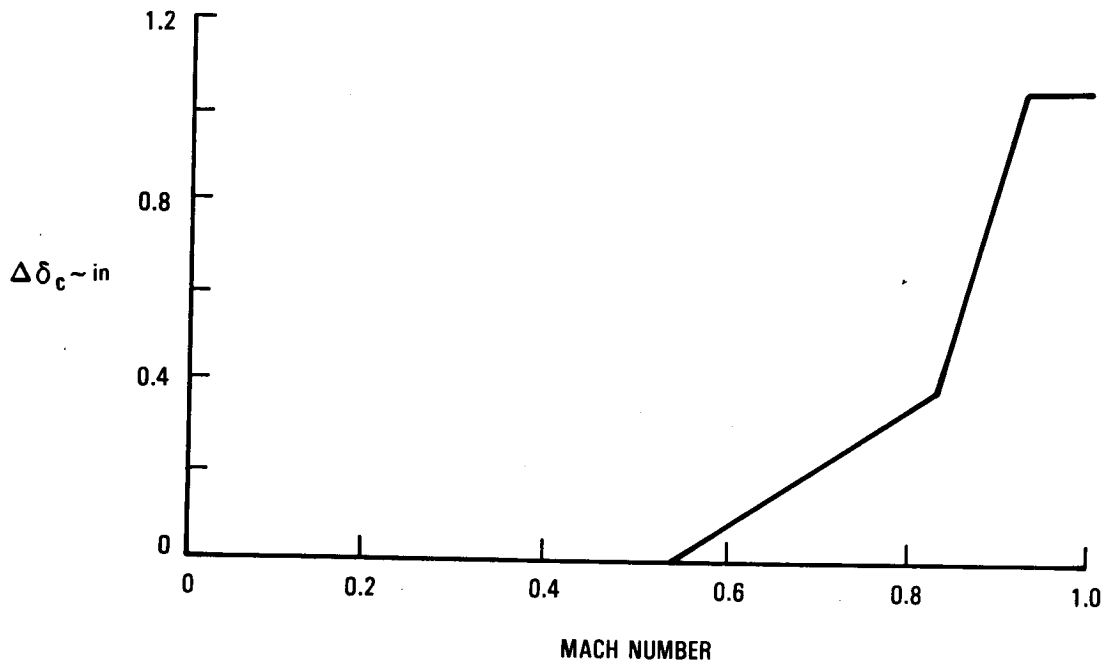


Figure 27. - Mach trim compensation.

The column force criteria for cruise are:

- Upper boundary = $\frac{120}{n_L - 1}$ lbs/g
- Lower boundary = Same as for takeoff

The value of n_L is 2.5 for the L-1011 aircraft.

ORIGINAL PAGE IS
OF POOR QUALITY

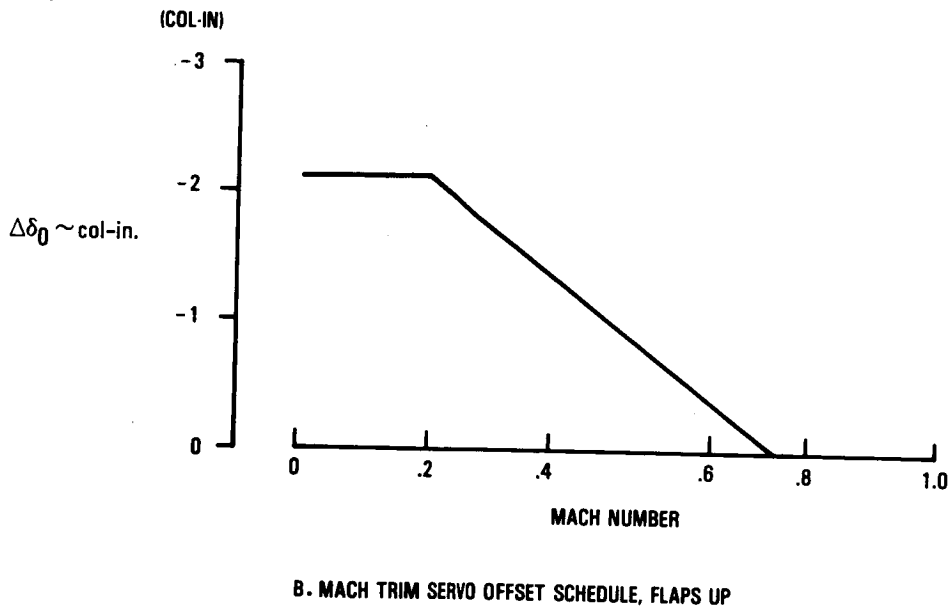
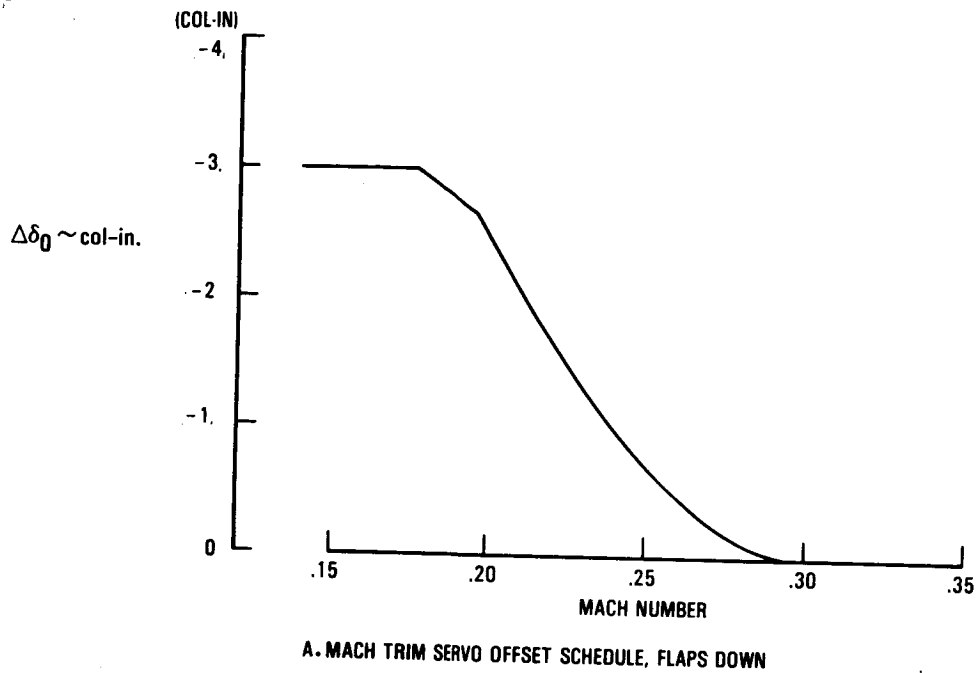


Figure 28. - Mach compensation circuit servo offset schedules.

ORIGINAL PAGE IS
OF POOR QUALITY

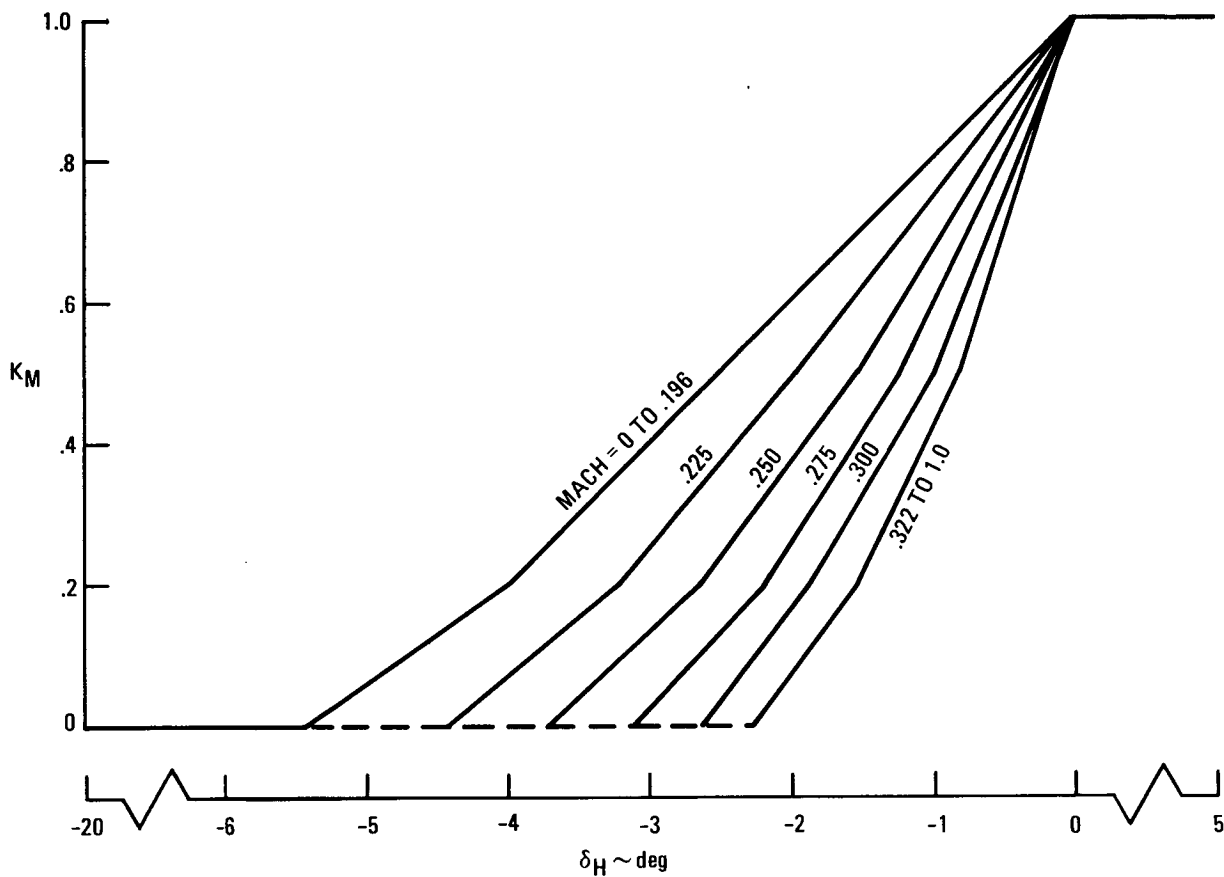
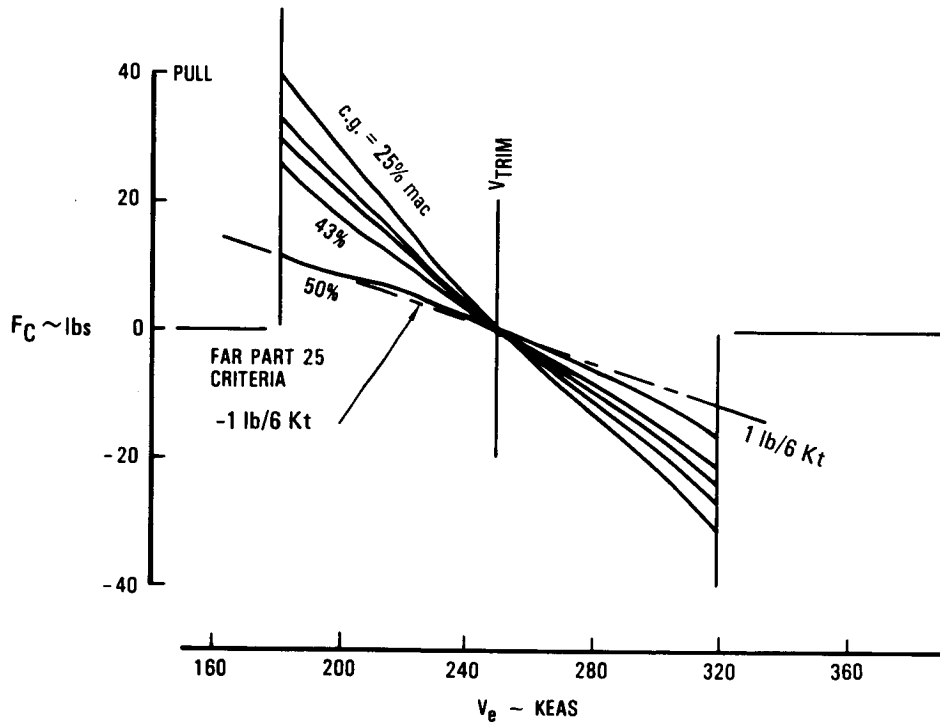
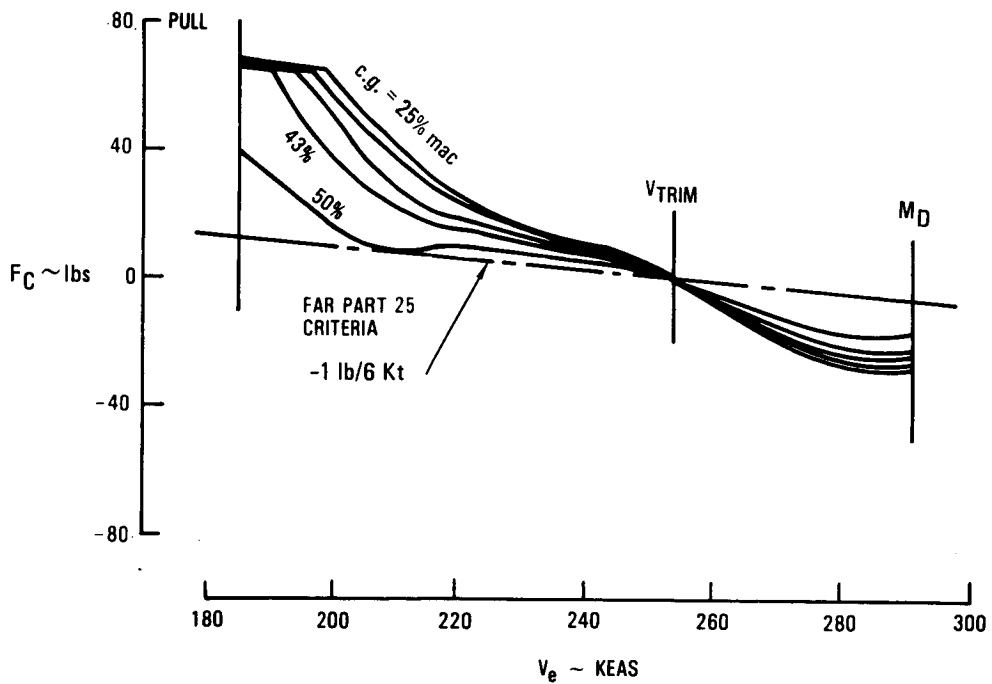


Figure 29. - Mach compensation gain schedule, flaps down.

ORIGINAL PAGE 19
OF POOR QUALITY



A. FLIGHT CONDITION 17: HOLD CONDITION



B. FLIGHT CONDITION 7: CRUISE

Figure 30. - PACS configured aircraft speed stability column force characteristics.

5.2.1 Takeoff Maneuver Stability. - Maneuver stability analysis of the baseline aircraft in the takeoff configuration showed that the column forces were stable throughout the c.g. range. However, the gradients were very steep for the aft c.g. position compared to MIL-F-8785C guidelines shown in Figure 31. The nature of these column forces can be attributed to the low speed aerodynamics and control system characteristics.

The pitching moment characteristics for takeoff are shown in Figure 32. The aircraft has close to zero static margin (neutral stability) for the center-of-gravity at the 50% mac position. However, it has a substantial positive maneuver margin because of pitching moment due to AACS engagement and due to pitch rate for the maneuver. Figure 33 shows the maneuver pitching moment increments of the aircraft due to pitch rate and the AACS. The maneuver margin is the nondimensional longitudinal distance from the center-of-gravity of the aircraft to the maneuver point which is the c.g. where the column force per g is zero. The maneuver point is always aft of the neutral point and increases the aircraft stability. The AACS engagement is shown to have a small effect on pitching moment. The pitch rate effect makes the pitching moment substantially more negative as the load factor increases. Increased stabilizer deflection is required to counteract this increased stability and maintain load factor during maneuvers.

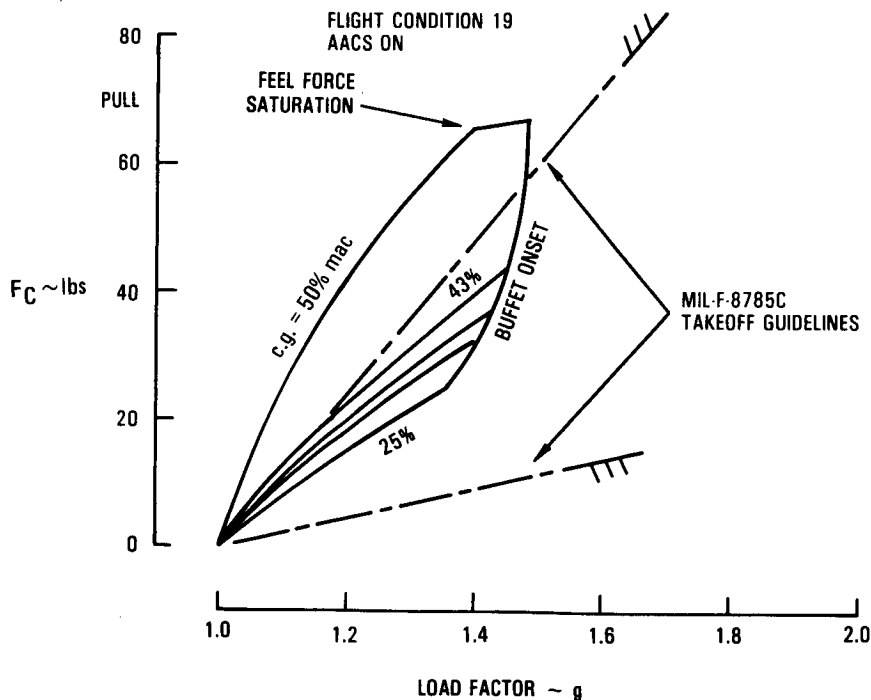


Figure 31. - Baseline aircraft takeoff maneuver stability column forces.

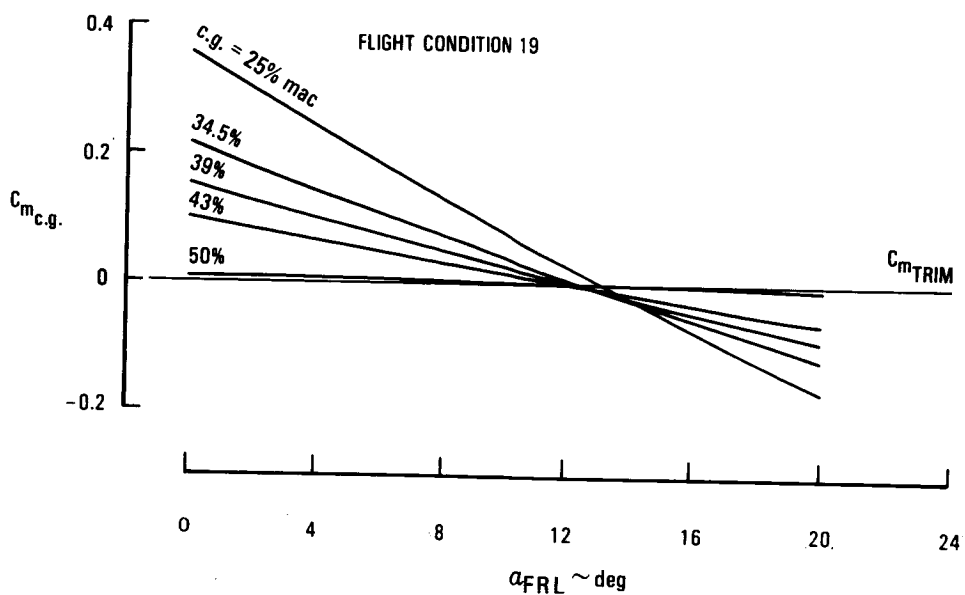


Figure 32. - Baseline aircraft takeoff pitching moments.

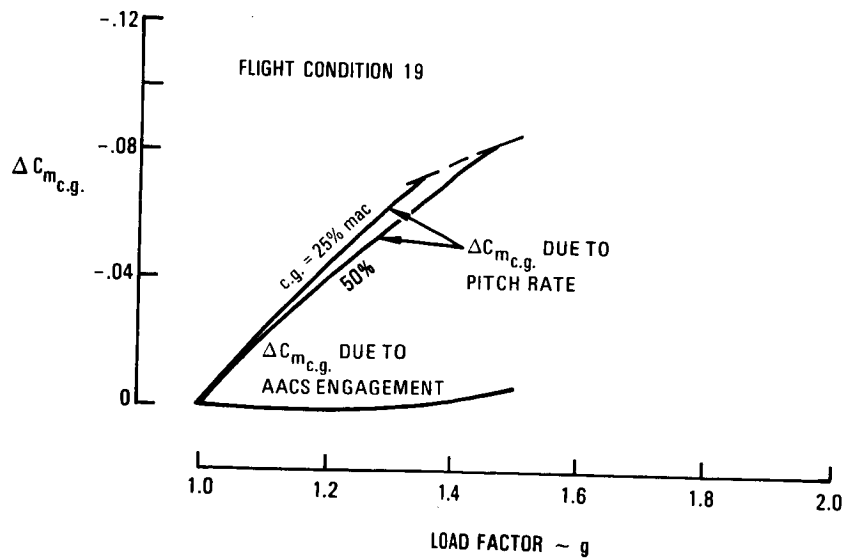


Figure 33. - AACCS engagement and pitch rate impact on pitching moment \sim takeoff.

ORIGINAL PAGE IS
OF POOR QUALITY

The takeoff maneuver stabilizer gradient decreases slightly as the c.g. is moved from 25% to 50% mac as shown in Figure 34.

Although the stabilizer gradient is higher at the forward c.g. than at the aft c.g., the control system characteristics causes the column force gradient to be higher at the aft c.g. than at the forward c.g. because the J-curve (Figure 4) was optimized to give good handling qualities for the L-1011 with c.g. range of 12% to 35% mac. The slope of the J-curve was designed to obtain a maneuver column force gradient at the aft c.g. similar to the gradient at the forward c.g. Thus, more control column displacement at the aft c.g. is required to obtain the same stabilizer displacement increment than at the forward c.g. Flaps down configurations which have a trim stabilizer setting of -4 degrees or less determined the upper portion of the curve, and the flaps up configurations which have a trim stabilizer setting at 1 degree or less determine the lower portion of the curve. In the c.g. range of interest (35% to 50% mac) for the advanced PACS, the trim stabilizer setting is greater than -1 degree (e.g., +1 degree for the takeoff configuration with the c.g. at 50% mac). This setting falls outside the optimal range of the J-curve and results in a higher column force gradient with c.g. aft than with c.g. forward.

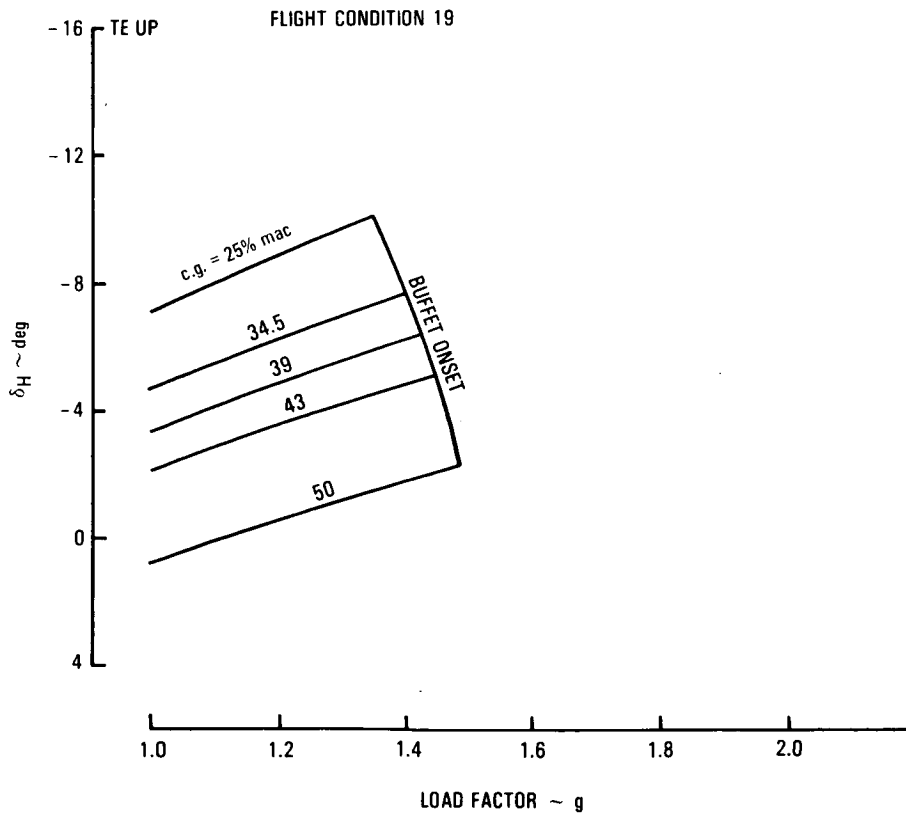


Figure 34. - Baseline aircraft takeoff maneuver stability stabilizer position characteristics.

Figure 35 shows maneuver stability characteristics of the aircraft in the takeoff configuration with the advanced PACS (Figure 26). These data show that the PACS reduces the spread of the column force gradients for the complete c.g. range so that they are similar to the baseline aircraft with c.g. at 25% mac.

5.2.2 Cruise Maneuver Stability. - Maneuver stability analysis of the baseline aircraft at cruise conditions (Figure 36) shows unsatisfactory column force characteristics for the complete c.g. range of 25 to 50% mac. The unsatisfactory force characteristics can be attributed to nonlinear high speed pitching moment characteristics and to the AACS.

The nonlinear pitching moment characteristics are illustrated in Figure 37. The pitching moment for Mach numbers greater than 0.7 are a strong function of angle of attack. At angles of attack greater than 5 degrees, there is a significant nose-up pitching moment caused by shock-induced boundary layer separation on the upper surface of the outer wing. This nose-up pitching moment for the angle of attack between 4.7 and 7.5 degrees causes a dip in the stabilizer displacement required to maintain load factor and results in column force lightening. The static stability of the airplane decreases as the c.g. is moved aft, and at 50% mac the c.g. location airplane is statically unstable.

The effect of pitch rate and the AACS on pitching moment characteristics are shown in Figure 38. The AACS reduces the maneuver margin by 4 to 5% mac

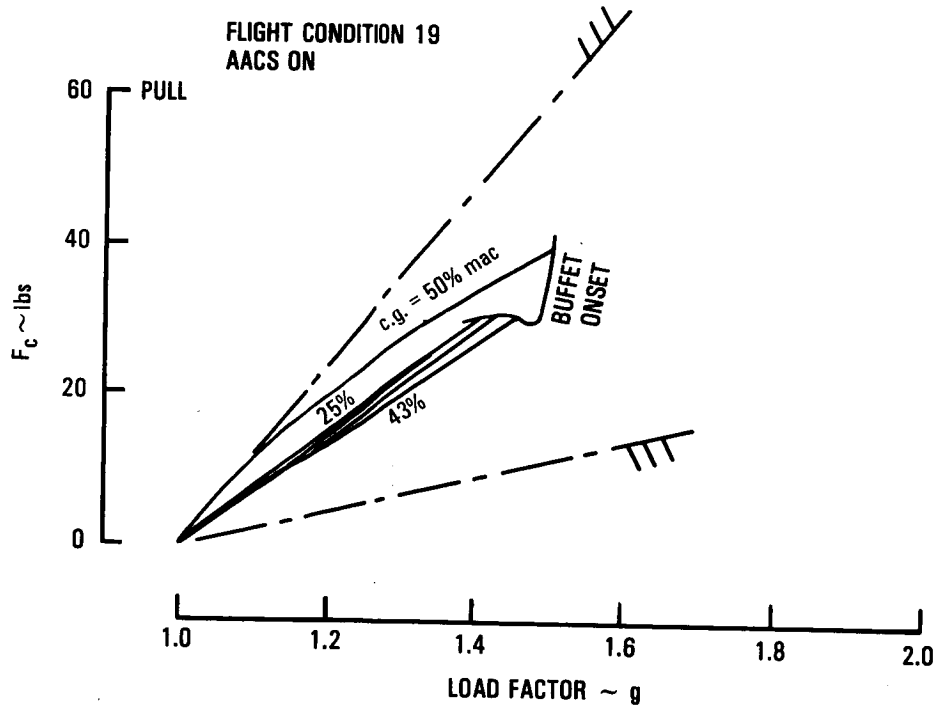


Figure 35. - PACS configured aircraft maneuver stability column force characteristics ~ takeoff.

ORIGINAL DRAFT IS
OF POOR QUALITY

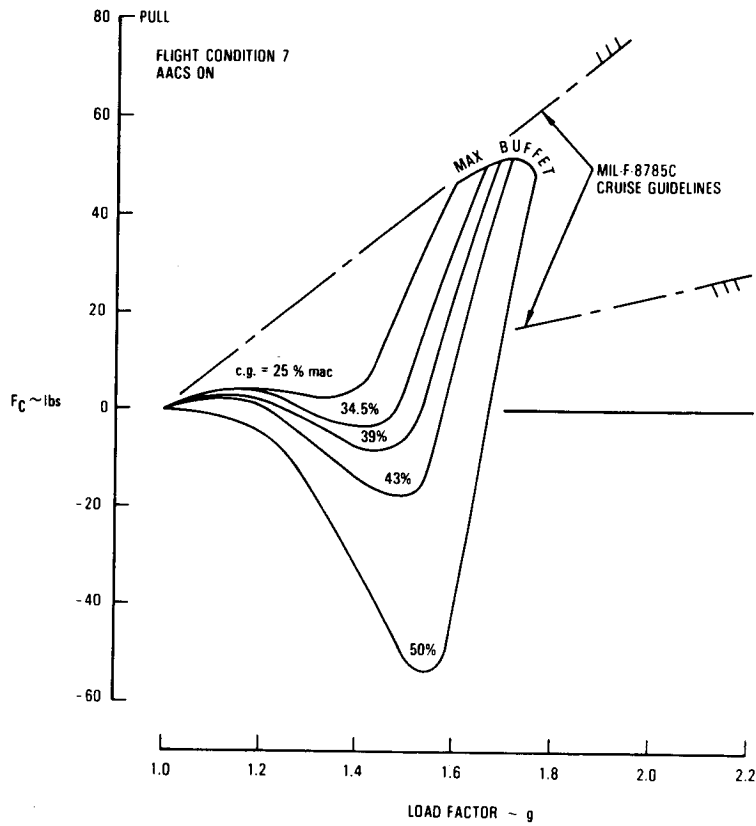


Figure 36. - Baseline aircraft maneuver stability column characteristics ~ cruise.

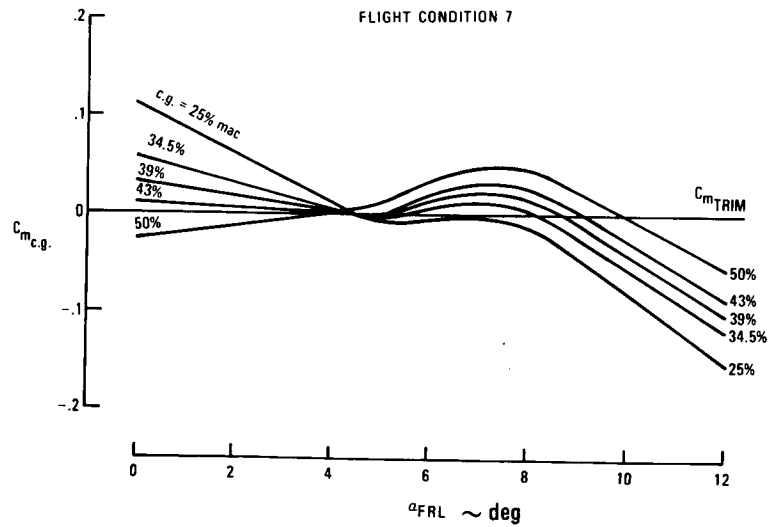


Figure 37. - Aircraft pitching moment versus angle-of-attack characteristics ~ cruise.

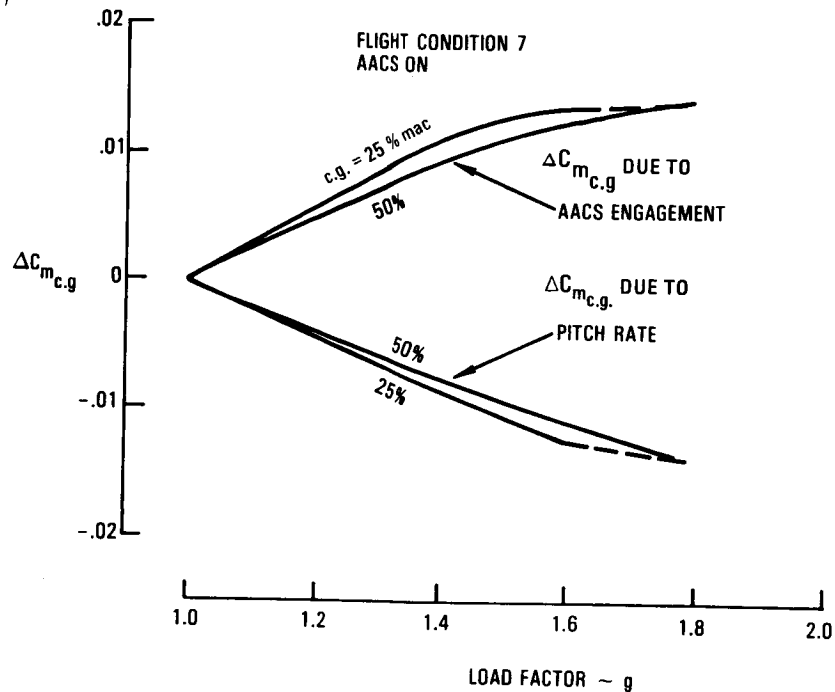


Figure 38. - AACS engagement and pitch rate impact on pitching moment ~ cruise.

at high speeds and completely negates the 3 to 4% mac increase in maneuver margin contributed by the pitch rate. There is a net reduction in stabilizer gradient throughout the load factor range which reduces the column force gradient.

The cruise maneuver stability stabilizer gradients are illustrated in Figure 39. At the 50% c.g. position there is an adverse stabilizer gradient at the trimmed load factor, and all c.g. locations have a dip in the middle of the stabilizer displacement curve.

Maneuver stability characteristics of the airplane with the advanced PACS are shown in Figure 40. These data show that the PACS completely removes the dip in column force gradient characteristics shown in Figure 36. This is accomplished primarily by the pitch-up controller which is scheduled with Mach number and angle of attack. These data show that the column force characteristics are satisfactory for all c.g. locations except for high load factors where the aircraft is very stable. The initial force gradients are essentially the same for the entire c.g. range.

5.3 Dynamic Stability

Analyses were performed to determine characteristic roots of the linear system dynamic stability and to demonstrate nonlinear time histories of the longitudinal dynamic response for discrete vertical gusts and control column

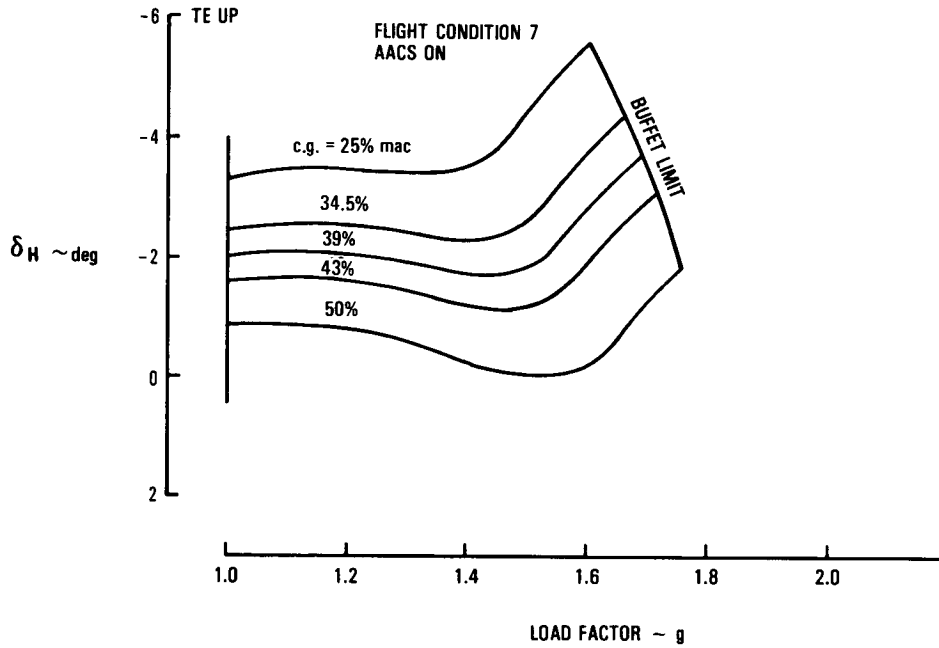


Figure 39. - Baseline aircraft cruise maneuver stability stabilizer position characteristics.

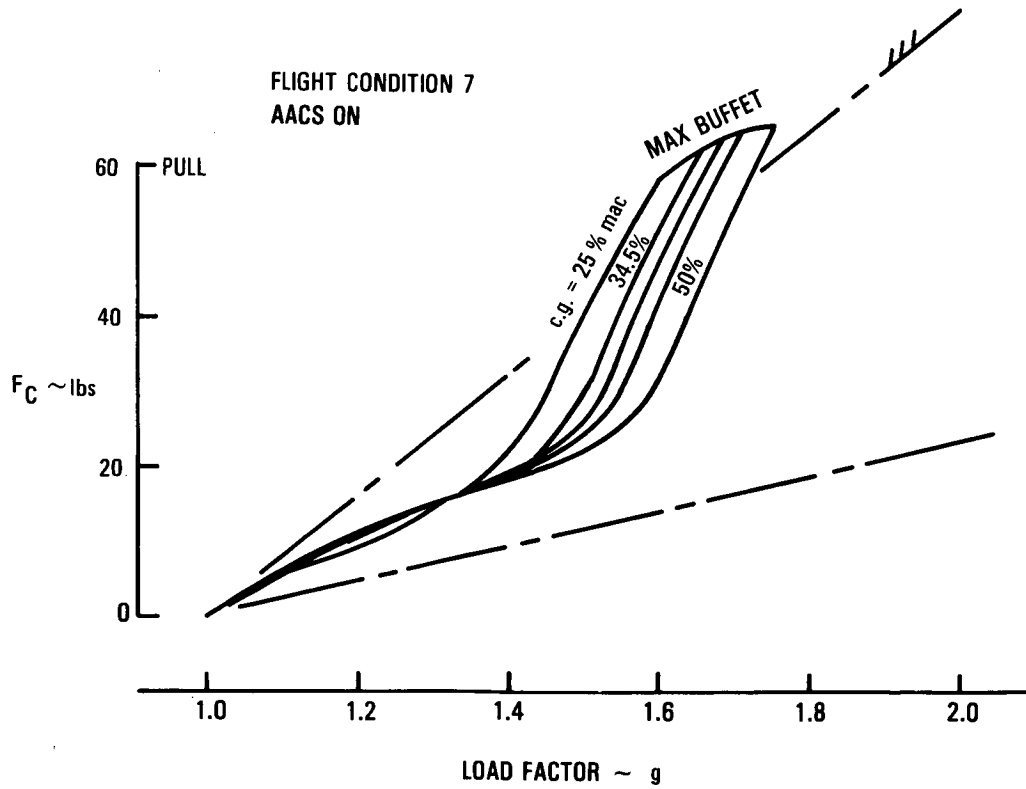


Figure 40. - PACS configured aircraft maneuver stability column force gradients \sim cruise.

step inputs. The linear analysis did not include the effects of aerodynamic and control system nonlinearities and is valid only for small disturbances about the trim condition.

5.3.1 Linear Analysis. - The purpose of the linear system analysis was to evaluate the dynamic stability characteristics of the aircraft for flight conditions and c.g. locations that were selected for piloted flight simulation tests (Table 12) and to determine effects of the Mach compensation loop (Section 1.4.1).

In general, an airplane that has satisfactory dynamic characteristics will have a short-period mode which is moderately damped and a phugoid mode which is lightly damped. Pitch angle and angle-of-attack perturbations are predominate for the short-period mode, and pitch angle and velocity perturbations are predominate for the phugoid mode.

The linear system dynamic stability characteristics were obtained by calculating eigenvalues of the small disturbance equations of motion. MIL-F-8785C specifications were used as guidelines to evaluate the dynamic stability.

Figure 41 presents s-plane eigenvalues (cruise condition 7) for the baseline aircraft short-period (x) and phugoid (o) modes. The short-period modes do not meet the MIL-F-8785C criteria when the c.g. is aft of 25 percent mac. Also, the phugoid characteristics become unstable as the c.g. is moved aft and violates the requirement for a minimum damping ratio of 0.04. The time-to-double amplitude for the most unstable phugoid nonoscillatory mode is 1.5 seconds.

The baseline aircraft exhibits the same general characteristics for the holding condition except that the phugoid instability at the aft c.g. limit has an increased time-to-double-amplitude of 4.6 seconds. The short-period characteristics of the aircraft for the low-speed conditions with flaps extended, are unsatisfactory for all c.g. locations and the phugoid mode goes unstable at 50% c.g. position with a time-to-double-amplitude of 10 seconds.

Figure 42 shows that the dynamic stability characteristics for the aircraft in cruise condition 7 with the advanced PACS engaged comply with MIL-F-8785C criteria. All of the flight conditions satisfied the dynamic stability characteristics except for the hold condition which has a mild phugoid instability with the c.g. at 25% mac. This instability resulted in a time-to-double-amplitude of 700 seconds and was considered acceptable.

5.3.2 Nonlinear Analysis. - Nonlinear aerodynamic and control system characteristics were modeled to compute responses of the aircraft with PACS on and off for discrete vertical gusts and column control step inputs. The analysis was concentrated on high altitude cruise flight (condition 7) because of the aircraft variable stability characteristics at this condition. The computer program used in the study consists of longitudinal equations of motion, nonlinear aerodynamic data, and models of the longitudinal control

ORIGINAL PAGE IS
OF POOR QUALITY

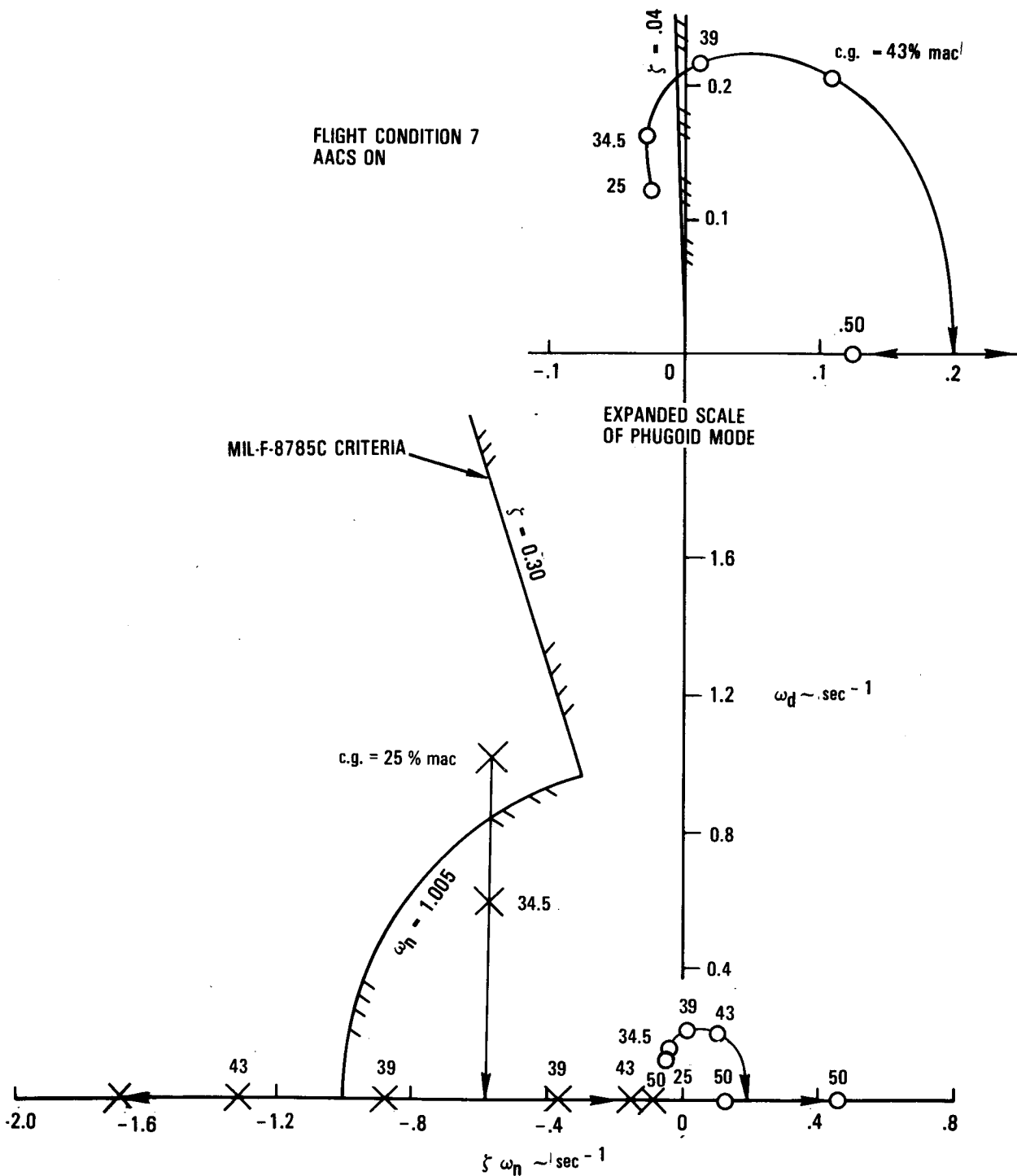


Figure 41. - Baseline aircraft dynamic stability characteristics.

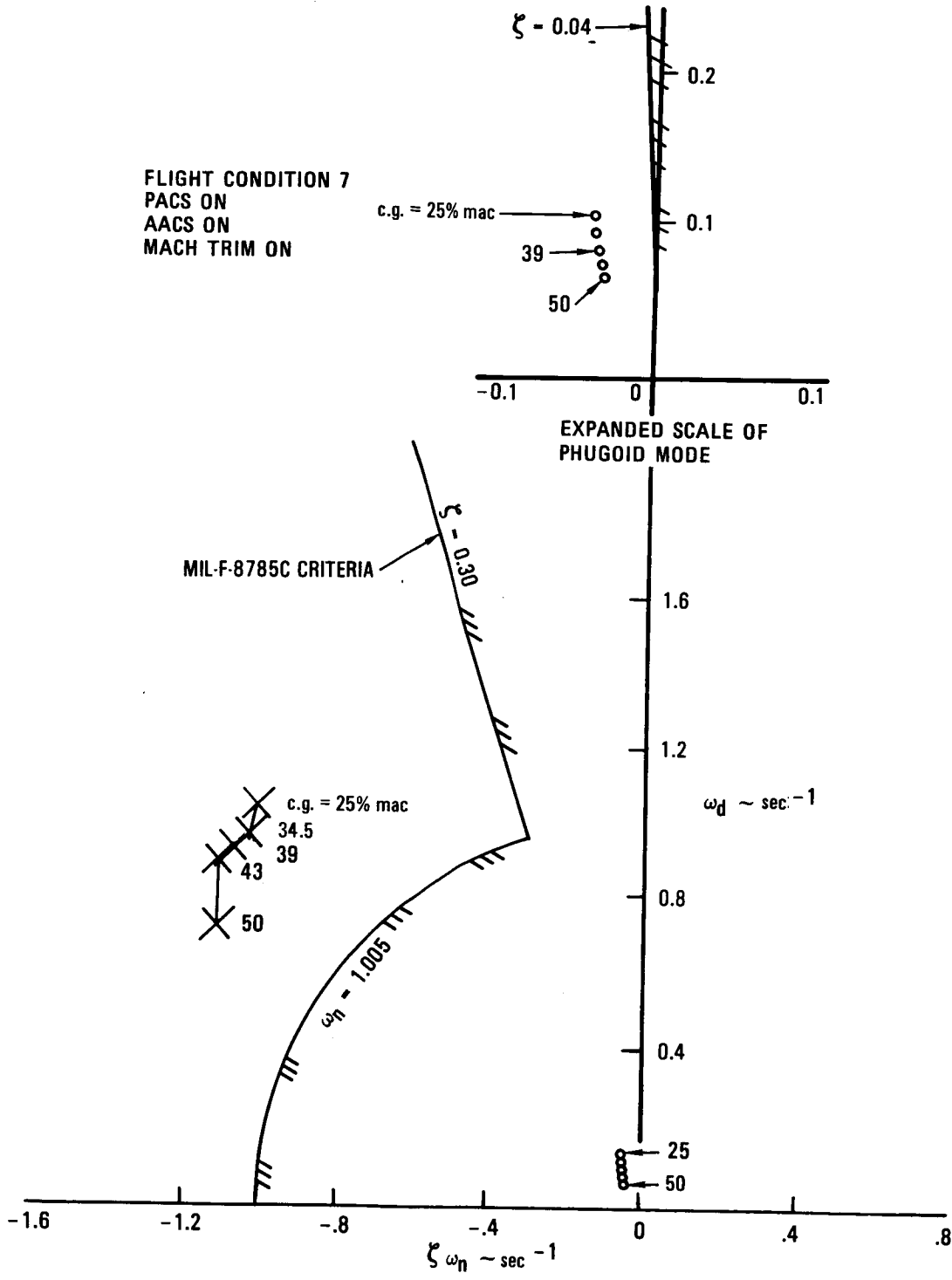


Figure 42. - PACS equipped aircraft stability characteristics.

and stability augmentation systems. Figure 43 shows the discrete vertical gust model used for the analysis. It was patterned after the model given in MIL-F-8785C. Horizontal distance of the disturbance is equivalent to distance the airplane travels during one cycle of a short-period response. A gust amplitude of -12 ft/sec is moderate and -54 ft/sec is a severe disturbance of heavy thunderstorm magnitude.

Satisfactory flying qualities are defined in terms of stable responses to external disturbances and pilot control inputs. After experiencing a discrete vertical gust, the aircraft should return quickly to its trim equilibrium condition and oscillations should be well damped. The airplane should respond predictably to a column force step input, and should quickly stabilize new equilibrium condition. The controls should give the pilot ability to change the pitch attitude precisely.

Figure 44 shows the response of the baseline airplane to a moderate vertical gust for various center of gravity positions. The aircraft is statically stable at initial trim conditions for the c.g. range of 25% to 43% mac. The angle-of-attack response is in the stable region for a disturbance of moderate magnitude and the aircraft returns to its initial trim condition naturally. The aircraft with c.g. at 43% mac is close to being neutrally stable and its pitch rate response is very flat. The short-period response matches results of the linear dynamics analysis for the 25 to 43% mac range. The aircraft is statically unstable about its initial equilibrium trim condition for the 50% mac c.g. case. The aircraft diverges from its trim position for any external disturbance at this c.g. and seeks a new equilibrium condition at a high angle of attack where a region of strong stability is encountered.

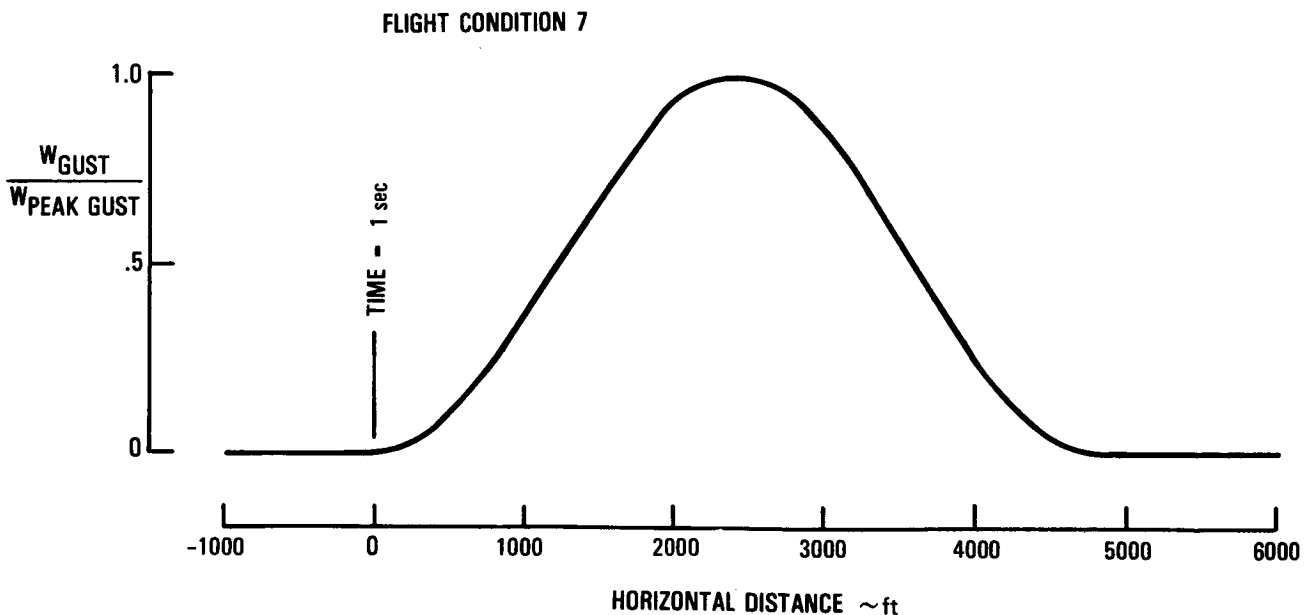


Figure 43. - Flight condition 7: discrete gust model, cruise.

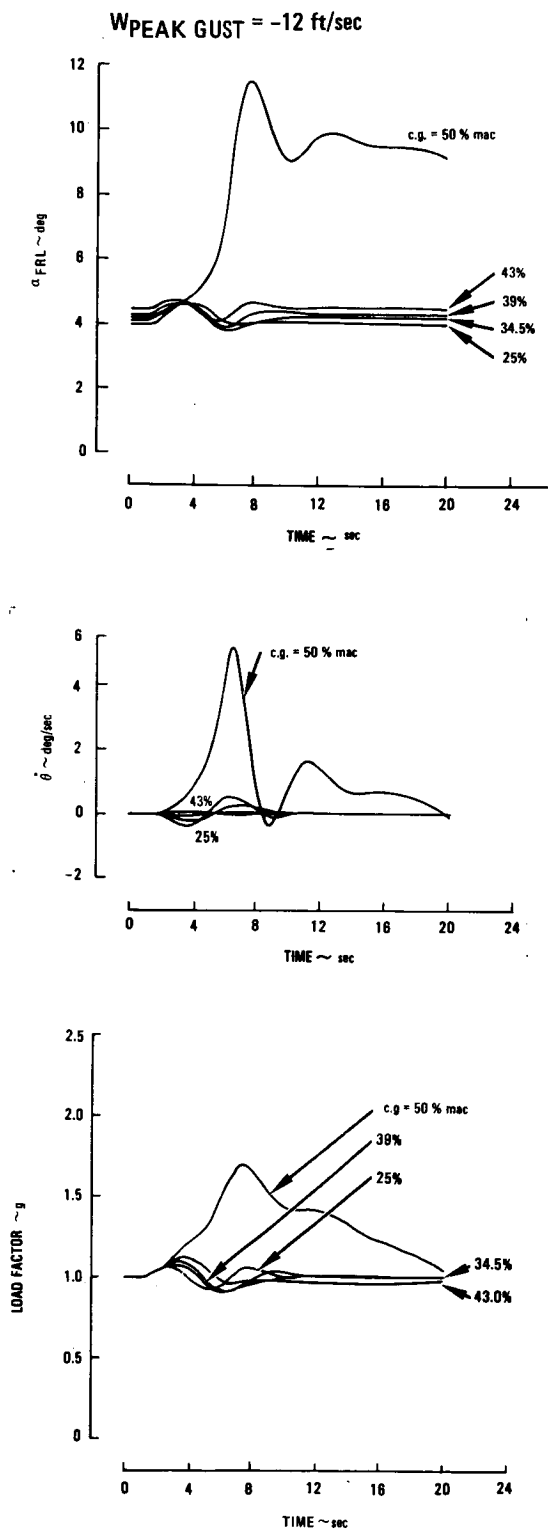


Figure 44. - Baseline aircraft response to a moderate vertical gust.

Figure 45 shows the baseline and PACS configured aircraft response to a -54 ft/sec gust. For this severe disturbance the baseline airplane with c.g. at 25% mac will return to its initial trim condition. The aircraft diverges from its trim condition for a c.g. position aft of 25% mac and seeks a new equilibrium at high angle of attack. The disturbance is strong enough to drive the aircraft into the high angle of attack heavy buffet region where the aircraft is excessively stable. The response of the PACS configured aircraft to a severe vertical gust has well-behaved, stable, response characteristics. The response characteristics were determined to be essentially the same for all c.g. positions from 25% to 50% mac as shown on the right side of Figure 45.

Figure 46 illustrates the aircraft response to various column force step inputs for the high altitude cruise condition with the c.g. at 50% mac. The baseline aircraft diverges quickly from its trim condition for any constant force input until it reaches a region of increased stability at high angle of attack.

The response of the PACS configured aircraft to column force step inputs show that the advanced PACS works to reduce excessive excursions in angle of attack and load factors.

5.4 Trimmability and Stabilizer/Elevator Limits

This analysis was performed to determine changes to the baseline aircraft control system that were required for the advanced PACS configured aircraft. Control system characteristics that were evaluated included: Stabilizer/elevator deflection range, trim servo range, elevator versus stabilizer gearing, control column limits, and pitch feel-spring rate.

The control system design criteria were:

- Capability must be provided to trim the aircraft for all flight conditions
- Sufficient control power must be provided to provide a minimum pitch angular acceleration of -5.73 deg/sec^2 for stall recovery from any flight condition
- Control power must be provided to recover from maneuvers in high angle-of-attack regions.

The standard L-1011 has a c.g. range of 12% to 35% mac. The corresponding stabilizer/elevator deflection range that provides sufficient control at all flight conditions is from -14 deg/-25 deg to +1 deg/0 deg. The stabilizer deflection range to trim the aircraft is -10 to 0 degrees. The advanced PACS configured aircraft has a c.g. range of 25% to 50% mac. Analyses show that the advanced PACS system with its further aft c.g. travel required more nose down trim and control capability. Therefore, the stabilizer/elevator deflection range was changed to -14 deg/-20 deg aircraft nose up and to +4 deg/+5 deg aircraft nose down. The trim range was increased to +1 degree aircraft nose down. The modified elevator versus stabilizer gearing curve is shown in Figure 47.

FLIGHT CONDITION 7
W_{PEAK GUST} = 16.46 M/SEC (-54 FT/SEC)

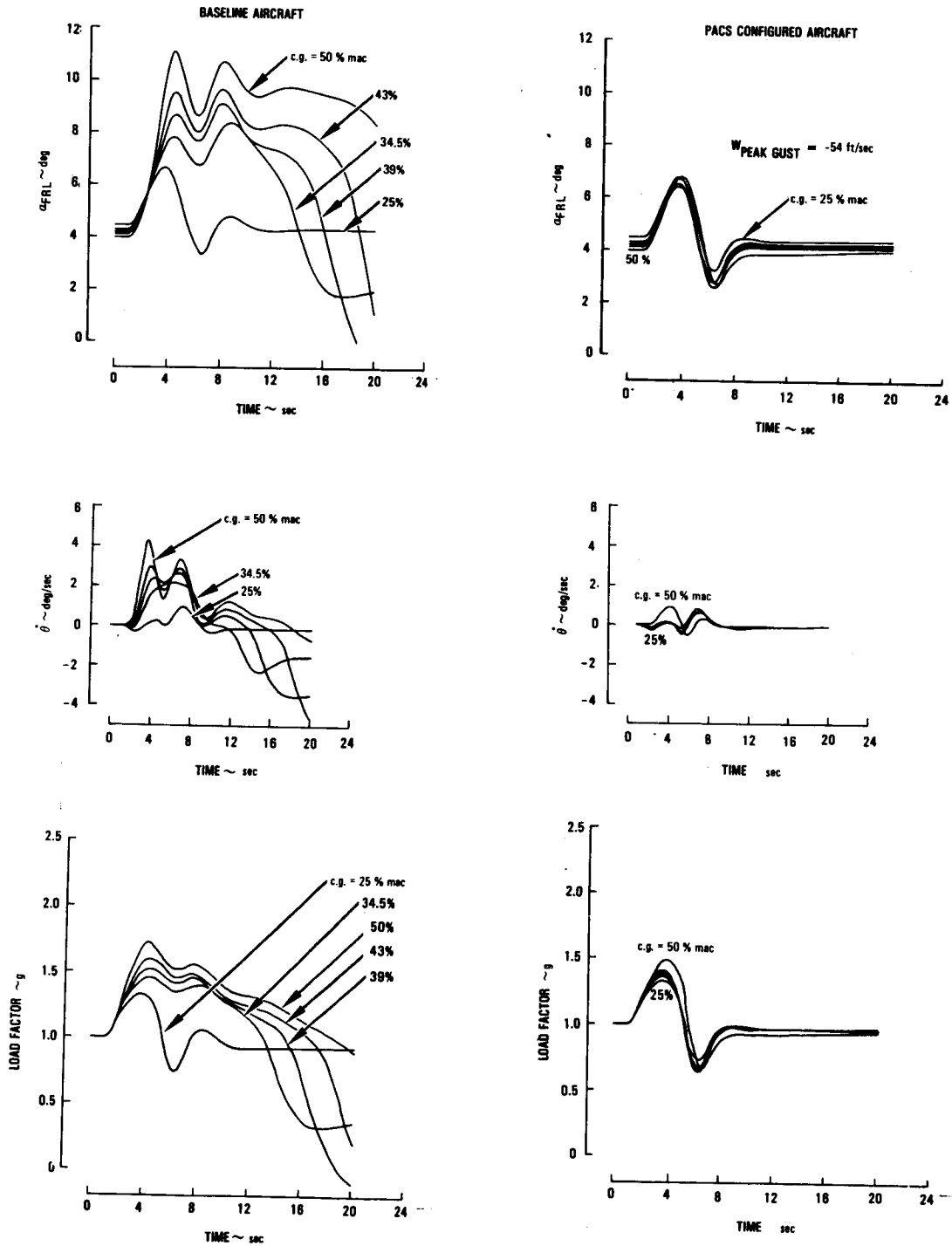


Figure 45. - Comparison of aircraft response with and without PACS engaged for a severe vertical gust.

FLIGHT CONDITION 7
AACs ON, c.g. AT 50% mac

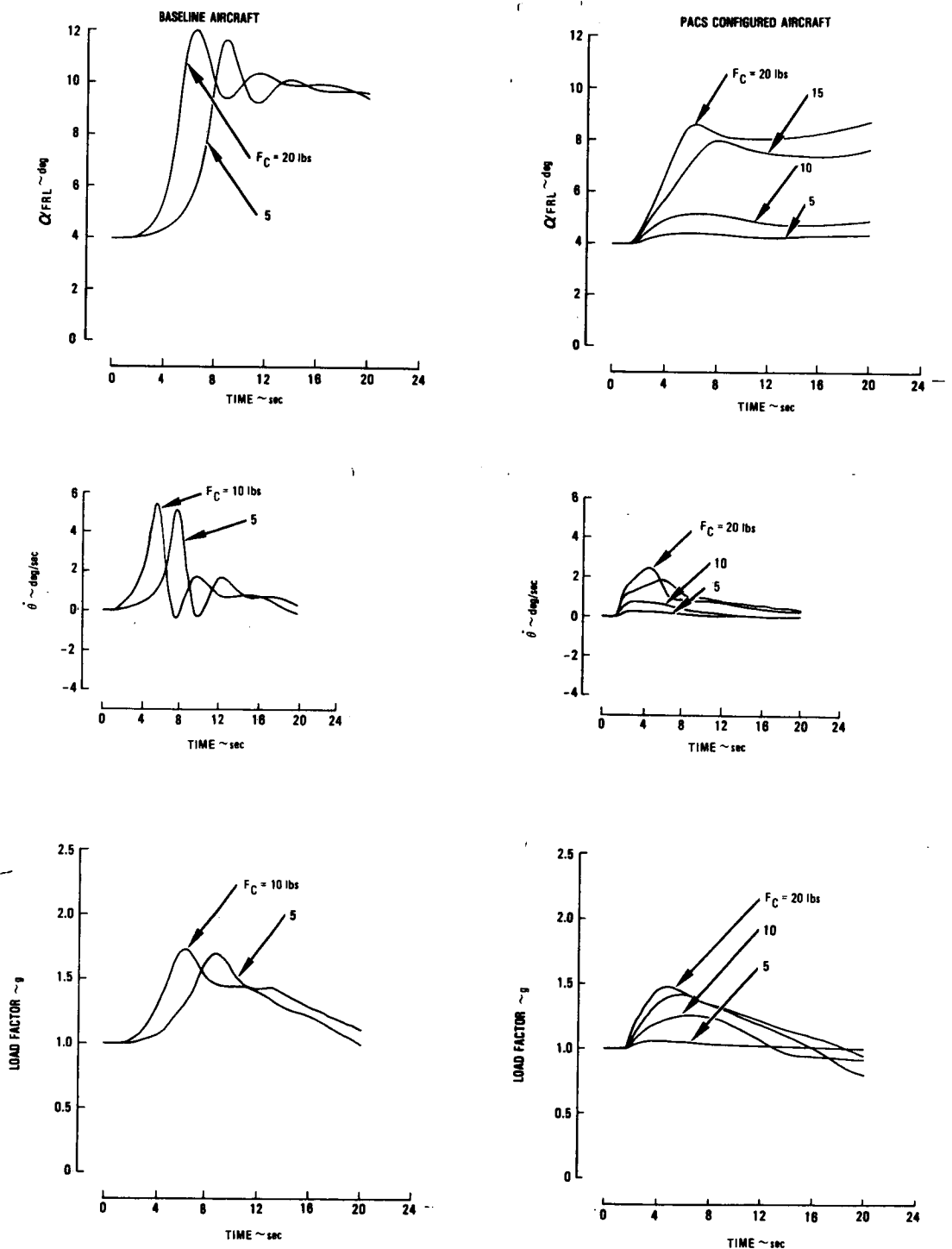


Figure 46. - Comparison of aircraft response with and without PACS engaged to various levels of control column step inputs.

ORIGINAL PAGE IS
OF POOR QUALITY

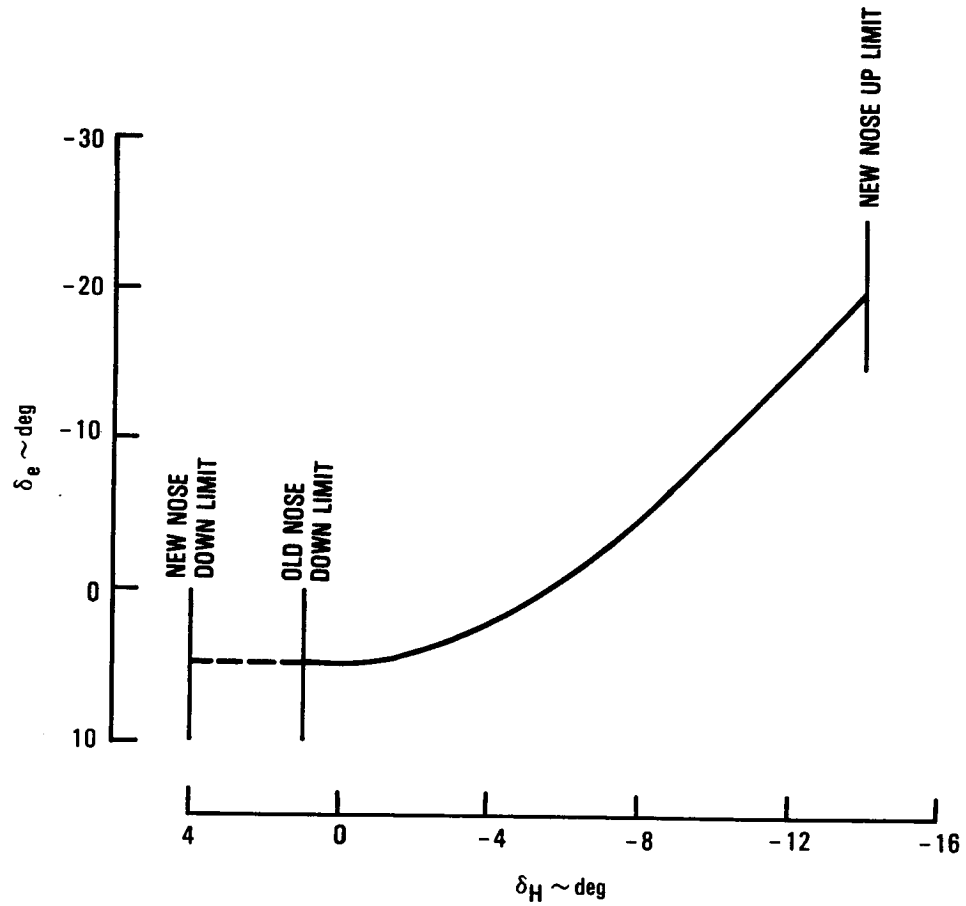


Figure 47. Modified elevator versus stabilizer gearing curve.

The PACS configured aircraft stabilizer deflection trim range for the flight conditions which were to be evaluated by piloted flight simulation tests is given in Figure 48. The +1 degree increase in the trim limit is required for the takeoff condition with the c.g. at the 50% mac position. The J-curve modification required because of the increased trim limit is indicated in Figure 49 by the dashed part of the curve. Travel of the trim servo displacement is shown to be increased by 1.15 inches to provide the +1 degree stabilizer deflection increase. It was also necessary to alter the pitch feel spring rate schedule as shown in Figure 50 by the dashed lines.

ORIGINAL PAGE IS
OF POOR QUALITY

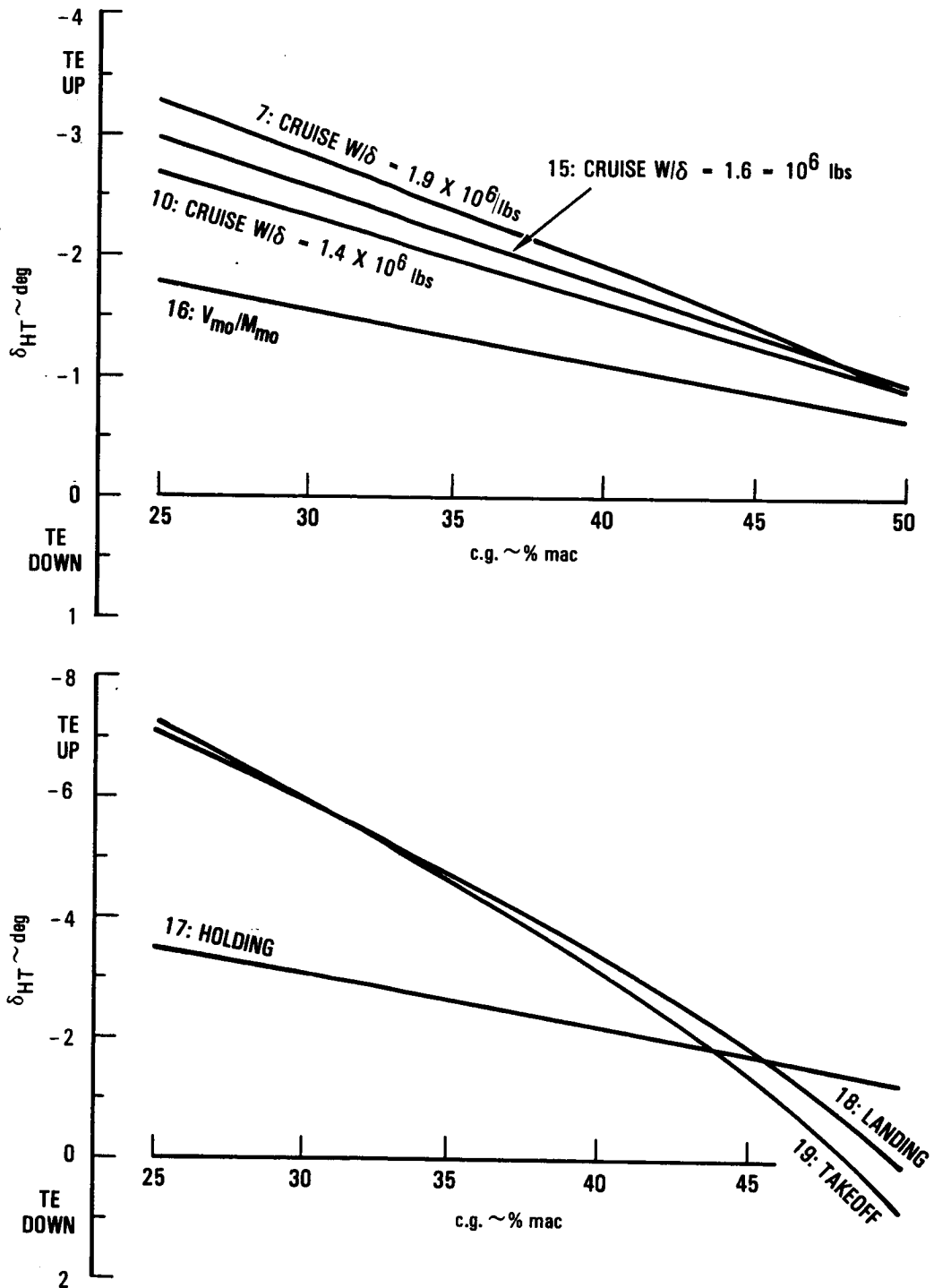


Figure 48. - Stabilizer deflection trim range for various flight conditions.

ORIGINAL PAGE IS
OF POOR QUALITY

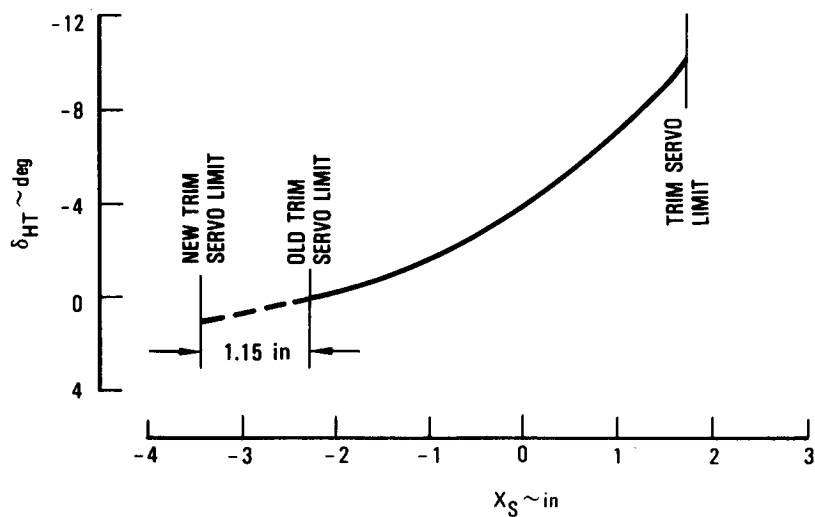


Figure 49. - Modified trim stabilizer position versus trim servo displacement characteristics.

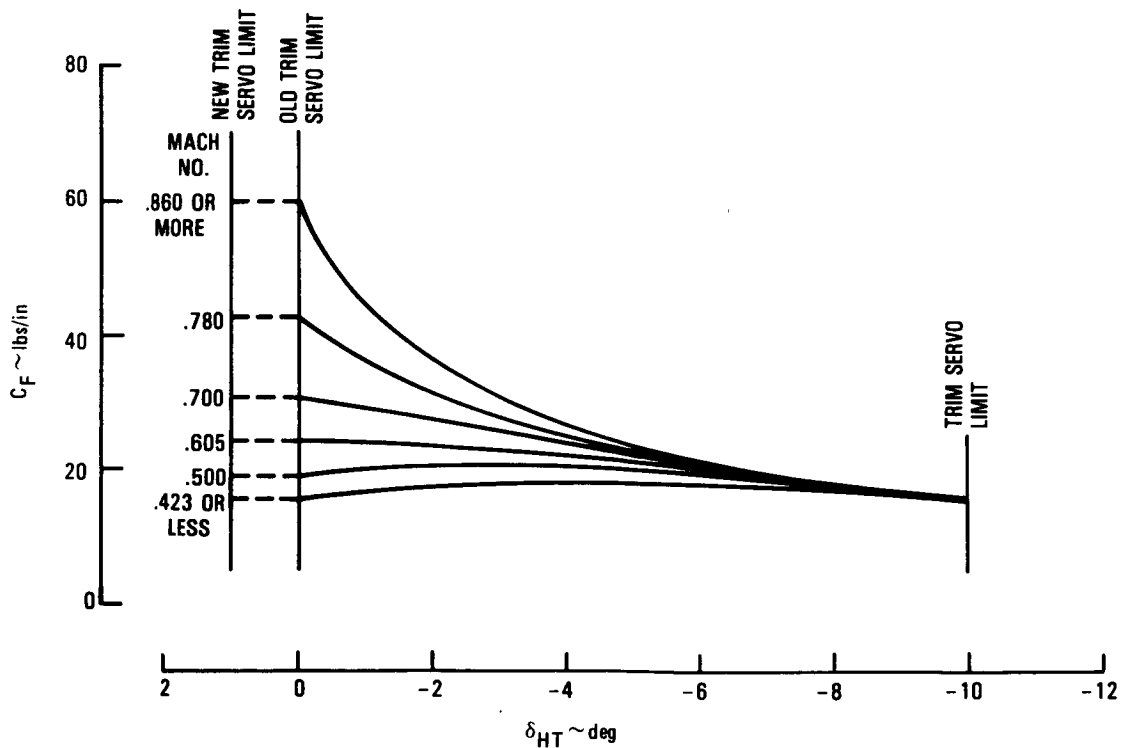


Figure 50. - Modified pitch feel spring rate schedule.

6. PILOTED FLIGHT SIMULATION TEST

The flight simulation test was performed to identify pilot/control interface problems and evaluate flying qualities of the advanced PACS.

The test was performed at the NASA Langley Flight Simulation Facilities. Setup of the simulator included a check-out of the computer program, motion system interface, cockpit controls, and instrumentation. Two Lockheed and three NASA pilots performed the flight simulation tests.

6.1 NASA Flight Simulator Center

The Langley simulator is a general purpose visual motion simulator consisting of a two-man cockpit on a six-degree-of-freedom synergistic motion base. A collimated visual display provides a 60 degree out-the-window color display which was activated during the landing approach task. A programmable hydraulic control loading system is provided for the column, wheel, and rudder. Instruments and displays are typical of transport aircraft. Photographs of the motion base, cockpit interior, and visual display are presented in Figures 51 through 53 respectively.

6.2 Simulation Math Model

The simulation mathematical model represented the L-1011 S/N 1001 aircraft. This L-1011 is a unique aircraft that has the Dash 1 version long fuselage, and the extended wing tips and AACS of the shorter fuselage Dash 500 derivative. Inertia characteristics of this configuration are given in Figure 54, and the weight/center-of-gravity envelope is presented in Figure 55.

The aerodynamic data model for the L-1011 S/N 1001 aircraft possesses a high-speed nonlinear pitch instability at high lift coefficients which is typical of swept wing designs. This characteristic defines the control system authority and aerodynamic control power requirements for the horizontal stabilizer and elevator. Figure 56 shows the aerodynamic longitudinal stability characteristics which were used in the simulation.

Engine characteristics were represented by the installed thrust for three Rolls Royce RB.211-22B high-bypass-ratio turbofan engines.

Control functions were represented by a complete dynamic model of the longitudinal system and a simplified model of the lateral-directional system. The advanced PACS block diagram is shown in Figure 26.

Longitudinal control forces in the simulator are supplied by a hydraulic column-loader which is a closed-loop servo system with position feedback and a high forward loop gain. The math model consisted of a second order system having position and rate feedback as follows:

$$\frac{F_C}{X_C} = \frac{s^2}{K} + s(K_v + K_c) + K_s + K_d$$

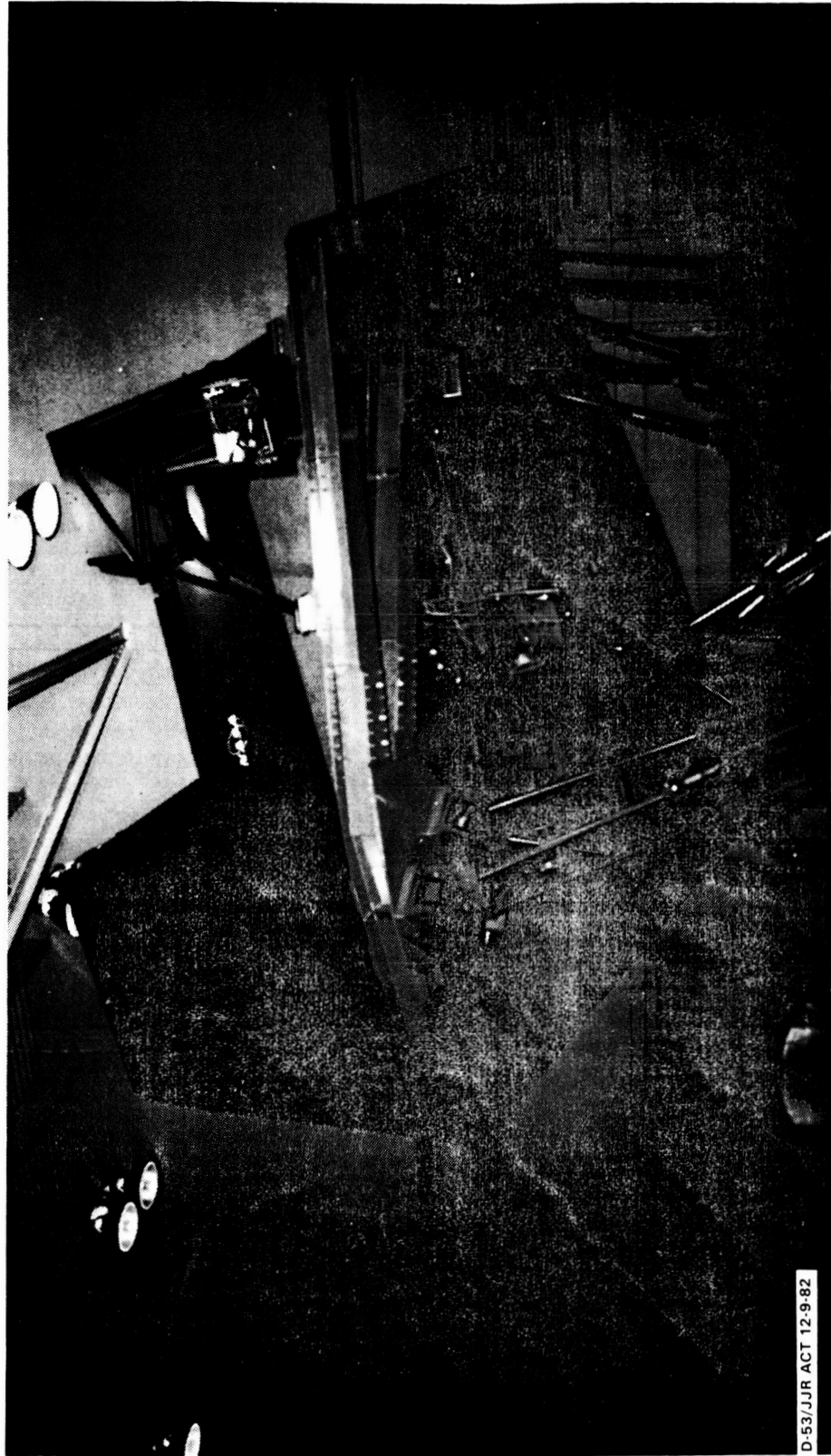


Figure 51. - NASA/Langley transport cab and motion base.

ORIGINAL PAGE 19
OF POOR QUALITY

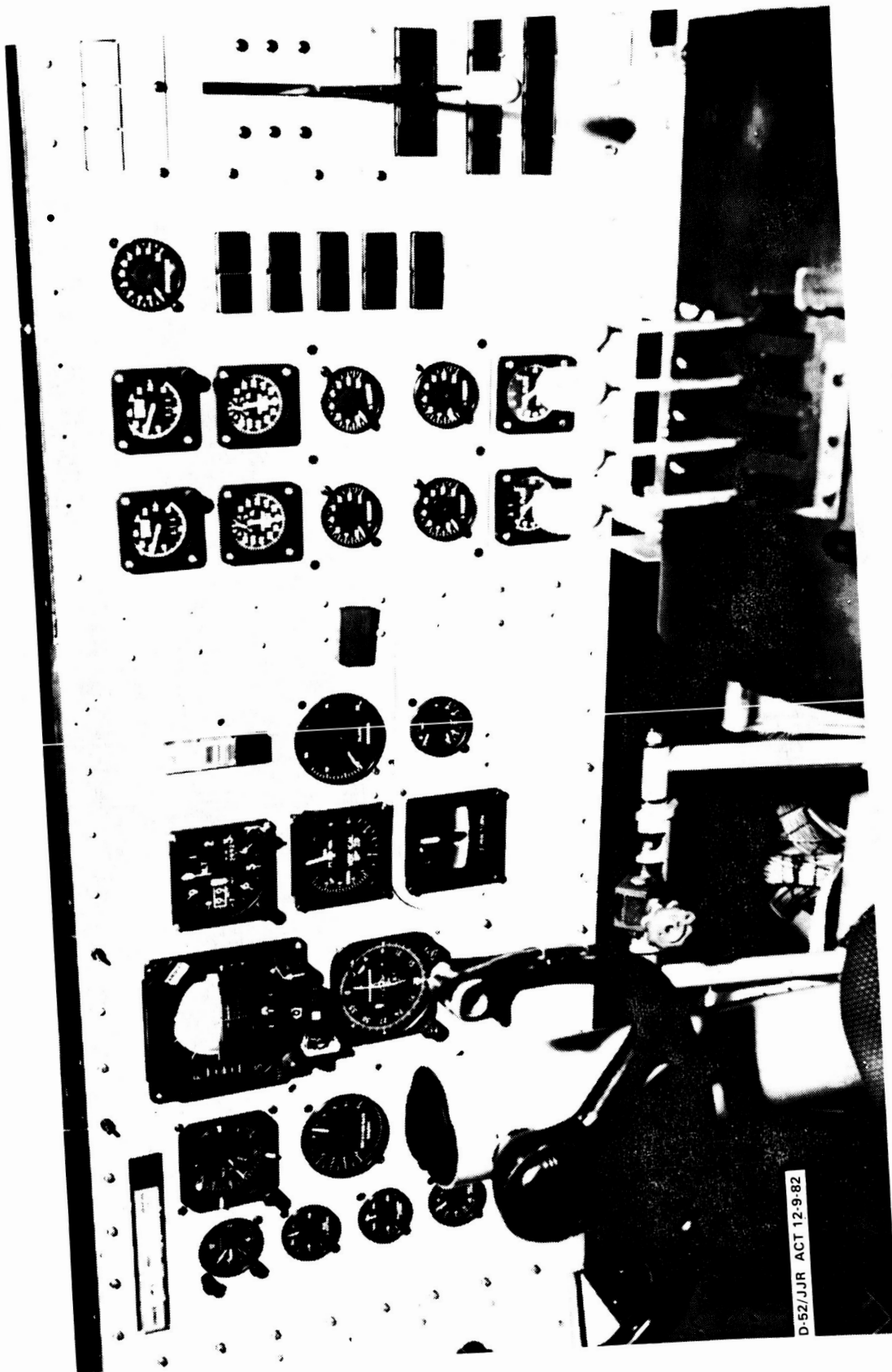


Figure 52. - NASA/Langley transport cockpit interior.



Figure 53. - NASA/Langley transport visual display.

ORIGINAL PAGE 19
OF POOR QUALITY

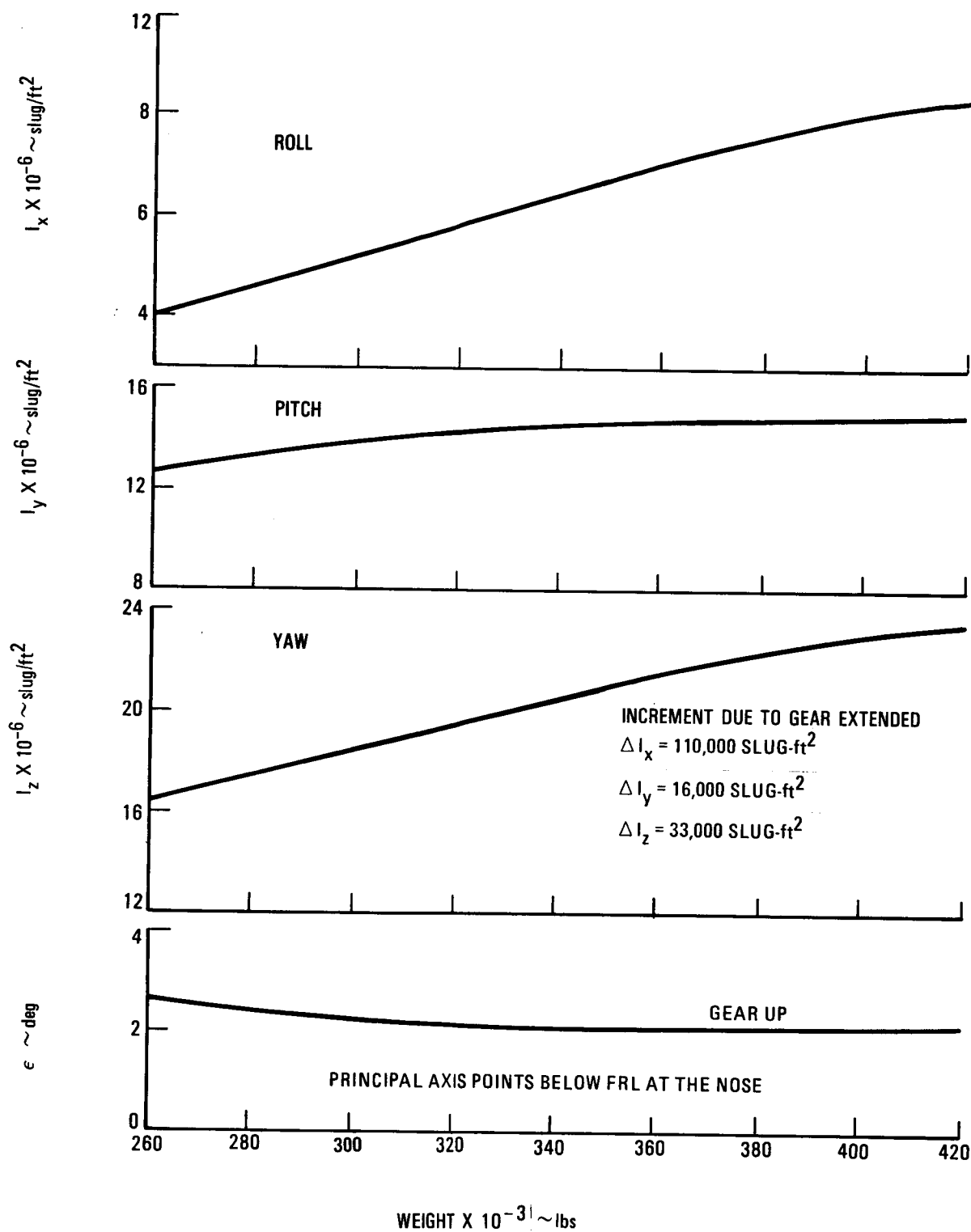


Figure 54. - L-1011 S/N 1001 weight/inertia characteristics.

ORIGINAL PAGE IS
OF POOR QUALITY

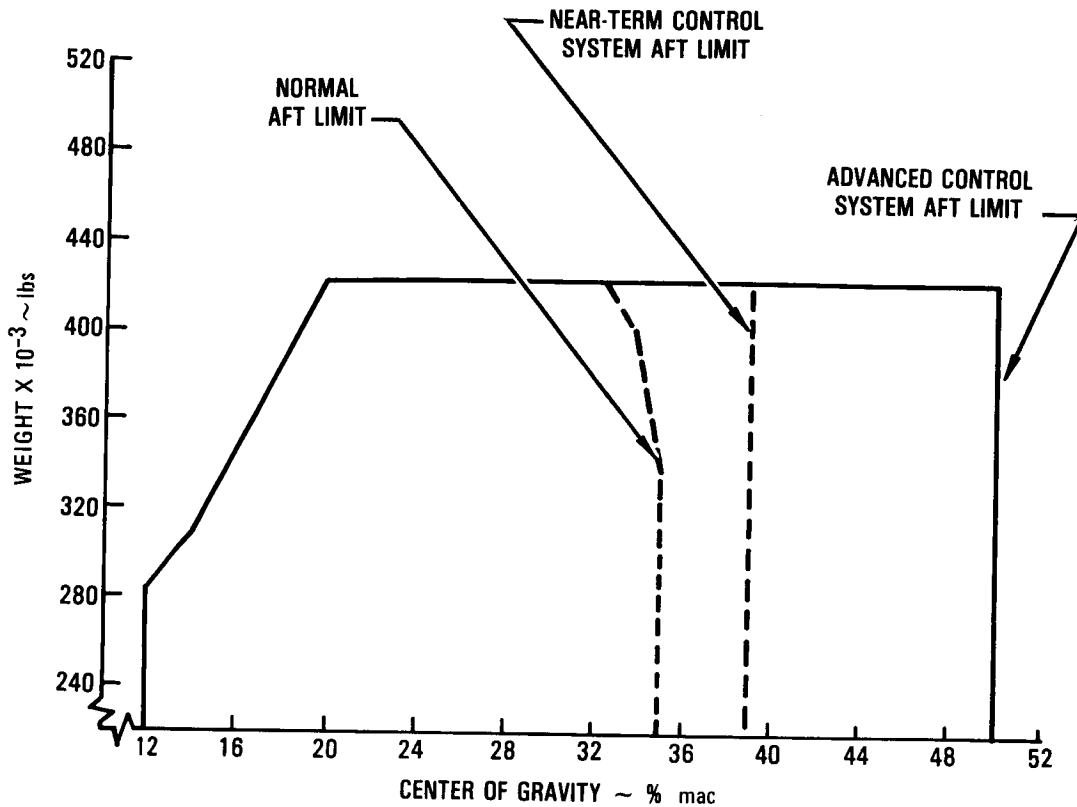


Figure 55. - L-1011 S/N 1001 weight/center-of-gravity envelope.

where

K_s = spring rate

K_d = detent spring rate

K_v = viscous friction

K_c = coulomb friction

$\frac{1}{K}$ = system mass

X_C = column position

F_C = column force

s = laplace operator

The spring rate is varied as a function of trim stabilizer position and Mach number as shown in Figure 50. Figure 57 presents a block diagram of the model which was used to generate the longitudinal column forces.

ORIGINAL PAGE IS
OF POOR QUALITY

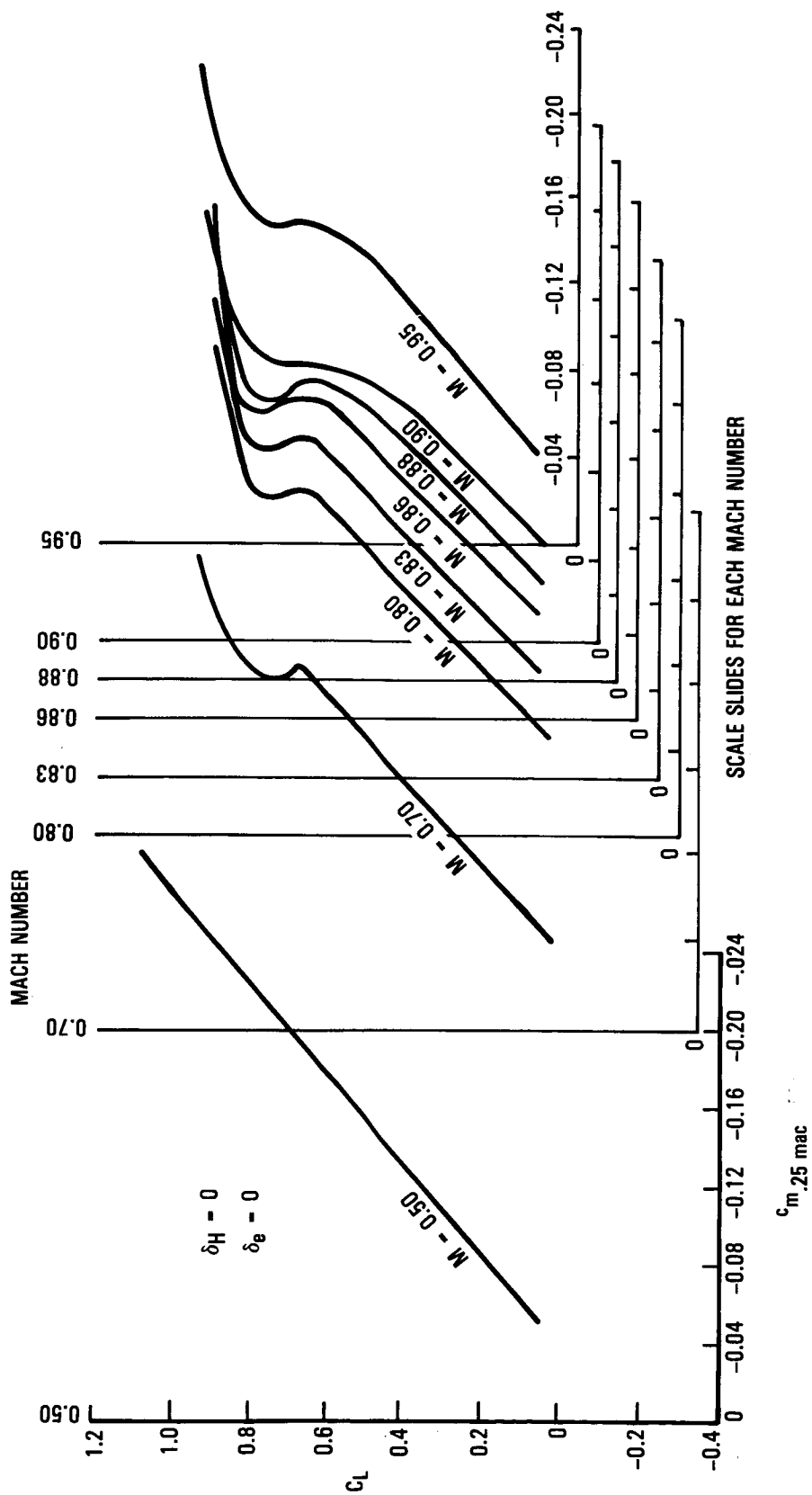


Figure 56. - L-1011-1 S/N 1001 high-speed pitching moment characteristics.

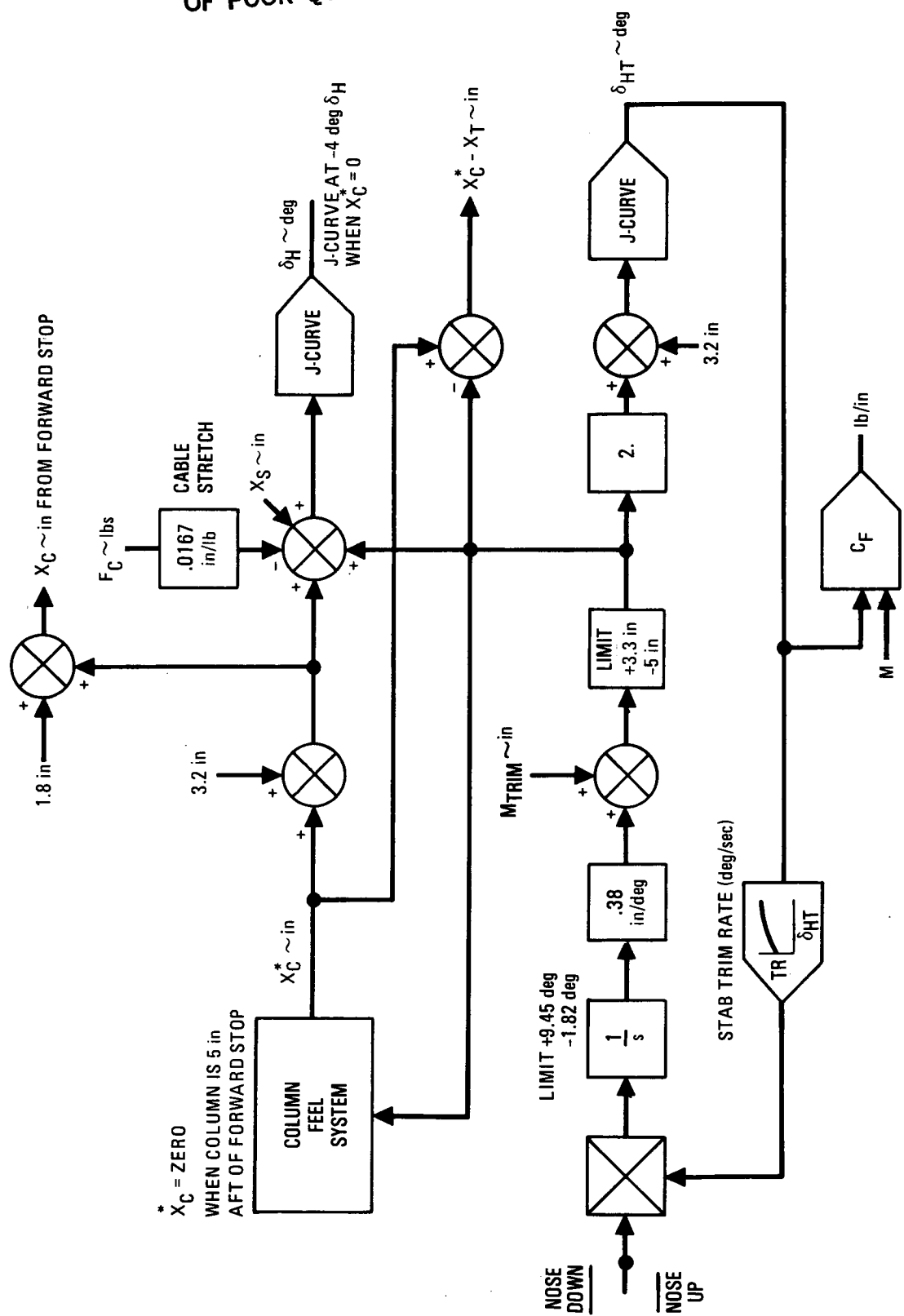


Figure 57. - Primary pitch trim system.

A block diagram of the lateral-directional control system is shown in Figure 58.

6.3 Flight Conditions

Specific flight conditions (Table 12) were selected for the simulation test. Simulation concentrated on regions of the flight envelope designated by the shaded areas in Figure 59. Stability characteristics of each flight condition are discussed in the following paragraphs.

Flight condition 10 is an average ($W/\delta = 1.4 \times 10^6$ lbs) cruise condition for commercial airline service. The L-1011 W/δ value of 1.4×10^6 lbs and Mach number of .83 represents a C_L value of .4. Since a constant C_L value is required to evaluate control characteristics, each flight condition 10 test was initiated at the same W/δ and Mach number values. Maneuver stability about trim is essentially linear at this flight condition. A region of reduced maneuver stability can be reached at high load factors. This condition can be considered a region of linear stability for small maneuvers with a region of nonlinear stability at high load factors.

Flight condition 15 is the maximum range cruise W/δ for the simulated aircraft. Stability characteristics at this flight condition are essentially the same as at the intermediate W/δ condition except that the region of nonlinear stability is encountered at a lower load factor.

Flight condition 7 is the highest W/δ at which the simulated aircraft can operate with a 1.3 g maneuver capability to buffet onset. The 1.3 g criterion is a typical aircraft operating restriction. This is a condition of non-linear stability caused by the wing aerodynamic flow separation which is perceived as buffet. The nonlinear region begins about 0.1 g from trim and is well into the unstable region of buffet onset which is 0.3 g.

Flight condition 16 is near the knee of the simulated aircraft maximum operational speed boundary (Figure 59). Because of the high dynamic pressure, the load factor to buffet onset is beyond the 2.5 g aircraft load factor limit. This condition can be considered a region of linear stability at high dynamic pressure.

Flight condition 17 is a typical intermediate-speed, flaps-up, holding pattern condition which is often encountered when approaching airports with heavy traffic. The condition provides linear stability at low dynamic pressure.

Flight condition 18 represents a typical landing configuration at normal approach speeds. The condition is characterized by linear stability characteristics.

Flight condition 19 represents the takeoff configuration for the second segment climb speed ($1.2 V_s$). Stability characteristics are linear at this condition.

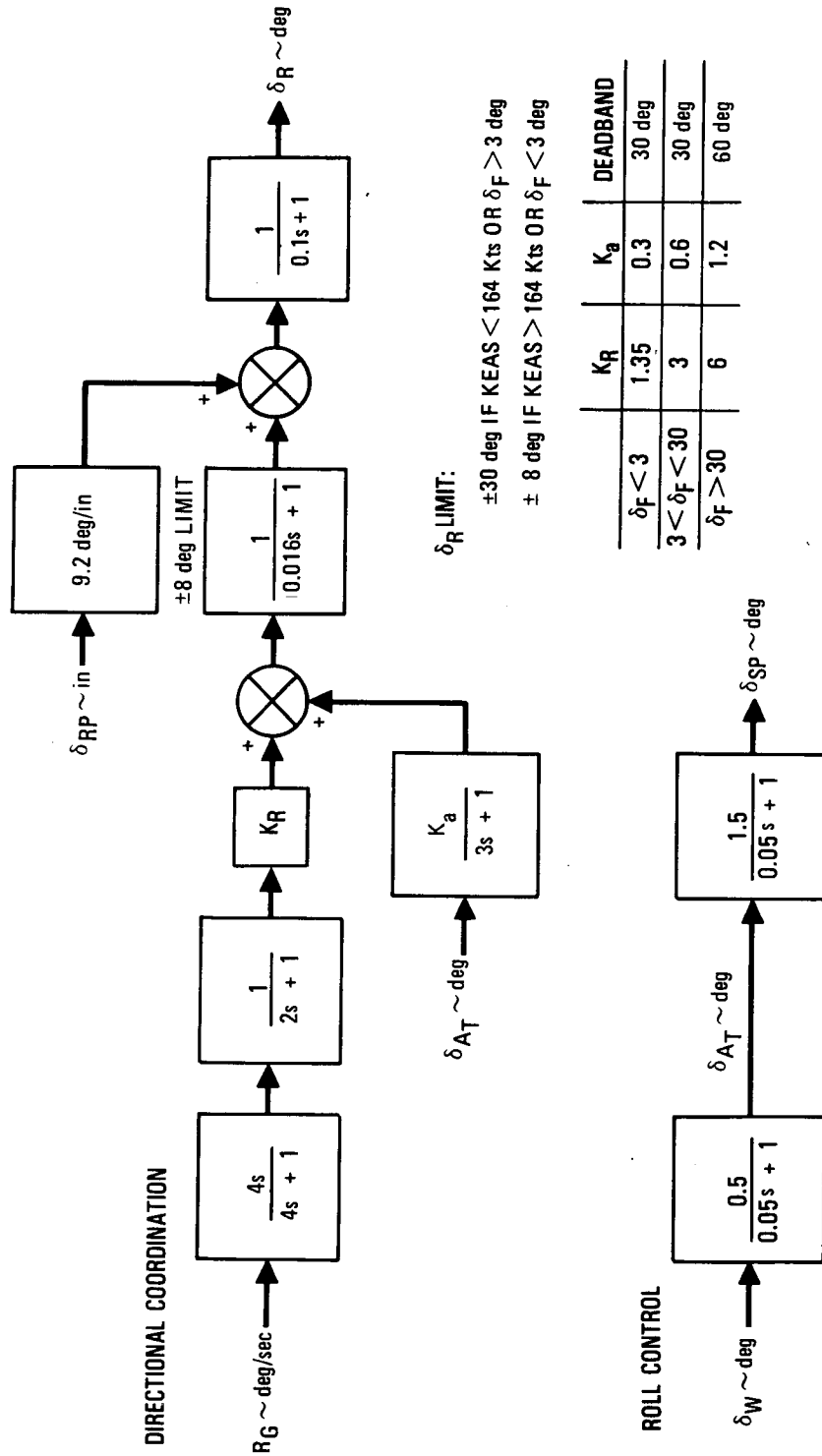


Figure 58. - Lateral-directional control system.

C 2

ORIGINAL PAGE IS
OF POOR QUALITY

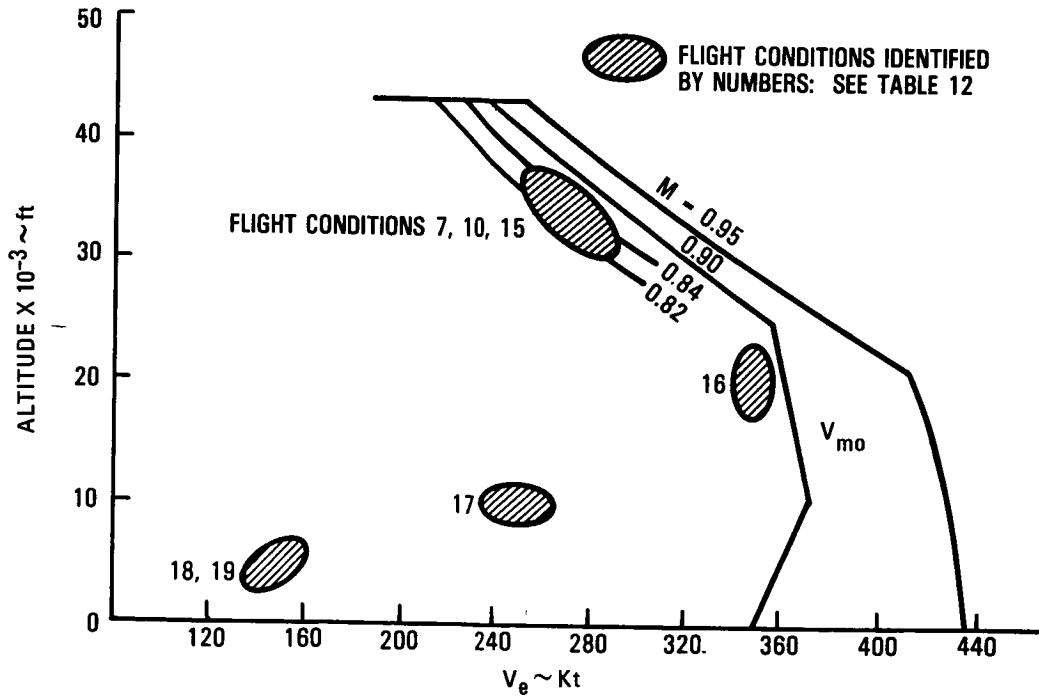


Figure 59. - Flight simulation test conditions.

The range of c.g. positions from 25% (positive 15% static stability margin) to 50% mac (negative 10% static stability margin) were covered for flying qualities evaluation of each flight condition. Also, c.g. positions to 60% mac were covered for flying qualities evaluation of some of the flight conditions.

The atmospheric conditions for each test condition were calm air and moderate turbulence ($\sigma = 4$ ft/sec rms at high speed and $\sigma = 6$ ft/sec rms at low speed).

6.4 Evaluation Tasks

The tasks performed in each flight regime were as follows:

Cruise

- Wind-up Turns: Wind-up turns were performed to evaluate maneuvering force and stability characteristics by stabilizing at increasing load factors.

- S-Pattern Turns: The aircraft was banked to a 4-minute turn attitude and flown through a 90 degree heading change while descending 500 feet. Then, the bank angle was reversed and the aircraft was turned back and rolled out on the initial heading while climbing 500 feet.
- Trimmability: The workload to initially trim the aircraft and to recapture trim from a disturbed condition was used as another measure of performance. The trim recapture was evaluated by advancing power to upset the aircraft altitude and flying back to the initial altitude without retrimming.
- Airline Operational Turns: 20 degree and 30 degree banked turns were performed while maintaining constant speed and using column force to control attitude and altitude. Turn entry and exit characteristics were also evaluated. This maneuver was limited to a 20 degree bank angle at a W/δ of 1.9×10^6 lbs because of the high angle-of-attack pitch divergence characteristics of the aircraft.
- Pitch Attitude Change: Attitude stability was evaluated by changing and holding a new pitch attitude with column force inputs.
- Power Effects: Power was advanced and retarded to restabilize the aircraft on a new pitch attitude while maintaining speed by holding column control force.
- Emergency Descent: Power was pulled back to idle and the nose was pushed over to start the aircraft descent. The aircraft was maneuvered into a banked turn after start of descent to increase drag.
- Short-Period Dynamic Stability: Short-period characteristics were evaluated by using quick forward and aft control column inputs and releasing the column to upset the aircraft from 1 g flight. Pitch attitude and load factor were observed while the aircraft returned to 1 g trim.
- Phugoid Dynamic Stability: The aircraft was displaced slightly from trim, and the phugoid damping and period were evaluated by observing excursions in rate of climb and pitch attitude.
- Static Stability: Longitudinal static stability, sometimes referred to as speed stability, was evaluated by determining the variation of column force with deviation from trim speed.

Maximum Operating Speed

- Tasks performed at maximum operational speeds included wind-up turns, operational turns, and trimmability. Descriptions of these tasks are similar to those for the cruise conditions.

Landing

- Wind-up Turns: Wind-up turns were conducted to evaluate maneuvering force characteristics by stabilizing at load factors up to 1.2 g.
- ILS Approach: The approach task was initialized 8 miles from the airport at 2000 feet above ground level with a 1000 foot lateral offset. The task entailed flying the airplane to the localizer, capturing the glide slope, and tracking the glide slope down to 50 feet. A few flares and touchdowns were attempted, but the pilots felt that this added nothing to the evaluation. The approaches were made on raw data displays.

Holding

- Airline Operational Turns: 30 degree banked turns were flown while maintaining speed and using column force to control attitude and altitude.

Takeoff

- 30 degree Heading Change: The takeoff condition was initialized with the aircraft climbing in the second segment configuration. Controllability was evaluated during 30 degree banked turns through 30 degree heading changes.

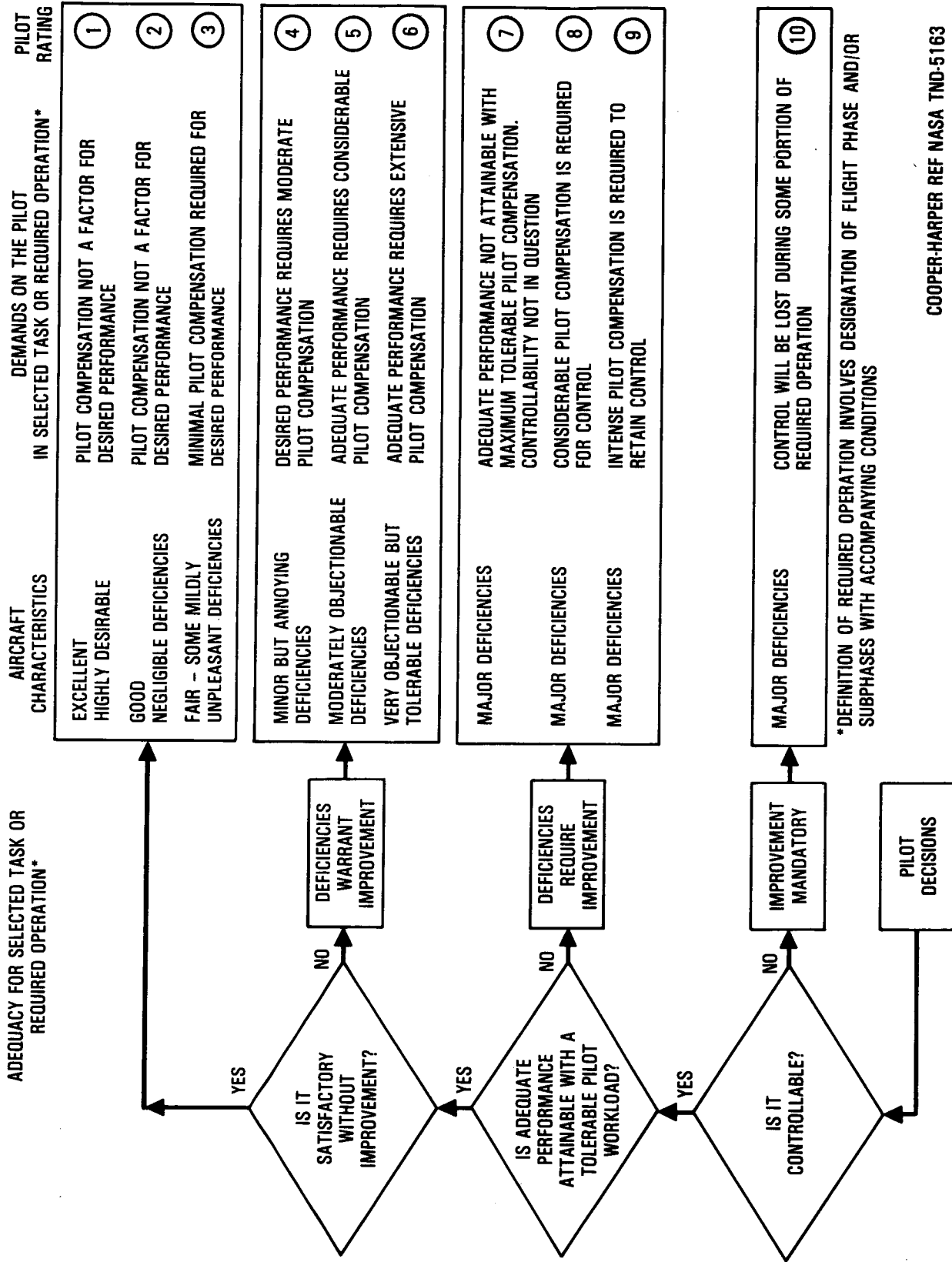
6.5 Evaluation Guidelines

Flying qualities of the aircraft were evaluated in terms of the Cooper-Harper pilot rating scale defined in Figure 60. In this report ratings 1 to 3.5 are designated as satisfactory, ratings 3.6 to 6.5 are unsatisfactory, and ratings 6.5 to 10 are unacceptable. Satisfactory/unsatisfactory and unsatisfactory/unacceptable divisions are shown on each of the rating charts at 3.5 and 6.5 respectively. Any rating higher than 3.5 indicates that improvements in the flying qualities are desired.

Basic flight parameters were recorded on analog strip charts with the PACS on and off and compared to show benefits achieved by engaging the PACS.

6.6 Simulation Test Results

Results of the simulation test show that the PACS fulfills the function for which it was designed. Pilot ratings indicate that flying qualities of the PACS configured aircraft with the c.g. at 50% mac are as good as the baseline aircraft with c.g. at 25% mac. The results are most impressive at high-speed conditions where handling qualities of the baseline aircraft quickly degrade to unacceptable levels (pilot ratings $>6-1/2$) for c.g. positions aft of 40% mac. Data for the PACS configured aircraft show satisfactory ratings (pilot ratings $\leq 3-1/2$) for c.g. position to 50% mac and very little degradation occurs when the c.g. is moved from 50 to 60% mac.



COOPER-HARPER REF NASA TND-5163

Figure 60. - Handling qualities rating scale.

Results of the simulation are presented for each flight condition in the following sections.

6.6.1 Flight Condition 10: Mid Altitude Cruise. - Flight condition 10 was evaluated by five pilots. However, all c.g. positions, which covered the range from 25 percent to 60 percent mac, were not tested by all of the pilots. Pilot ratings for the c.g. positions tested by each pilot in calm air and moderate turbulence conditions are presented in Figures 61 and 62 respectively. The solid symbols show ratings for the baseline aircraft (PACS off) and the open symbols show ratings for the PACS configured aircraft (PACS on).

The baseline aircraft ratings for the calm air and turbulence conditions showed unacceptable flying qualities for c.g. positions of 40 percent and aft. The wide scatter in ratings at 39% is due to the sensitivity of the pilot in judging the onset of unacceptable flying qualities. Engagement of the PACS in calm air showed satisfactory flying over the entire c.g. range of 25 percent to 60 percent mac. Flying qualities in moderate turbulence were not as good as in calm air but were considered to be satisfactory for c.g. positions to 55 percent mac. At a c.g. position of 60 percent mac, the ratings showed the flying qualities to be unsatisfactory.

Pilot comments were evaluated to determine specific flying quality characteristics for each c.g. position. An example of the pilot comments for Flight Condition 10 in calm air is given in Table 13.

6.6.2 Flight Condition 15: Maximum Range Cruise. - Flight condition 15 was evaluated by Pilot 5. The Cooper-Harper ratings for calm air and moderate turbulence are presented in Figures 63 and 64 respectively.

The baseline aircraft flying qualities degrade rapidly aft of 40 percent mac. Engagement of the PACS in calm air provides a rating that is near the satisfactory/unsatisfactory boundary for the entire c.g. range. In turbulence with the PACS on, ratings are about the same over the c.g. range but are not as good as for the calm air ratings.

6.6.3 Flight Condition 7: High W/δ Cruise. - Flight condition 7 was evaluated by three pilots. The Cooper-Harper ratings for calm air and moderate turbulence are presented in Figures 65 and 66 respectively.

Flight condition 7 was the least stable of the three cruise conditions due to the close proximity of the nonlinear static stability flight region. This reduced stability is reflected in the rapid degrading of the baseline aircraft flying qualities. Engaging the PACS in calm air provided satisfactory flying qualities to 50 percent mac and near satisfactory flying qualities at

ORIGINAL PAGE IS
OF POOR QUALITY

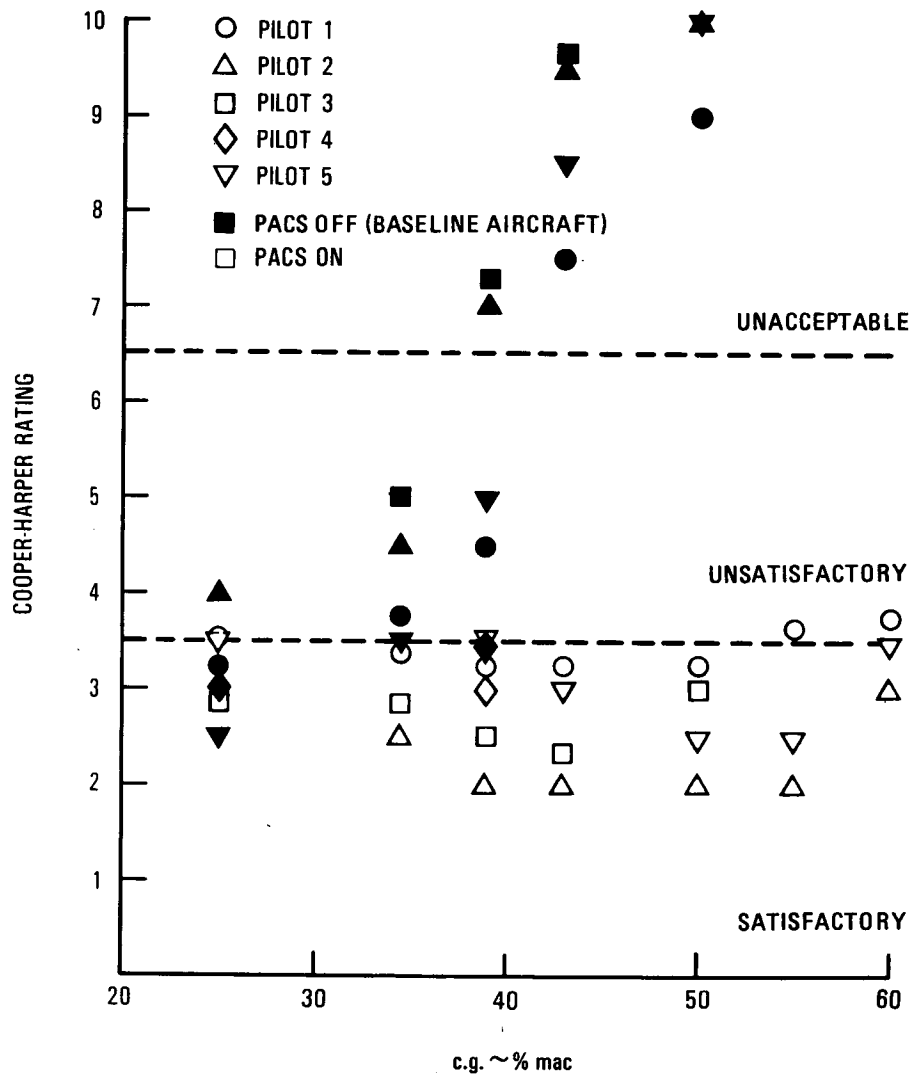


Figure 61. - Cooper-Harper rating for
Flight Condition 10, calm air.

ORIGINAL PAGE IS
OF POOR QUALITY

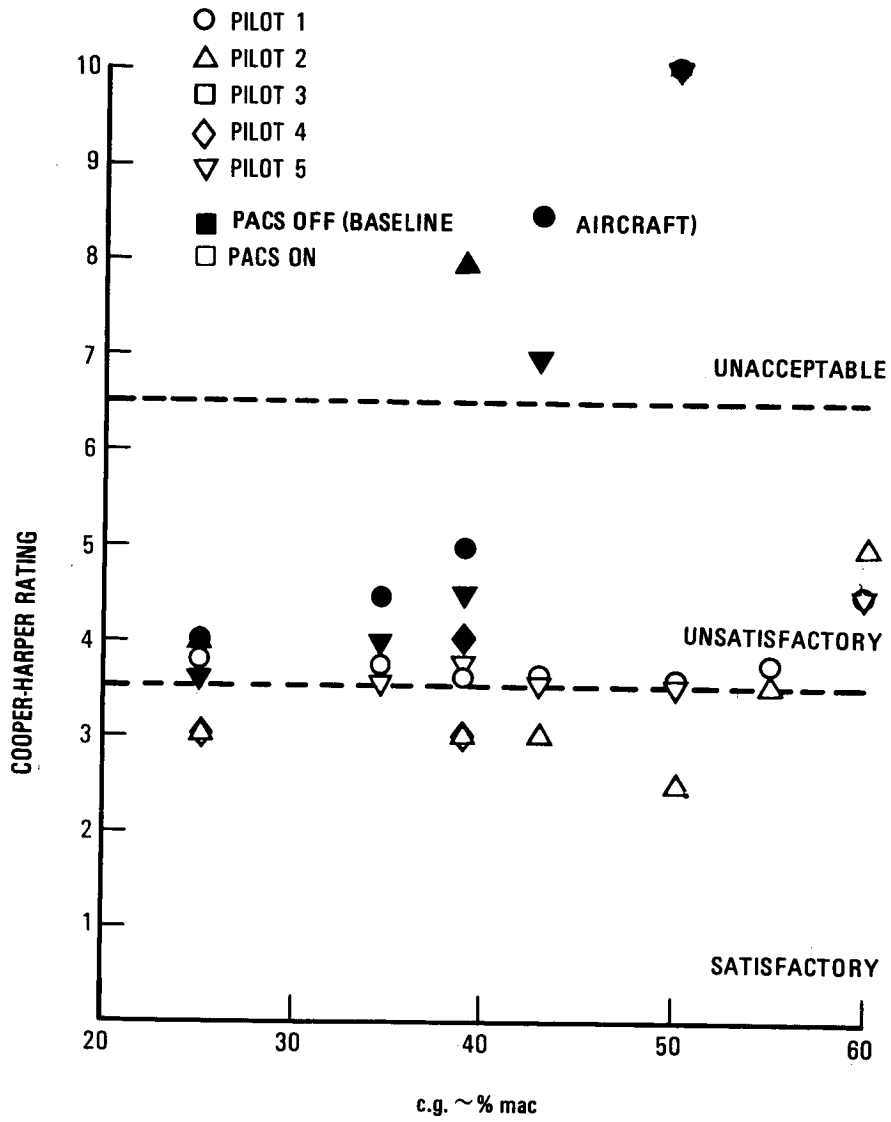


Figure 62. - Cooper-Harper rating for flight condition 10, moderate turbulence.

TABLE 13. PILOT COMMENTS, FLIGHT CONDITION 10, CALM AIR

c.g. Position	PACS Off	PACS On
25%	<ul style="list-style-type: none"> ● Trimmability was good. ● Altitude hold was ± 20 feet in 20 degree banked turns. ● Stability about trim was good and column forces were acceptable. ● High column forces during large maneuvers made control difficult. ● Short-period mode was well damped. ● Pitch attitude response was crisp and there was no bobble around the new attitude. 	<ul style="list-style-type: none"> ● PACS improved attitude control but forces to maneuver around trim were heavier. ● Column forces were objectionably high during large maneuvers. ● Short period mode was more heavily damped.
34.5%	<ul style="list-style-type: none"> ● Trimmability was degraded. ● Altitude hold was ± 40 feet in 20 degree banked turns. ● Force lightening was apparent at about 1.8 g. ● Short-period mode damping was good. ● Phugoid mode was divergent. ● Airplane appeared looser and precise control was more difficult. 	<ul style="list-style-type: none"> ● Altitude hold was ± 30 feet in 20 degree banked turns. ● Forces were higher but the airplane was much easier to control since it appeared more stable.
39%	<ul style="list-style-type: none"> ● Trimmability was difficult. ● Altitude hold was ± 50 feet in 20 degree banked turns. ● Significant force lightening was observed at high load factors. ● Forces were too light. ● Short-period mode was reasonably damped. ● Phugoid mode was rapidly divergent. ● Pitch attitude oscillations were observed. ● Considerable pilot attention was required. 	<ul style="list-style-type: none"> ● Trimmability was significantly improved. ● Forces were heavier and maneuvering characteristics were improved. ● Attitude control was improved.
43%	<ul style="list-style-type: none"> ● Controllability was marginal. ● Trimmability was very difficult. ● Altitude hold was ± 150 feet in 20 degree banked turns. ● ± 0.5 g oscillations occurred during 20 degree banked turns. ● Large maneuvers were no longer considered possible. 	<ul style="list-style-type: none"> ● Trimmability was excellent. ● Forces and controllability in turns and high-g maneuvers were good.

ORIGINAL PAGE 19
OF POOR QUALITY

TABLE 13. PILOT COMMENTS, FLIGHT CONDITION 10, CALM AIR (Continued)

c.g. Position	PACS Off	PACS On
50%	<ul style="list-style-type: none"> ● Airplane was no longer considered flyable. 	<ul style="list-style-type: none"> ● Same comments as PACS On at 43% mac.
55%	<ul style="list-style-type: none"> ● Not flyable 	<ul style="list-style-type: none"> ● Altitude control was slightly looser than at 50% mac.
60%	<ul style="list-style-type: none"> ● Not flyable 	<ul style="list-style-type: none"> ● Altitude control noticeably looser. ● Nose wandering occurred during S turns. ● Aware of reduced forces around 1.8 g. ● Control sensitivity was increased because of reduced stability and lighter forces.

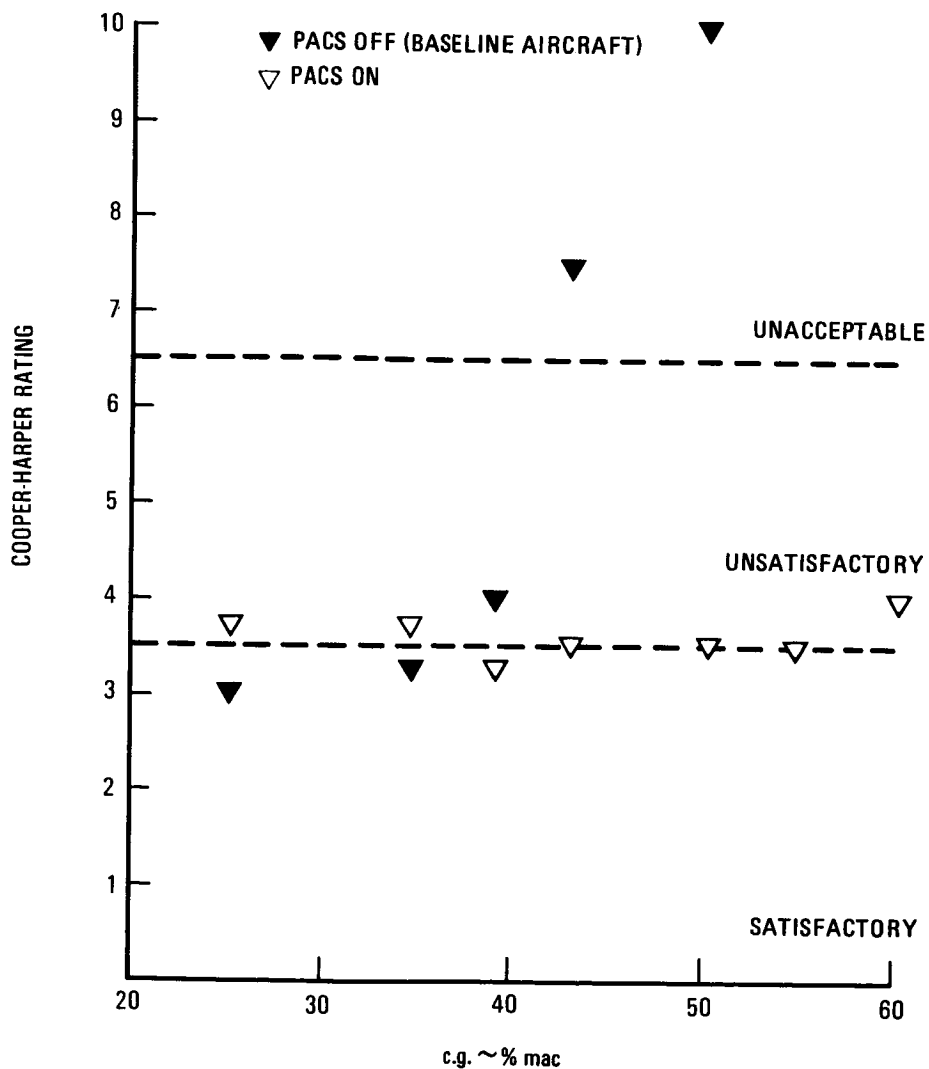


Figure 63. - Pilot 5 Cooper-Harper rating for flight condition 15, calm air.

ORIGINAL PAGE IS
OF POOR QUALITY

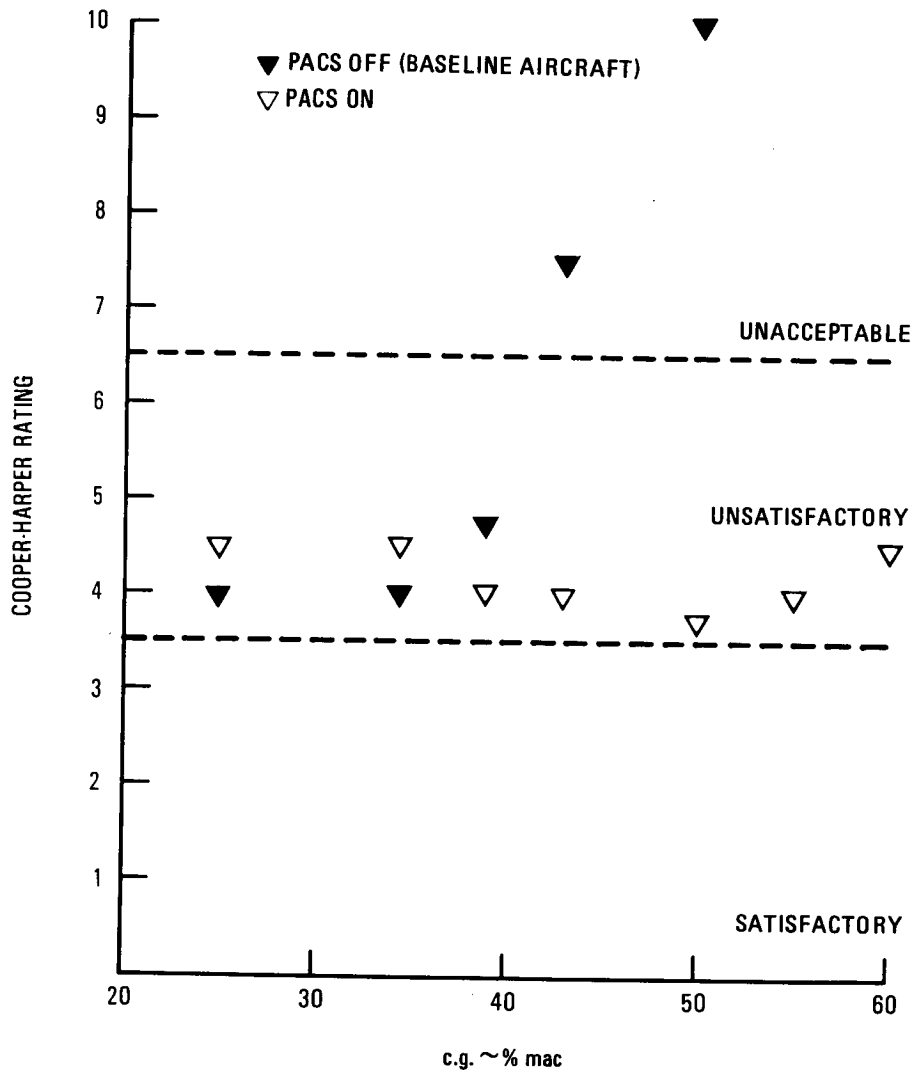


Figure 64. - Pilot 5 Cooper-Harper rating for flight condition 15, moderate turbulence.

ORIGINAL PAGE IS
OF POOR QUALITY

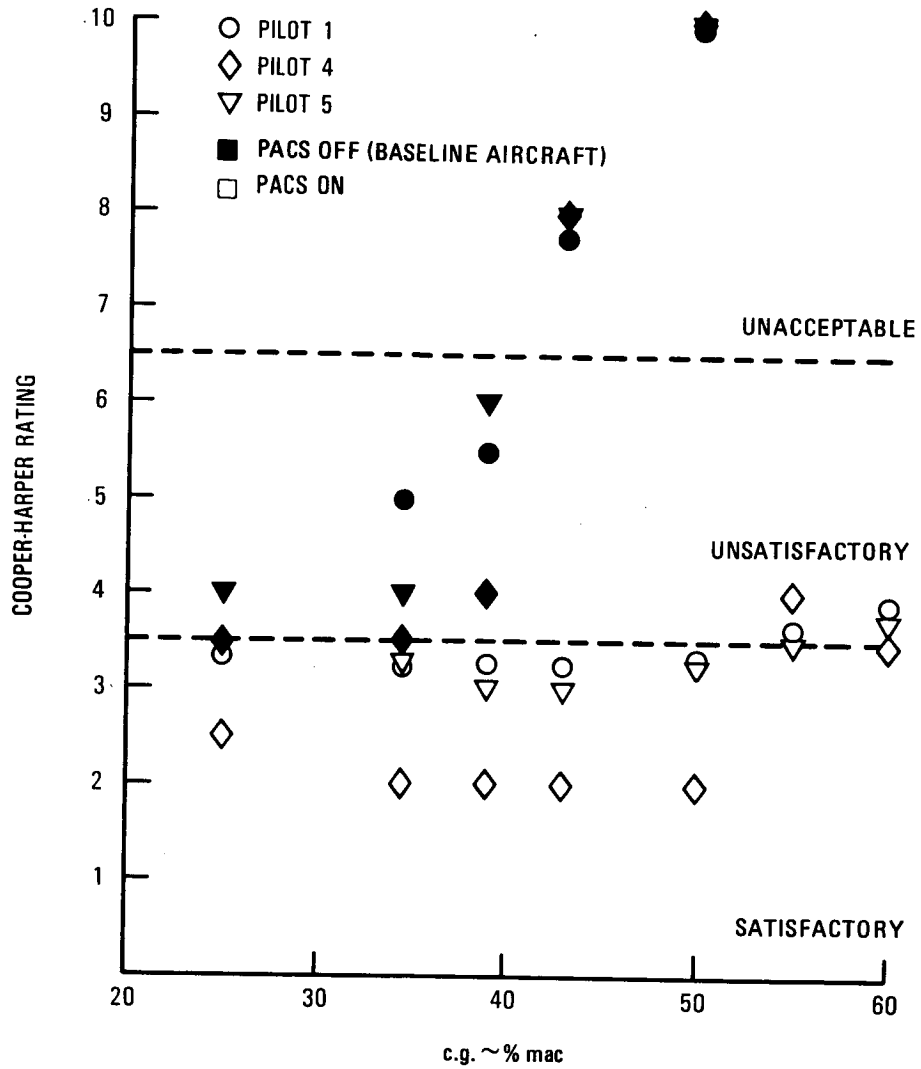


Figure 65. - Cooper-Harper rating for flight condition 7, calm air.

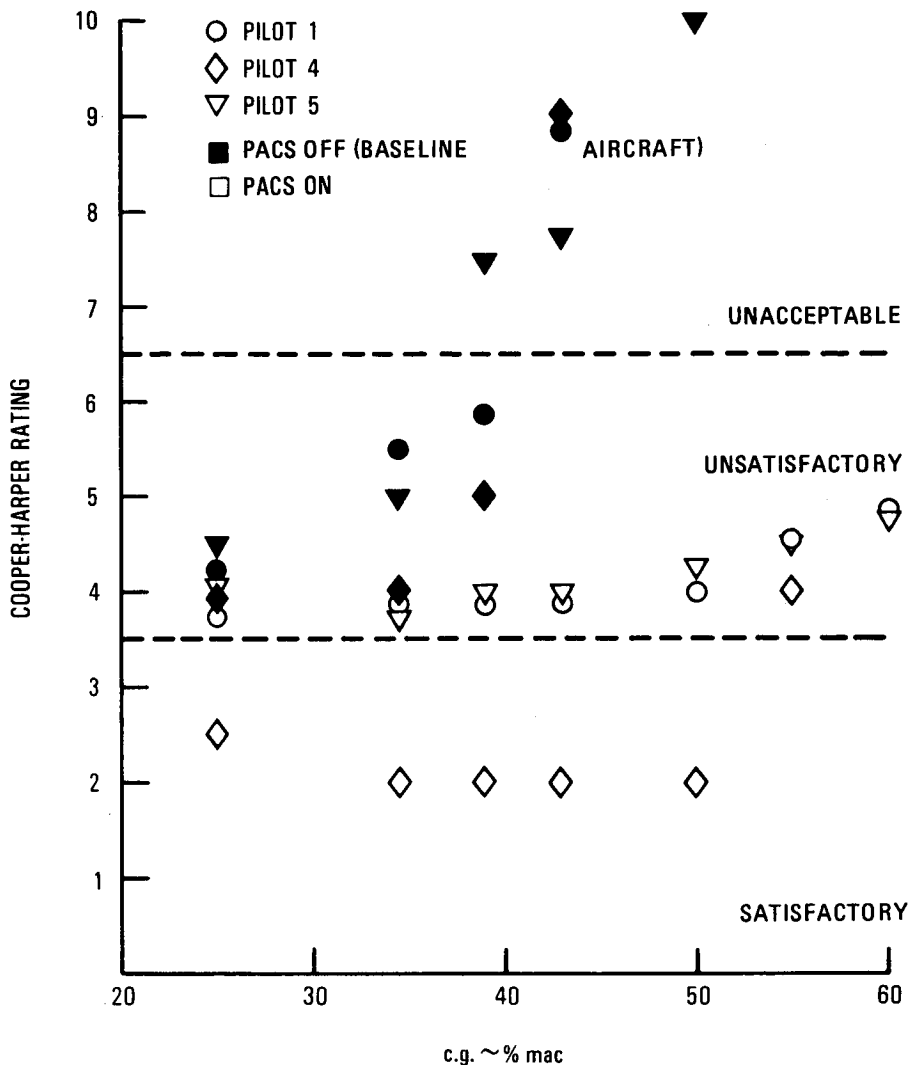


Figure 66. - Cooper-Harper rating for flight condition 7, moderate turbulence.

55 percent and 60 percent mac. The turbulence ratings indicate a trend toward degraded flying qualities at the 55 percent and 60 percent mac c.g. positions. Pilot 4 ratings were satisfactory in calm air and turbulence to the 50 percent mac c.g. position which he evaluated.

Pertinent parameters were recorded on strip charts during the pilot evaluations. Three strip chart segments have been selected to illustrate the difference between the baseline and PACS configured aircraft for the Pilot 1 evaluation of flying condition 7. Figures 67 through 69 compare the flight characteristics at c.g. positions of 39%, 43%, and 50% mac respectively.

ORIGINAL PAGE IS
OF POOR QUALITY

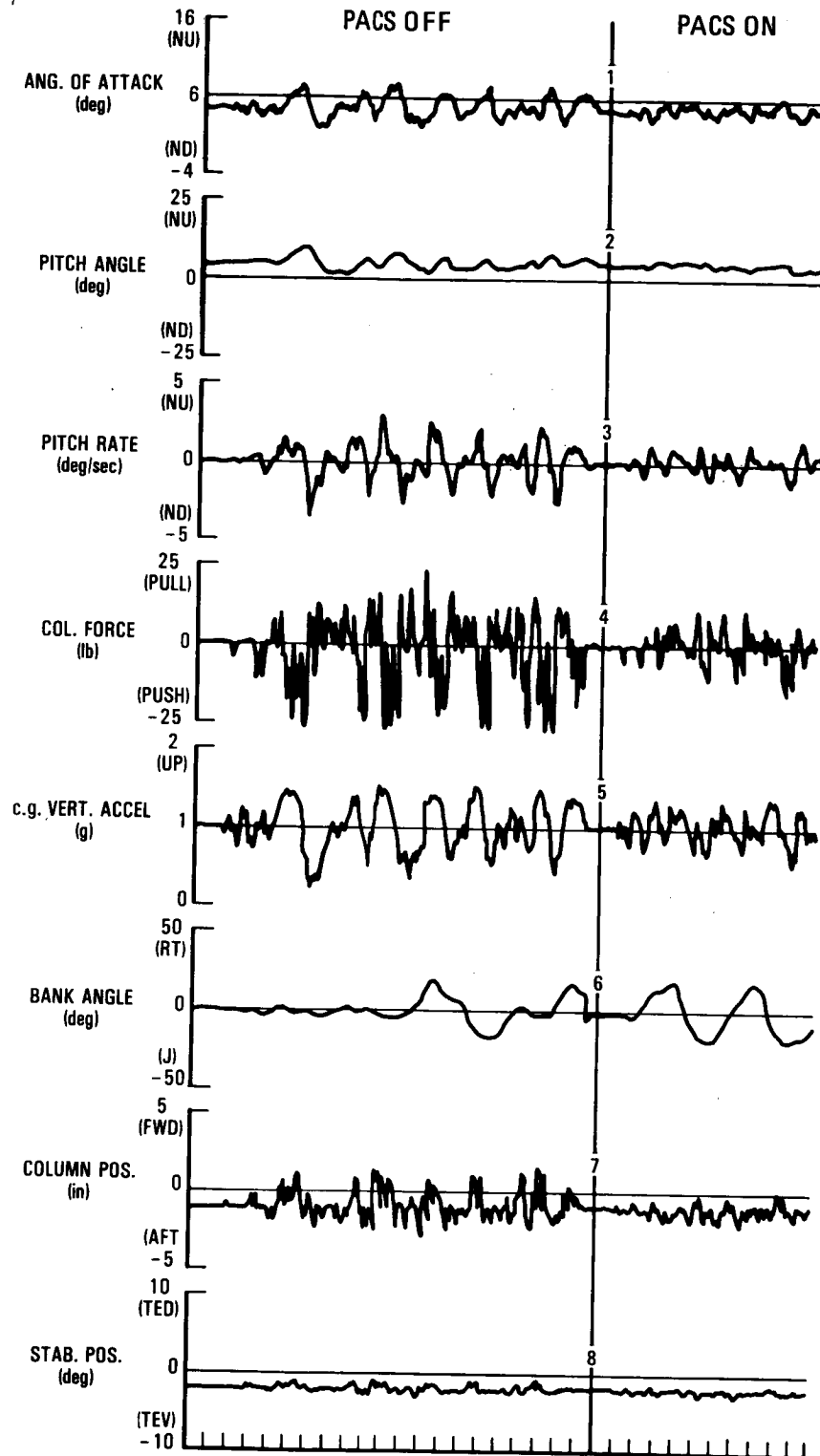


Figure 67. - Flight condition 7 comparison of damping response characteristics with PACS on and off, c.g. at 39 percent mac.

ORIGINAL COPY IS
OF POOR QUALITY

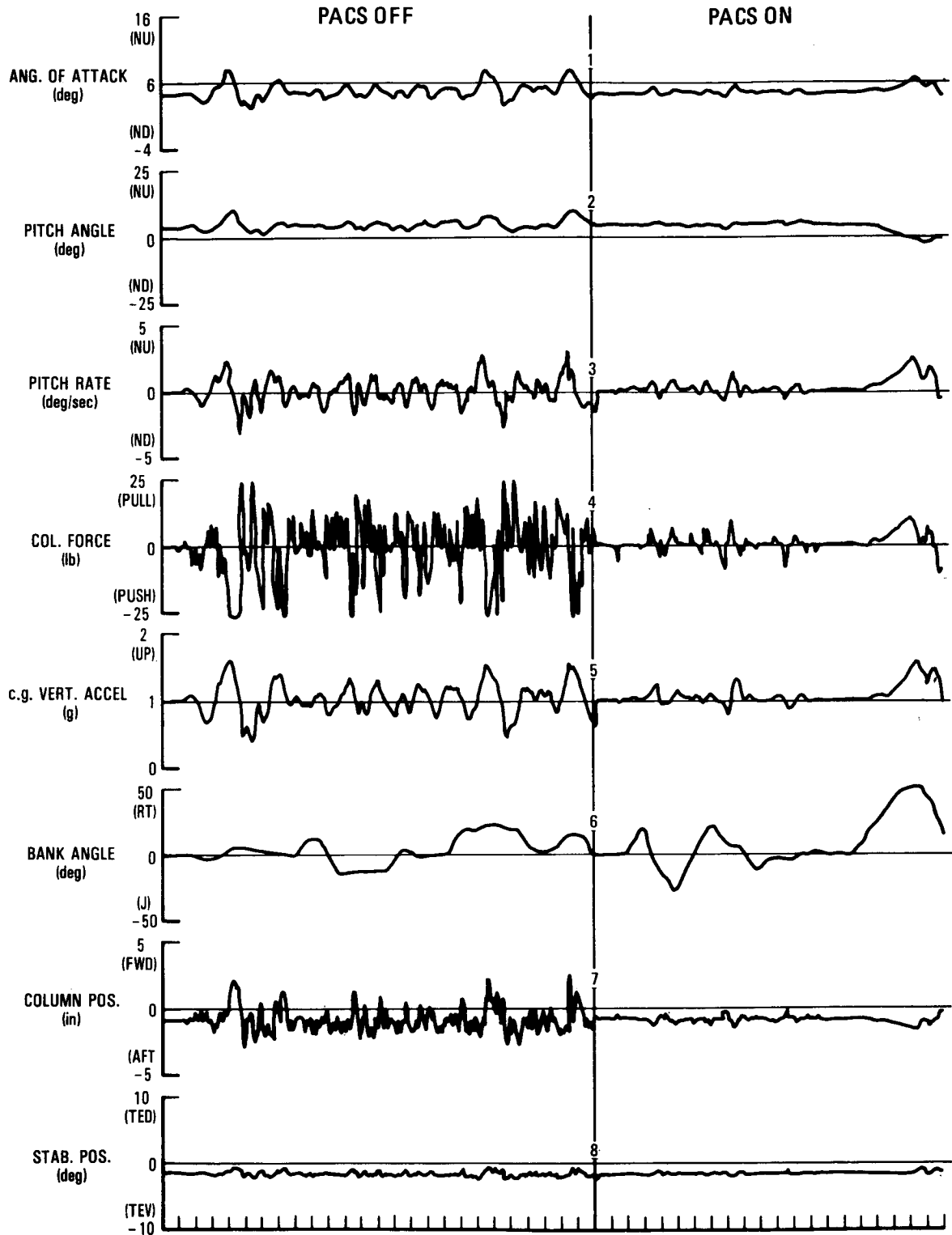


Figure 68. - Flight condition 7 comparison of damping response characteristics with PACS on and off, c.g. at 43 percent mac.

ORIGINAL PAGE IS
OF POOR QUALITY

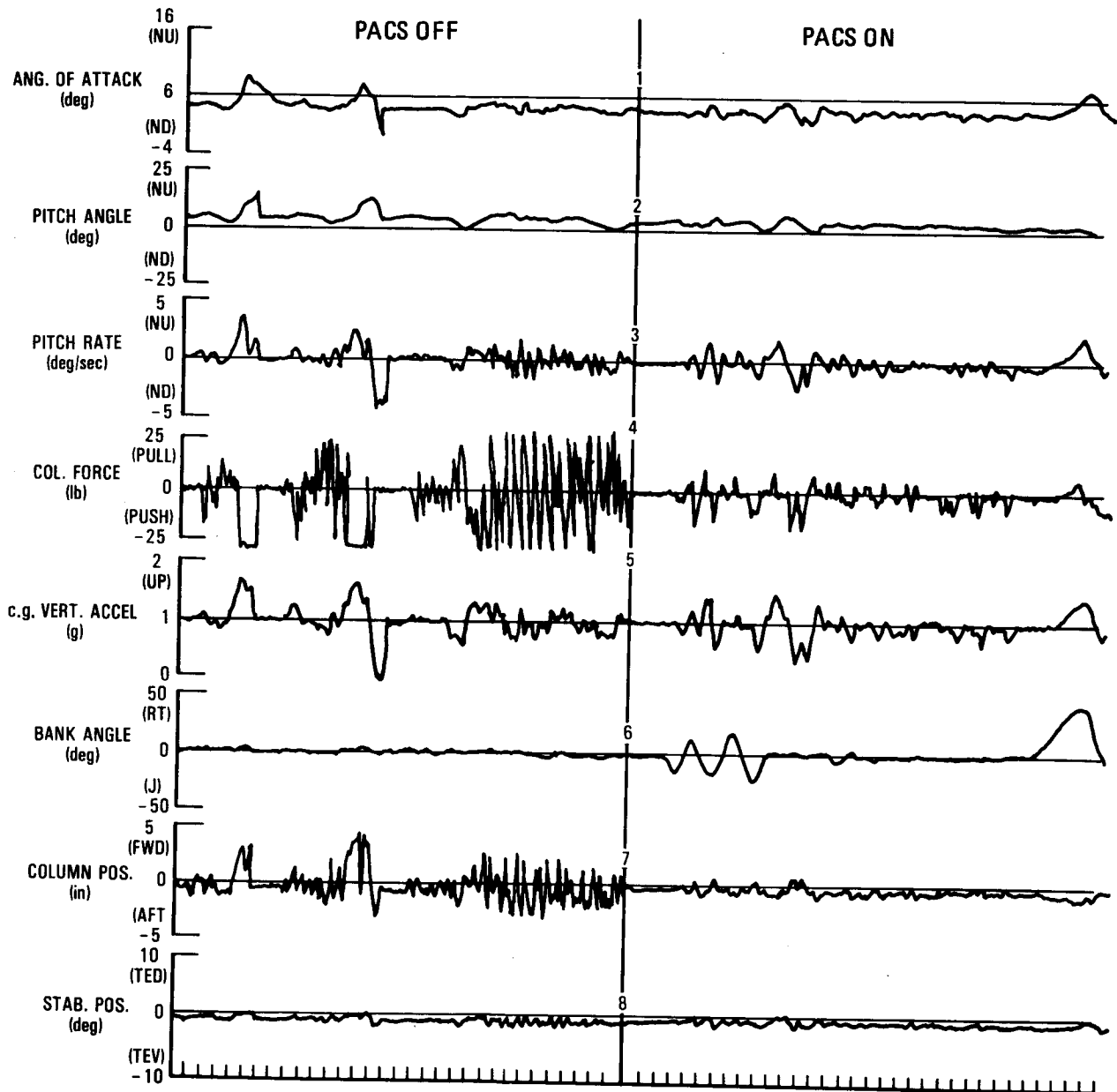


Figure 69. - Flight condition 7 comparison of damping response characteristics with PACS on and off, c.g. at 50 percent mac.

The 39 percent mac condition (Figure 67) was flown in moderate (4 fps RMS) turbulence only for shallow banked turns. In each instance the airplane was first evaluated with PACS off, after which the PACS was engaged and the evaluation was repeated. The pilot workload shown by the control force was high and excursions in c.g. normal acceleration were approaching ± 0.5 g with the PACS disengaged. After engaging the PACS, the c.g. vertical acceleration excursion and the control column input forces were less than half.

Figure 68 shows the evaluation at a c.g. of 43 percent mac in calm air. With PACS disengaged the workload was about the same as the c.g. of 39 percent mac in turbulence. Again only shallow banked turns were attempted. With the PACS engaged the pilot workload was dramatically reduced and the pilot comfortably rolled into a 30 degree banked turn.

Figure 69 shows the evaluation in calm air with the c.g. at 50% mac. With PACS disengaged the aircraft was difficult to control and large, rapid, cyclic, control column inputs were required to fly level. The PACS was engaged and the airplane could be comfortably rolled into a 30 degree banked turn.

6.6.4 Flight Condition 16: High Speed

Flight condition 16 was evaluated by three pilots in calm air and by one pilot in moderate turbulence (4 ft/sec rms). The Cooper-Harper ratings for calm air and moderate turbulence are presented in Figures 70 and 71 respectively. The PACS on ratings showed satisfactory flying qualities for the calm air condition and near satisfactory for the turbulence condition.

6.6.5 Flight Condition 18: Landing

Flight condition 18 was evaluated by three pilots in calm air and moderate turbulence (6 ft/sec rms) for the c.g. range of 25 percent to 50 percent mac. The aft c.g. position was limited to 50 percent by the nose-down authority of the trim system. The ratings are presented in Figures 72 and 73.

The baseline aircraft flying qualities in calm air were near the satisfactory/unsatisfactory rating line over the entire c.g. range. Engagement of the PACS did not show significant improvements in the flying qualities.

The baseline aircraft Cooper-Harper ratings for turbulence conditions were scattered throughout the unsatisfactory rating band. Engagement of the PACS reduced the scatter and indicated some improvement of the flying qualities.

6.6.6 Flight Condition 17: Holding

Flight condition 17 was evaluated by pilot 5. Ratings in calm air and moderate turbulence (4 ft/sec rms) are presented in Figures 74 and 75 respectively.

ORIGINAL PAGE IS
OF POOR QUALITY

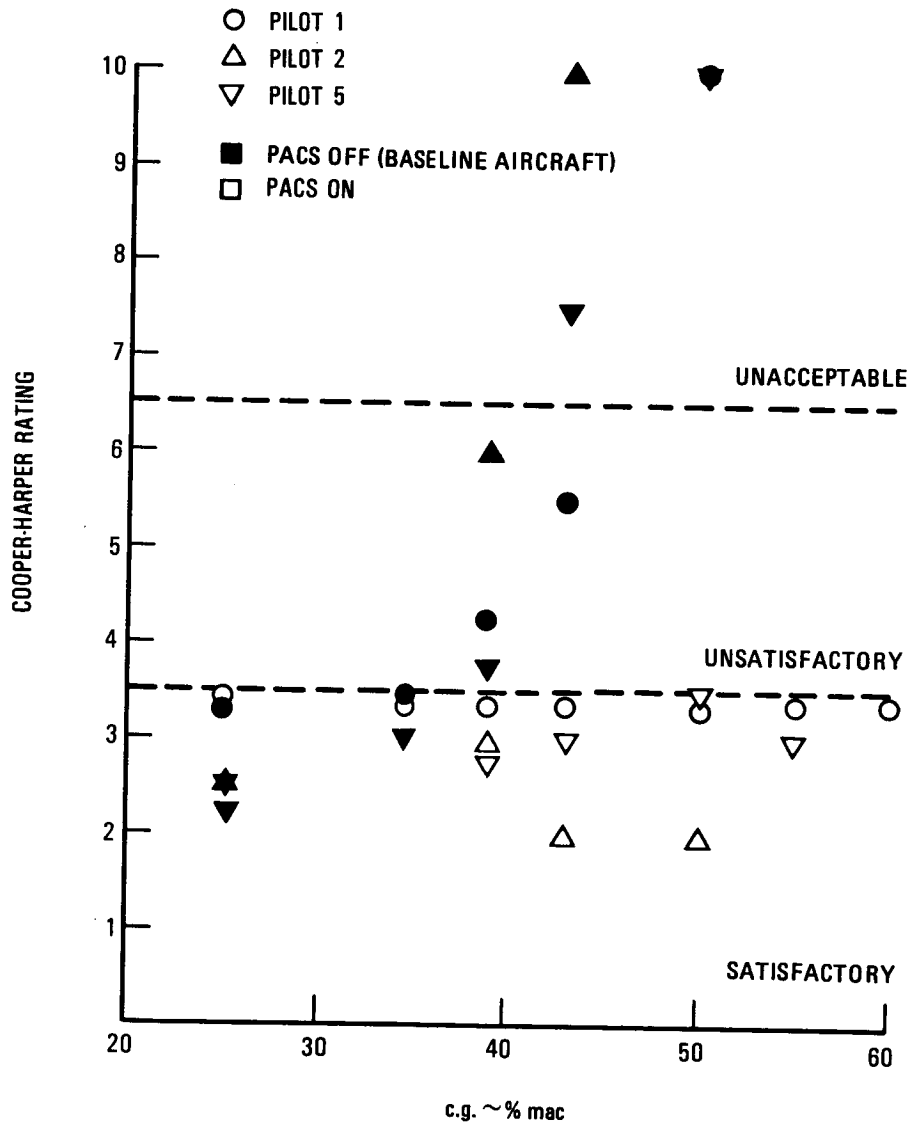


Figure 70. Cooper-Harper rating for flight condition 16, calm air.

ORIGINAL PAGE IS
OF POOR QUALITY

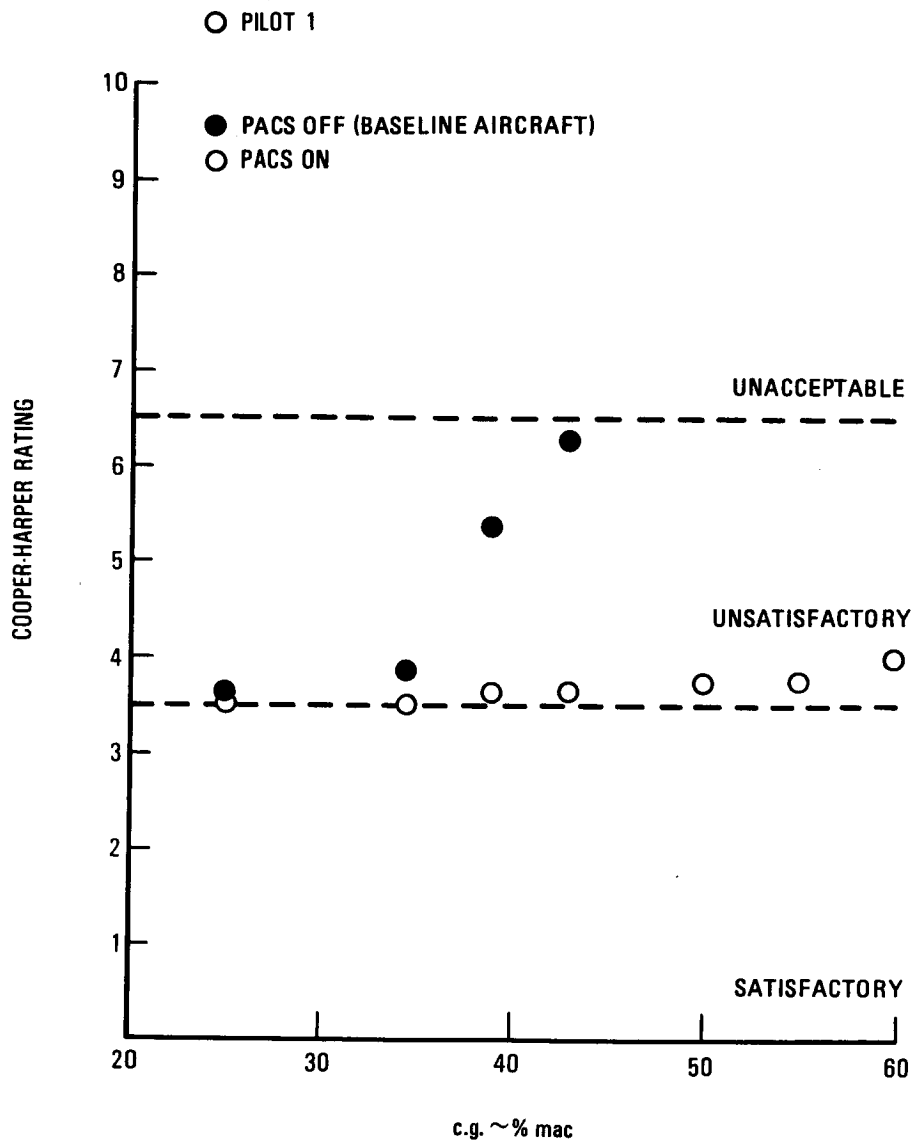


Figure 71. - Cooper-Harper rating for flight condition 16, moderate turbulence.

ORIGINAL PAGE IS
OF POOR QUALITY

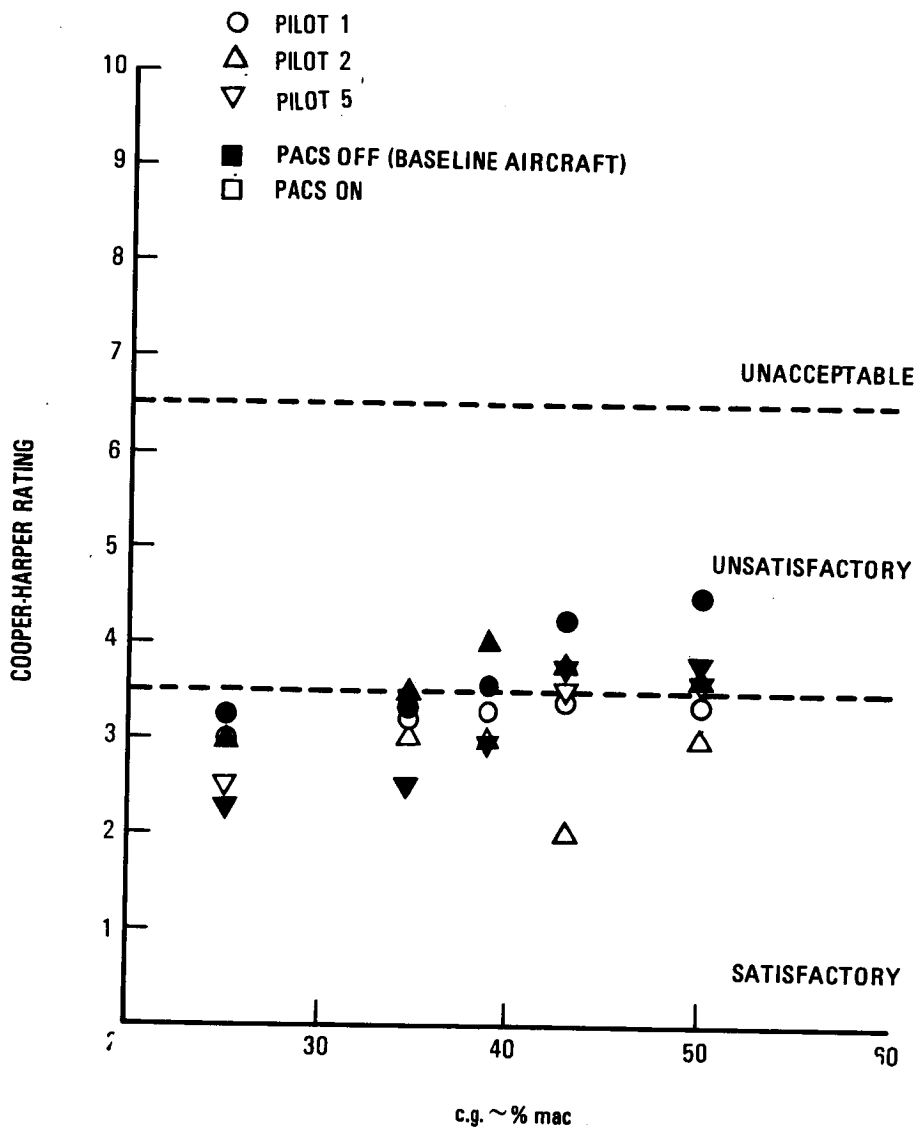


Figure 72. - Cooper-Harper rating for flight condition 18, calm air.

ORIGINAL PART 19
OF PGOR QUALITY

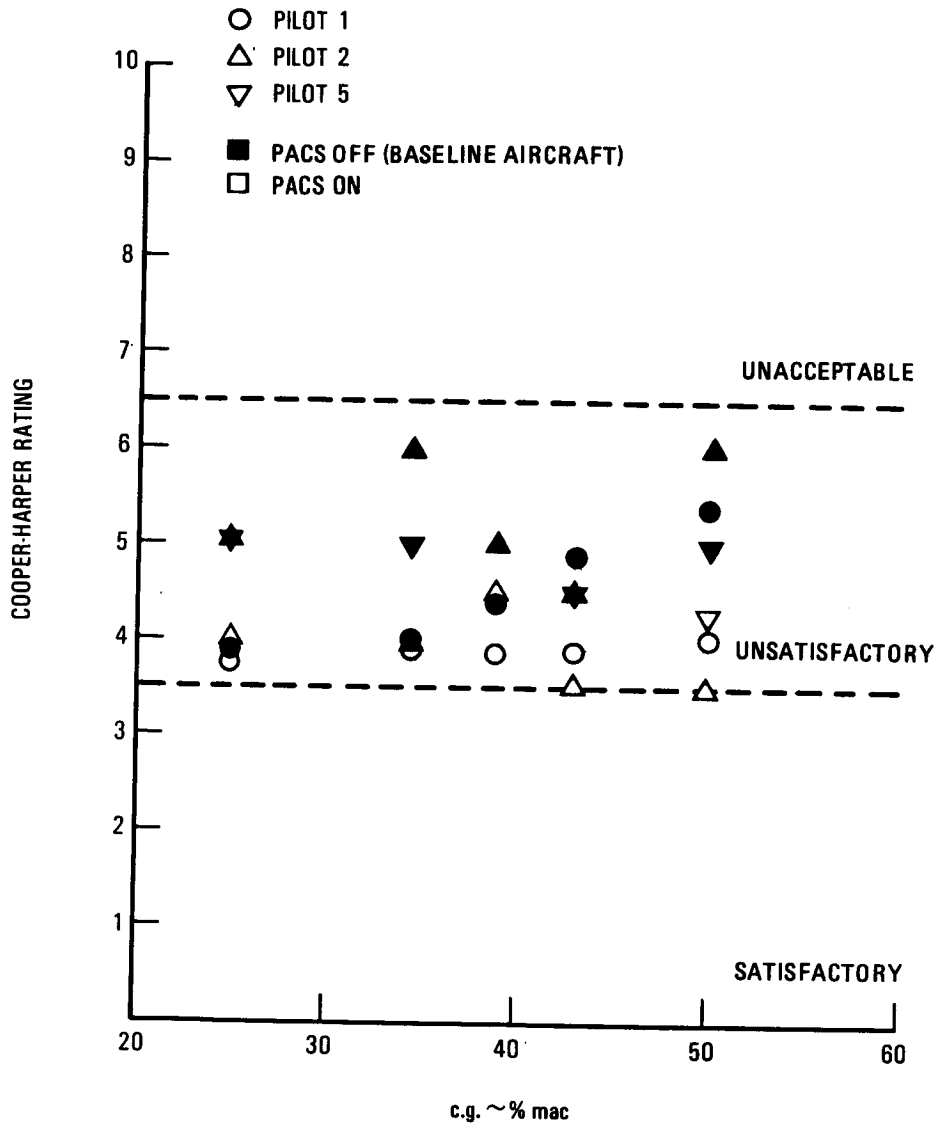


Figure 73. - Cooper-Harper rating for flight condition 18, moderate turbulence.

ORIGINAL PAGE IS
OF POOR QUALITY

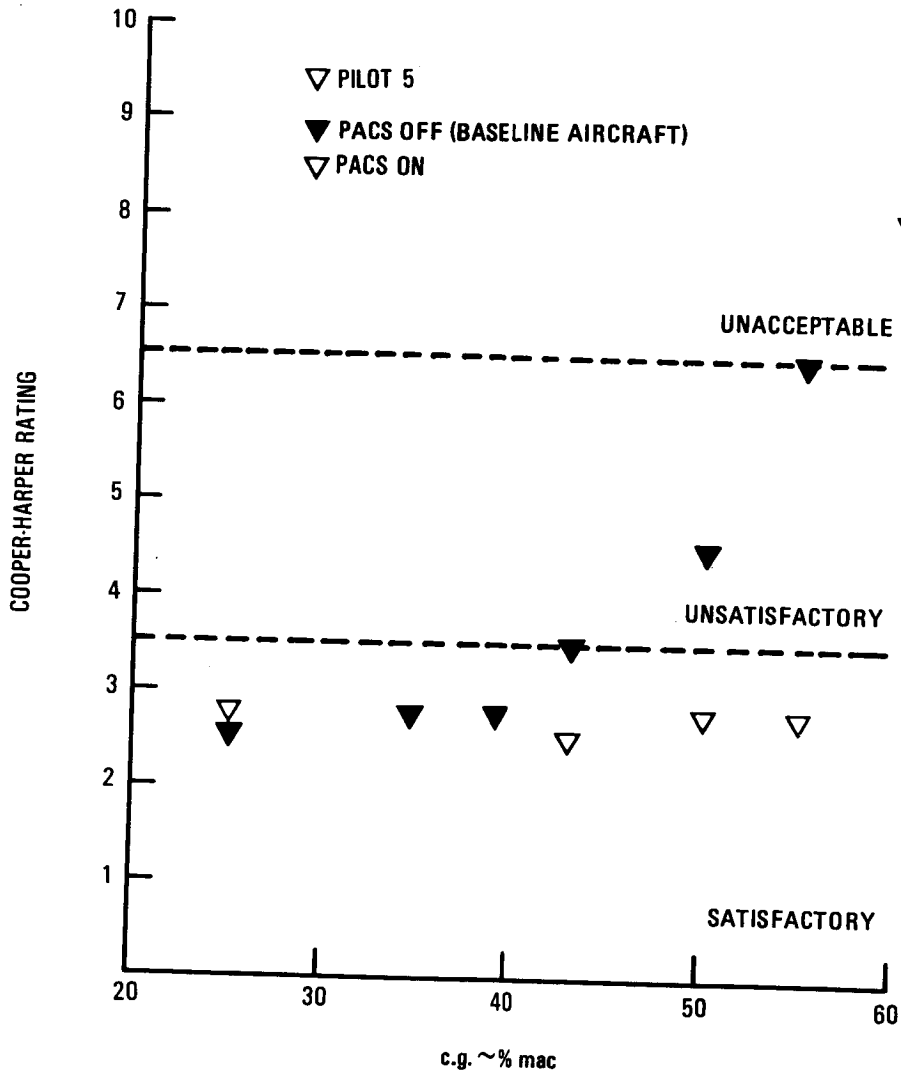


Figure 74. - Cooper-Harper rating for flight condition 17, calm air.

ORIGINAL PAGE IS
OF POOR QUALITY

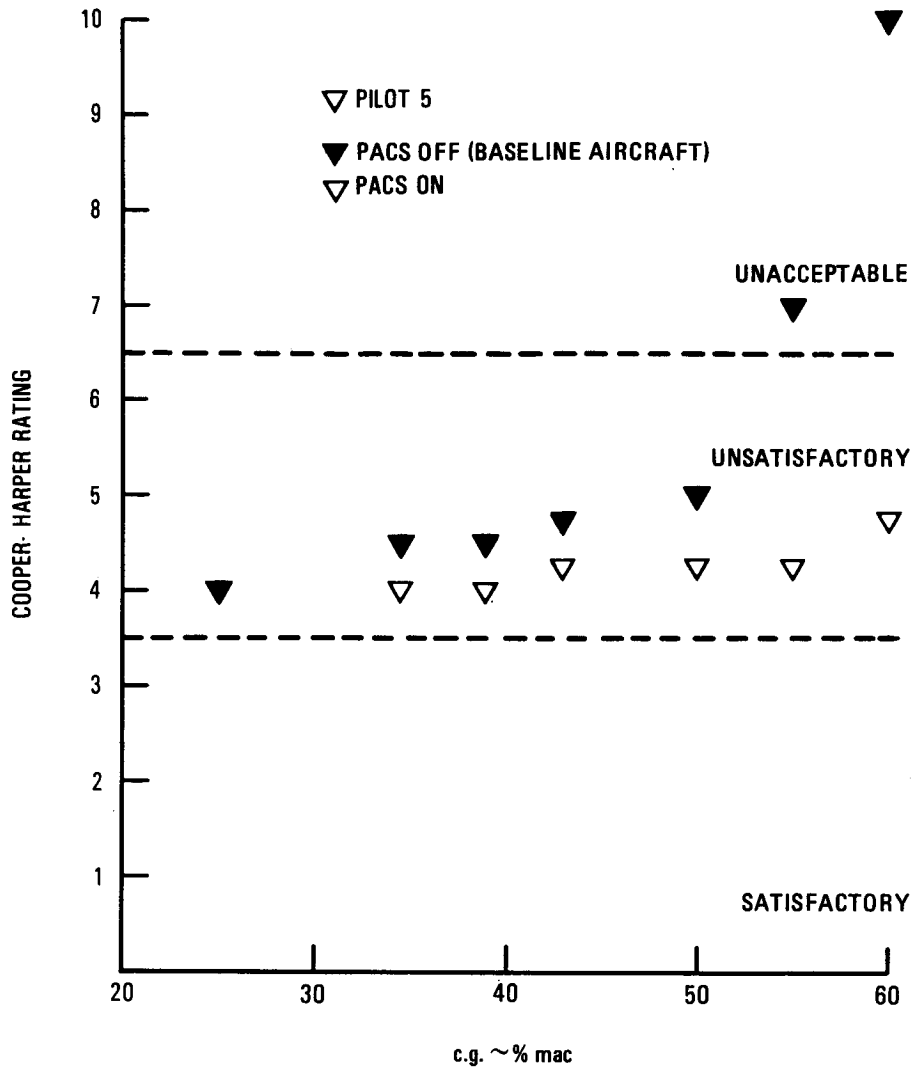


Figure 75. - Cooper-Harper rating for flight condition 17, moderate turbulence.

The baseline aircraft had reasonably good flying qualities (satisfactory to mid unsatisfactory ratings) to c.g. positions of 50 percent mac. The flying qualities became unacceptable at approximately 55 percent. Engagement of the PACS resulted in unsatisfactory flying qualities over the entire c.g. range for calm air conditions. Turbulence conditions resulted in unsatisfactory flying qualities with Cooper-Harper ratings between 4 and 5 over the entire c.g. range.

6.6.7 Flight Condition 19: Takeoff

Flight condition 19 was rated by pilot 5 for calm air and moderate turbulence (6 ft/sec rms) over a c.g. range from 25 percent to 50 percent mac. The ratings are presented in Figures 76 and 77.

The baseline aircraft had good flying qualities for the calm air flight condition and engagement of the PACS did not show a significant improvement. Flight in turbulence degraded the flying qualities and resulted in baseline aircraft Cooper-Harper ratings between 4 and 5. Engagement of the PACS enhanced the flying qualities slightly.

6.6.8 Summary of Simulation Test Results

The solid lines in Figure 78 show the spread in Cooper-Harper ratings of the baseline aircraft for the cruise and high speed flight conditions (7, 10, 15 and 16). Engagement of the PACS results in a rating spread shown by the dashed lines. The rating spreads include calm air and turbulence conditions ratings. The holding condition (18) is not included in Figure 78 but the rating trend is similar. The PACS did not provide a significant benefit for the landing and takeoff conditions (18 and 19) although some improvement of flying qualities in turbulent flight were shown.

A summary of the Cooper-Harper ratings for the PACS configured aircraft are given in Table 14 for all of the flight conditions. The Cooper-Harper ratings shown are the typical best estimate for each test point. In general the turbulence Cooper-Harper ratings have a value of one greater than the ratings for the calm air conditions. The most unsatisfactory rating in the table is 5.

ORIGINAL PAGE 19
OF POOR QUALITY

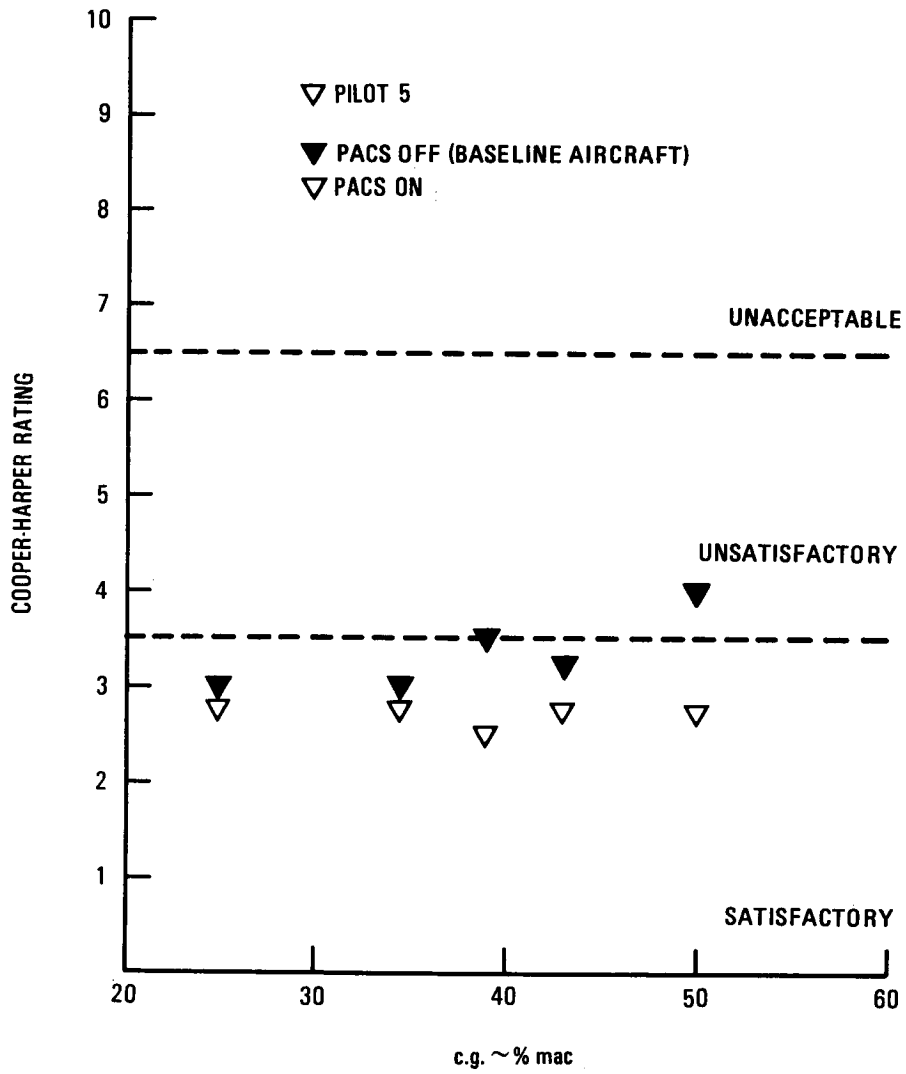


Figure 76. - Cooper-Harper rating for flight condition 19, calm air.

ORIGINAL PAGE IS
OF POOR QUALITY

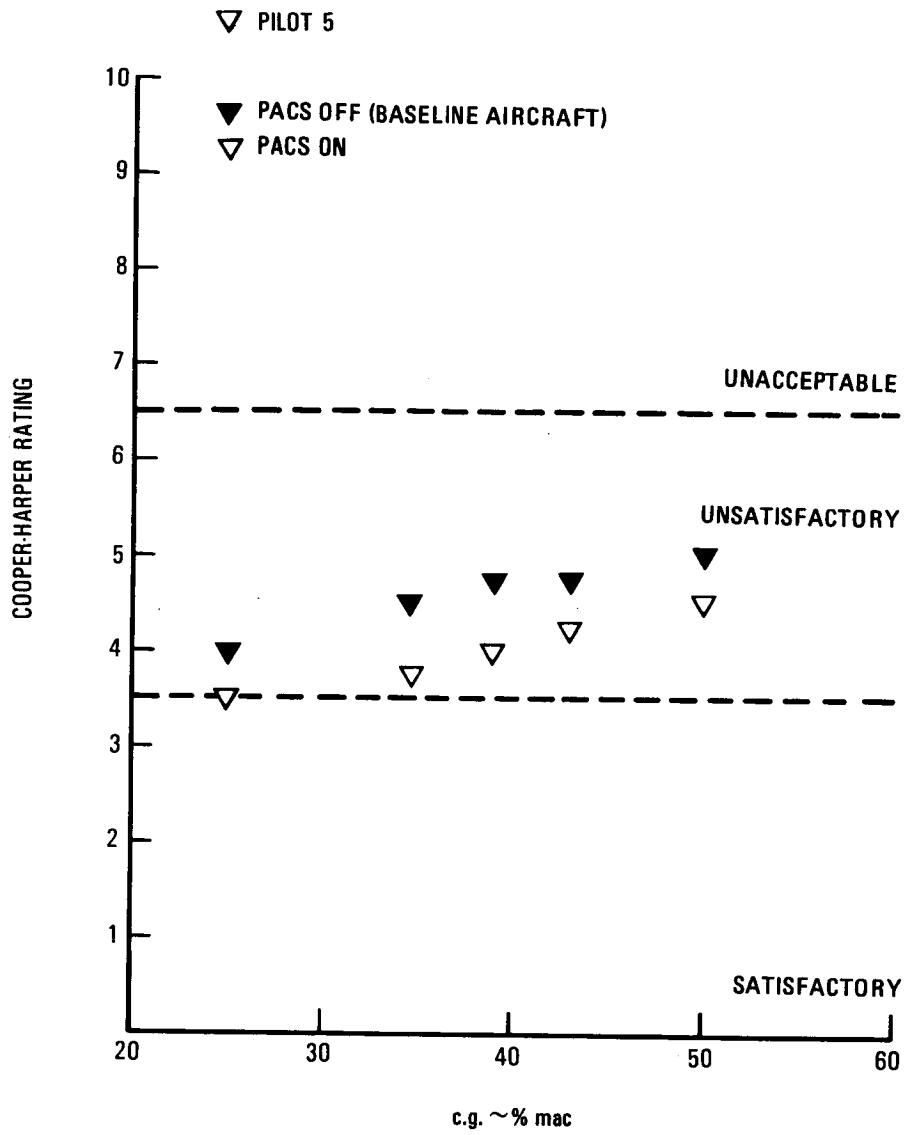


Figure 77. - Cooper-Harper rating for flight condition 19, moderate turbulence.

ORIGINAL PAGE IS
OF POOR QUALITY

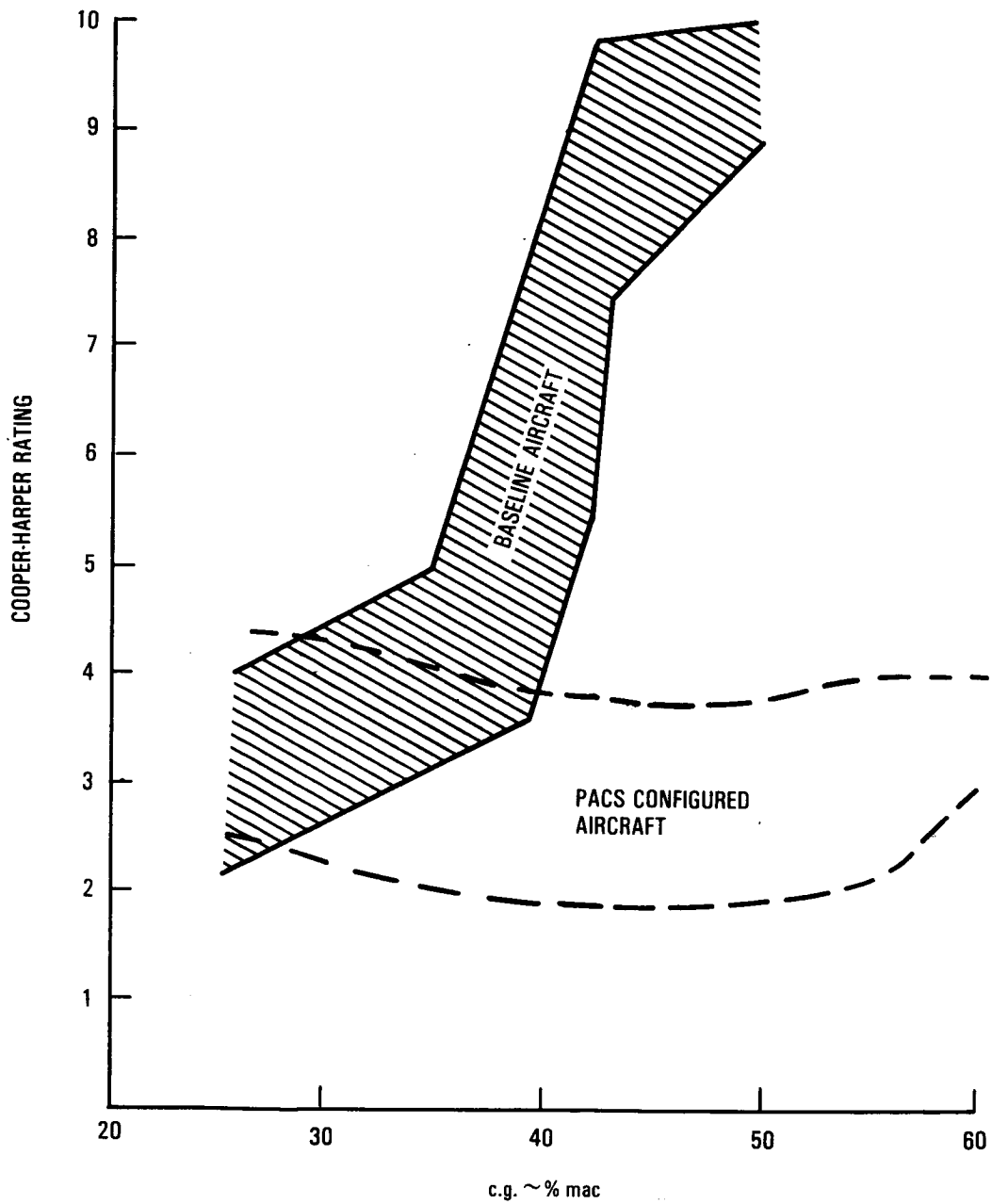


Figure 78. - Summary of Cooper-Harper ratings for cruise and high speed flight conditions.

ORIGINAL PAGE IS
OF POOR QUALITY

TABLE 14. - SUMMARY OF COOPER-HARPER RATINGS WITH PACS ON

Flight Condition	Atm. Cond.	c.g. Position ~% mac						
		25	34.5	39	43	50	55	60
7	C.A.	3.0	3.0	2.5	2.5	3.0	3.5	3.5
	T	3.0	3.5	3.5	3.5	4.0	4.0	4.5
10	C.A.	3.5	3.0	3.0	2.5	2.5	3.0	3.5
	T	3.5	3.5	3.5	3.5	3.0	3.5	5.0
15	C.A.	3.5	3.5	3.5	3.5	3.5	3.5	4.0
	T	4.5	4.5	4.0	4.0	3.5	4.0	4.5
16	C.A.	3.5	3.5	3.0	3.0	3.0	3.5	3.5
	T	3.5	3.5	3.5	3.5	3.5	3.5	4.0
17	C.A.	3.0			3.0	3.0	3.0	
	T		4.0	4.0	4.5	4.5	4.5	5.0
18	C.A.	3.0	3.0	3.5	3.5	3.5		
	T	4.0	4.0	4.0	4.0	4.0		
19	C.A.	3.0	3.0	2.5	3.0	3.0		
	T	4.0	4.5	5.0	5.0	5.0		

7. PACS ARCHITECTURE

This section shows the control law mechanization for an advanced PACS which would be suitable for a Lockheed L-1011 (S/N 1001) flight test program. Although the advanced PACS control law was developed to provide good flying qualities to a 50 percent mac aft c.g. position and shown by simulation test to provide good cruise and high speed flying qualities to a 60 percent mac aft c.g. position, the PACS architecture that is suitable for an L-1011 flight test program was based on an aft 43 percent mac c.g. limit. This represents a negative 3 percent static stability margin and is the maximum aft c.g. limit that the Lockheed L-1011 (S/N 1001) can operate without significant structural modifications.

The advanced PACS interface block diagram is shown in Figure 79. The controller input signals from each component are shown on the diagram. Output signals were provided to the series servo channels and failure signals were provided to the Flight Control Electronic System (FCES) panel.

Tasks performed by the controller (digital computer) are analog-to-digital conversion, signal monitoring and voting, automatic configuration switching after failures, digital-to-analog, gain scheduling, and filtering operations. Redundancy of the advanced PACS components are shown in Figure 80. The architecture design was based on the following rationale. Single failures are bound to occur and it is impossible to predict exactly when they will happen. Therefore, the design aim is to incorporate safety provisions to protect the system against critical effects of any single failure. Also, the flight crew needs to be warned of any failure, critical or not, so that exposure time for the build up of a possible hazardous multiple failures is limited. The design aim is accomplished when there are no critical single failures and the probability of potential hazardous single failures is acceptably remote.

The advanced PACS equipment specification document was completed in August, 1981. Its contents covered a normal Lockheed specification format for submittal to vendors. The section specifying system requirements included functional requirements, performance (including safety), interface (including sensors and servos), environment, operational utility (including reliability), monitoring, and software procedures. Several appendices were included to expand the specification with background.

PRECEDING PAGE BLANK NOT FILMED

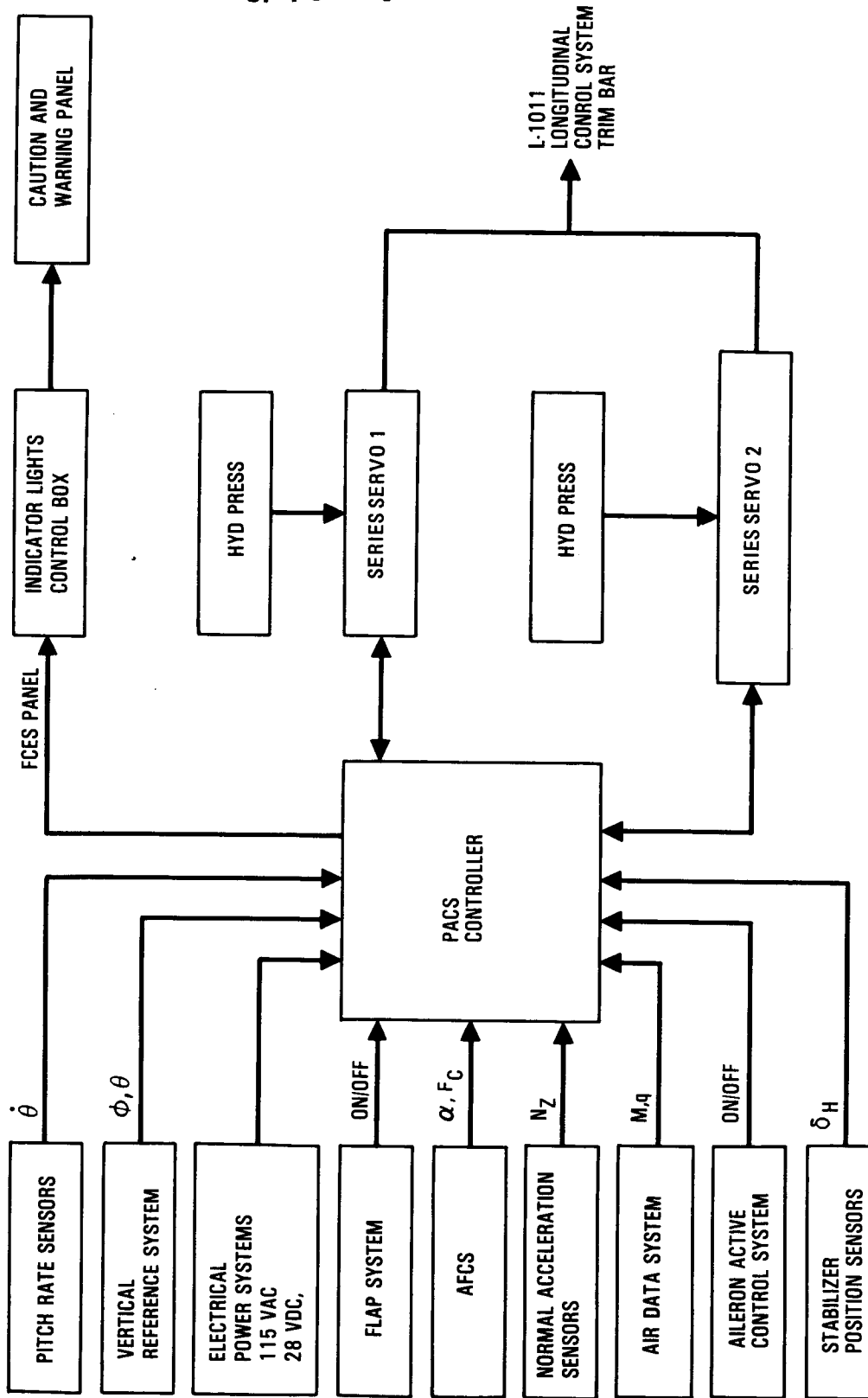


Figure 79. - Advanced PACS interface block diagram.

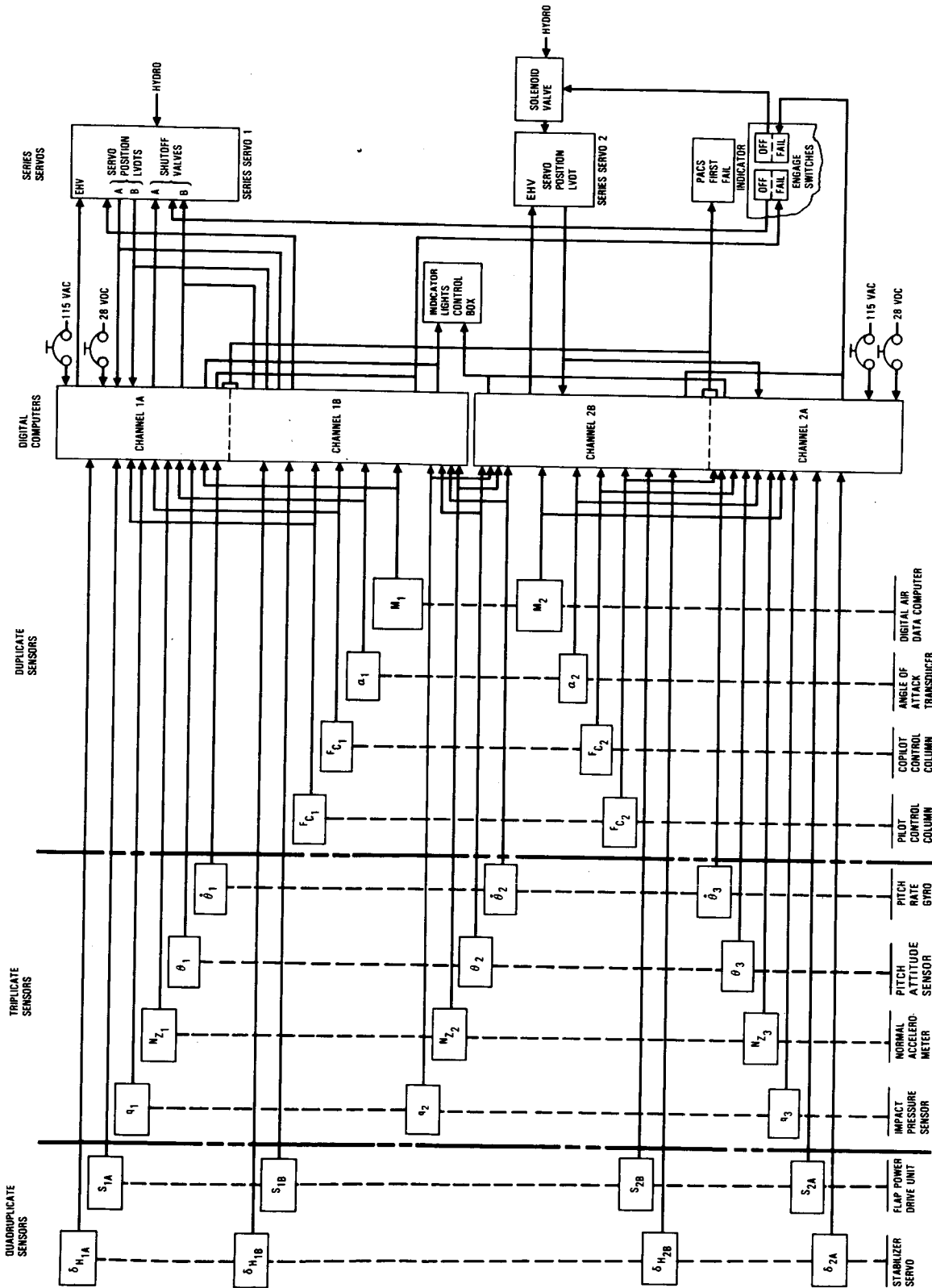


Figure 80. - Advanced PACS component diagram.

CONCLUSIONS

The piloted flight simulation test showed that addition of the advanced PACS to the L-1011 longitudinal control system provided flying qualities to a 20% negative static stability margin which were comparable with the best baseline aircraft flying qualities (15% positive stability margin). The PACS sensor inputs required for flight in the linear stability region are normal acceleration, pitch rate, and pitch attitude. Additional sensor inputs required for nonlinear stability flight conditions are angle of attack, bank angle, and Mach number.

Analyses and piloted flight simulation tests also showed that handling qualities for the flight test L-1011 (S/N 1001), which was the baseline aircraft used for the study, become unsatisfactory at about a negative 3% static stability margin. Consequently, a commercial transport equipped with a PACS that has the capability to fly at 10% negative static stability margin should have a longitudinal control system that has a reliability equivalent to the structure reliability. Thus, a major step toward implementation of a PACS for commercial airline service is to determine that it satisfies the reliability requirement. The advanced PACS architecture shown in this report was designed for a flight test program with static stability margins to negative 3%.

The advanced PACS program provides strong evidence that technology is available to develop PACS control laws which provide good handling qualities for commercial transports for the c.g. range from +15% to -10% static stability margins. Further validation of the advanced PACS control laws developed during the current program requires hardware development and flight testing. However, indications are that the analytical methods developed during the program can be applied to reduce the number of sensor inputs required by the PACS.

PRECEDING PAGE BLANK NOT FILMED

APPENDIX A

Aero Data

Table 15 is a computer output sheet of the aircraft trim conditions and dimensionless stability derivatives for flight case 7b (Table 2). The nomenclature for this table is given below:

- DLC - Direct lift control
- DAC - Aileron active control
- DARIG - $(\delta_{a_{right}} + \delta_{a_{left}})/2$, aileron deflection due to aileron active control system \sim deg
- FLAP - Flap setting \sim degrees
- W - Gross weight \sim lbs
- C.G. - Center of gravity location \sim % mac
- ALT - Altitude above sea level \sim ft.
- VE - V_e , Equivalent air speed \sim knots
- M - Mach number
- UO - True airspeed, ft/sec
- RHO - , air density \sim slugs/ft³
- IY - I_y , Pitch axis inertia \sim slugs/ft²
- ALPHA - α , trim angle of attack \sim degrees
- THETA - θ , climb angle \sim degrees
- GAMMA - γ , yaw angle \sim degrees
- WLCG - center-of-gravity position on the water line
- DH - δ_H , horizontal stabilizer trim angle \sim degrees
- T1 - Thrust of engine 1 \sim lbs
- T2 - Thrust of engine 2 \sim lbs
- T3 - Thrust of engine 3 \sim lbs

TABLE 15. LONGITUDINAL AERO DATA, CASE 7b

<u>TRIM CONDITIONS, AEROELASTIC EFFECTS INCLUDED</u>			
GEAR UP			
DLC OFF			
OUT OF GROUND EFFECT			
DAC ON, DARIG = 0.0			
FLAP = 0	W = 408000.	CG = 25.0	ALT = 37000.
VE = 254.3	M = 0.830	UO = 803.5	RHO = 0.000678
IY = 1.49500E 07			
ALFA = 4.37	THETA = 4.37	GAMMA = 0.0	WLCG = 186.5
DH = -3.15			
T1 = 9773.	T2 = 9773.	T3 = 9773.	
MBT1 = 6.33	MBT2 = -12.77	MBT3 = 6.33	
<u>LONGITUDINAL STABILITY DERIVATIVES (LINEARIZED)</u>			
CD = 0.03845	CL = 0.535	CM = -0.00171	
CDA = 0.01685	CLA = 0.1243	CMA = -0.0151	
	CLQ = 9.88	CMQ = -20.45	
	CLADT = 4.16	CMADT = -10.16	
	CLDH = 0.0297	CMDH = -0.0671	
CDDAC = -0.00014	CLDAC = 0.00182	CMDAC = -0.00427	
CDU = 0.1859	CLU = 0.4942	CMU = -0.1019	
DTDM = 6739.	DTDU = 6.96	DTDH = -0.53	DTDTHR = 303.1

MBT1 - Perpendicular distance from center of gravity to thrust line of left engine (positive for nose-up pitching moment) ~ ft.

MBT2 - Perpendicular distance from center of gravity to thrust line of center engine ~ ft.

MBT3 - Perpendicular distance from center of gravity to thrust line of right engine ~ ft.

CD - C_D , Drag coefficient

CL - C_L , Lift coefficient

CM - C_m , Pitching moment coefficient

CDA - $\frac{\partial C_D}{\partial \alpha}$, change in drag coefficient due to angle of attack ~ 1/deg

CLA - $\frac{\partial C_L}{\partial \alpha}$, change in lift coefficient due to angle of attack ~ 1/deg

ORIGINAL PAGE IS
OF POOR QUALITY

$$\begin{aligned} \text{CMA} - \frac{\partial C_m}{\partial \alpha}, & \text{ change in pitching moment coefficient due to angle of} \\ & \text{attack } \sim 1/\text{deg} \\ \text{CLQ} - C_{L\dot{\theta}} &= -\frac{2U}{\text{mac}} \frac{\partial C_L}{\partial q}, \text{ change in lift coefficient due to pitch} \\ & \text{rate } \sim 1/\text{rad} \\ \text{CMQ} - C_{m\dot{\theta}} &= -\frac{2U}{\text{mac}} \frac{\partial C_m}{\partial q}, \text{ change in pitching moment coefficient due to} \\ & \text{pitch rate } \sim 1/\text{rad} \\ \text{CLADT} - C_{L\dot{\alpha}} &= \frac{2U}{\text{mac}} \frac{\partial C_m}{\partial \dot{\alpha}}, \text{ change in lift coefficient due to rate of change} \\ & \text{of angle of attack } \sim 1/\text{rad} \\ \text{CMADT} - C_{m\dot{\alpha}} &= \frac{2U}{\text{mac}} \frac{\partial C_m}{\partial \dot{\alpha}}, \text{ change in lift coefficient due to rate of change} \\ & \text{of angle of attack } \sim 1/\text{rad} \\ \text{CLDH} - C_{L\delta_H} &= -\frac{\partial C_L}{\partial \delta_H}, \text{ change in lift coefficient due to stabilizer} \\ & \text{deflection } \sim 1/\text{deg} \\ \text{CMDH} - C_{m\delta_H} &= -\frac{\partial C_m}{\partial \delta_H}, \text{ change in pitching moment coefficient due to} \\ & \text{stabilizer deflection } \sim 1/\text{deg} \\ \text{CDDAC} - C_{m\delta_{AC}} &= -\frac{\partial C_D}{\partial \delta_{AC}}, \text{ change in drag coefficient due to AACS} \\ & \text{deflection } \sim 1/\text{deg} \\ \text{CLDAC} - C_{L\delta_{AC}} &= -\frac{\partial C_L}{\partial \delta_{AC}}, \text{ change in lift coefficient due to AACS} \\ & \text{deflection } \sim 1/\text{deg} \\ \text{CMDAC} - C_{m\delta_{AC}} &= -\frac{\partial C_D}{\partial \delta_{AC}}, \text{ change in drag coefficient due to AACS} \\ & \text{deflection } \sim 1/\text{deg} \\ \text{CDU} - C_{D_U} &= -\frac{U}{2} \frac{\partial C_D}{\partial U}, \text{ change in drag coefficient due to speed} \\ \text{CLU} - C_{L_U} &= -\frac{U}{2} \frac{\partial C_L}{\partial U}, \text{ change in lift coefficient due to speed} \\ \text{CMU} - C_{m_U} &= -\frac{U}{2} \frac{\partial C_m}{\partial U}, \text{ change in pitching moment due to speed} \end{aligned}$$

DTDM - $\frac{\partial T}{\partial M}$, change in thrust due to Mach number \sim lbs.

DTDU - change in thrust due to speed change \sim lbs.

DTDH - $\frac{\partial T}{\partial h}$, change in thrust due to height \sim lbs/ft.

DTDTHR - $\frac{\partial T}{\partial X_{\text{THROTTLE}}}$, change in thrust due to throttle position \sim lbs/in.

**ORIGINAL PAGE IS
OF POOR QUALITY**

APPENDIX B

Baseline Aircraft Math Model

The baseline aircraft math model is a state-space equation (Reference 4) for open loop condition of the PACS control model shown in Figure 9. In matrix notation the state-space equation is:

$$\{\dot{x}\} = [A]\{x\} + [B]\{u\} \quad (\text{Eq. B.1})$$

The matrices are defined as follows:

- x - state vector
- \dot{x} - derivative of the state vector
- u = input vector
- A = dynamic matrix
- B = input distribution matrix

The expanded form of equation B-1 is given below:

$$\begin{bmatrix} \dot{\alpha} \\ \ddot{\theta} \\ \dot{\theta} \\ \dot{u} \\ \dot{N}_{Z_F} \\ \ddot{\theta}_F \\ \ddot{\theta}_H \\ \dot{\delta}_H \\ \dot{\delta}_H \end{bmatrix} = \begin{bmatrix} A_{11} & A_{12} & A_{13} & A_{14} & A_{15} & A_{16} & A_{17} & A_{18} \\ A_{21} & A_{22} & A_{23} & A_{24} & A_{25} & A_{26} & A_{27} & A_{28} \\ A_{31} & A_{32} & A_{33} & A_{34} & A_{35} & A_{36} & A_{37} & A_{38} \\ A_{41} & A_{42} & A_{43} & A_{44} & A_{45} & A_{46} & A_{47} & A_{48} \\ A_{51} & A_{52} & A_{53} & A_{54} & A_{55} & A_{56} & A_{57} & A_{58} \\ A_{61} & A_{62} & A_{63} & A_{64} & A_{65} & A_{66} & A_{67} & A_{68} \\ A_{71} & A_{72} & A_{73} & A_{74} & A_{75} & A_{76} & A_{77} & A_{78} \\ A_{81} & A_{82} & A_{83} & A_{84} & A_{85} & A_{86} & A_{87} & A_{88} \end{bmatrix} \begin{bmatrix} \alpha \\ \dot{\theta} \\ \theta \\ u \\ N_{Z_F} \\ \dot{\theta}_F \\ \dot{\theta}_H \\ \dot{\delta}_H \end{bmatrix} + \begin{bmatrix} B_{11} & B_{12} \\ B_{21} & B_{22} \\ B_{31} & B_{32} \\ B_{41} & B_{42} \\ B_{51} & B_{52} \\ B_{61} & B_{62} \\ B_{71} & B_{72} \\ B_{81} & B_{82} \end{bmatrix} \begin{bmatrix} \delta_{HC} \\ \delta_{AC} \end{bmatrix}$$

Elements of the state vector (x) and the input matrix (u) are defined as follows:

$$\{x\} = \begin{bmatrix} \alpha \\ \dot{\theta} \\ \theta \\ u \\ N_{Z_F} \\ \dot{\theta}_F \\ \dot{\delta}_H \\ \delta_H \end{bmatrix} \begin{array}{l} \text{angle of attack increment} \\ \text{pitch rate} \\ \text{pitch attitude increment} \\ \text{normalized airspeed increment } (\Delta u/U_o) \\ \text{filtered normal acceleration increment} \\ \text{filtered pitch rate} \\ \text{horizontal stabilizer angular velocity} \\ \text{horizontal stabilizer angular increment} \end{array}$$

$$\{u\} = \begin{bmatrix} \delta_{H_C} \\ \delta_{A_C} \end{bmatrix} \begin{array}{l} \text{horizontal stabilizer command signal} \\ \text{Outboard aileron symmetric command signal} \end{array}$$

Elements of the dynamic matrix (A) and the input distribution matrix (B) are derived from the aerodynamic data trim conditions and stability derivatives of Appendix A. The elements of these matrices are defined in Table 16. The symbols in the table are defined below.

- m - Mass of Aircraft (slugs)
- V_o - True Air Speed (ft/sec)
- q - Dynamic Pressure $(1/2\rho V_o^2)$ (lbs/ft²)
- S_w - Wing Area (ft²)
- C_{x_u} - Coefficient of Drag Change due to Speed Change
- C_{x_α} - Coefficient of Drag Change due to Angle-of-Attack Change (deg⁻¹)
- C_{L_o} - Coefficient of Lift Change due to Gravity as Pitch Attitude Changes (deg⁻¹)
- C_{z_u} - Coefficient of Lift Change due to Speed Change

- $C_{z\dot{\alpha}}$ - Coefficient of Lift Change due to Angle-of-Attack Rate (rad^{-1})
- $C_{z\alpha}$ - Coefficient of Lift Change due to Angle-of-Attack (deg^{-1})
- C_{zq} - Coefficient of Lift Change due to Pitch Rate (rad^{-1})
- g - Constant Acceleration due to Gravity (ft/sec)
- τ_z - Time Constant of Accelerometer Filter (sec)
- $C_{z\delta_H}$ - Coefficient of Lift Change due to Horizontal Stabilizer Change (deg^{-1})
- $C_{z\delta_a}$ - Coefficient of Lift Change due to Horizontal Symmetrical Aileron Change (deg^{-1})
- C_{m_u} - Coefficient of Pitching Moment Change due to Speed Change
- $C_{m\dot{\alpha}}$ - Coefficient of Pitching Moment Change due to Angle-of-Attack Rate (rad^{-1})
- $C_{m\alpha}$ - Coefficient of Pitching Moment Change due to Angle-of-Attack Change (deg^{-1})
- S_W - Wing Area (ft^2)
- \bar{c} - Mean Aerodynamic Chord of Wing (ft)
- C_{mq} - Coefficient of Pitching Moment Change due to Pitch rate (rad^{-1})
- $C_{m\delta_H}$ - Coefficient of Pitching Moment Change due to Horizontal Stabilizer Change (deg^{-1})
- $C_{m\delta_a}$ - Coefficient of Pitching Moment Change due to Horizontal Stabilizer Change (deg^{-1})
- $\tau_{\dot{\theta}}$ - Time Constant of Pitch Rate Sensor Filter (sec)
- $C_{x\delta_a}$ - Coefficient of Drag Change due to Symmetrical Aileron Change (deg^{-1})
- l - Distance of Accelerometer Forward of c.g. (ft)
- τ_s - Time Constant of Series Servo (sec)
- τ_p - Time Constant of Horizontal Stabilizer Servo (sec)

ORIGINAL PAGE IS
OF POOR QUALITY

TABLE 16. DEFINITION OF ELEMENTS FOR MATRICES A AND B

[A] =	G/F	H/F	0	E/F	0 0	0	J/F	[B] =	0	K/F
	$\frac{GN}{FQ} + \frac{P}{Q}$	$\frac{HN}{FQ} + \frac{R}{Q}$	0	$\frac{EN}{FQ} + \frac{M}{Q}$	0 0	0	$\frac{JN}{FQ} + \frac{S}{Q}$		0	$\frac{KN}{FQ} + \frac{T}{Q}$
	0	1	0	0	0 0	0	0		0	0
	C/A	0	-D/A	B/A	0 0	0	0		0	V/A
	-(GW+YP)	-(HW+RY-I)	0	-(EW+MY)	-L 0	0	-(JW+SY)		0	-(KW+TY)
	0	U	0	0	0 -U	0	0		0	0
	0	0	0	0	0 0	$-(Z_1+Z_2)$	$-Z_1Z_2$		Z_1Z_2	0
	0	0	0	0	0 0	1	0		0	0

where:

$A = \frac{m V_0}{q S_w}$	$B = C_{X_u}$	$C = C_{X_\alpha}$	$D = C_{L_0}$	$E = C_{Z_u}$
$F = A - X C_{Z_\alpha}$	$G = C_{Z_\alpha}$	$H = A + X C_{Z_q}$	$I = \frac{V_0}{g \tau_z}$	$J = C_{Z_{\delta_H}}$
$K = C_{Z_{\delta_a}}$	$L = -\frac{1}{\tau_z}$	$M = C_{m_u}$	$N = X C_{m_\alpha}$	$P = C_{m_\alpha}$
$Q = \frac{l y}{q S_w \bar{c}}$	$R = X C_{m_q}$	$S = C_{m_{\delta_H}}$	$T = C_{m_{\delta_a}}$	$U = \frac{1}{\tau_\theta}$
$V = C_{X_{\delta_a}}$	$W = \frac{N l + Q V_0}{g \tau_z F Q}$	$X = \frac{\bar{c}}{2 V_0}$	$Y = \frac{l}{g \tau_z Q}$	$Z_1 = \frac{1}{\tau_s}$
$Z_2 = \frac{1}{\tau_p}$				

APPENDIX C

Modal Control Method

The eigenvalue/eigenvector assignment problem is generalized for both the output feedback and full state cases. Therefore, the C-matrix referenced throughout this report is assumed to be a general matrix of dimensions $r \times n$. If all C-matrices are set equal to an n^{th} order identity matrix, this will convert the generalized eigenvalue/eigenvector assignment problem into a full state feedback problem.

The development of the eigenvalue/eigenvector assignment problem will include the following three major areas:

- Eigenvalue assignment
- Eigenvector assignment
- Feedback gain calculation

C.1 Eigenvalue Assignment.- We consider the standard multivariable linear time-invariant feedback control system.

$$\dot{x} = Ax + Bu, \quad x(t_0) = x_0 \quad (\text{Eq C.1})$$

$$y = Cx \quad (\text{Eq C.2})$$

$$u = Fy \quad (\text{Eq C.3})$$

By substituting the feedback equation (C.3) into the system equation (C.1), we obtain the closed loop state equation

$$\dot{x} = (A + BFC)x \quad (\text{Eq C.4})$$

The closed loop system has the eigenvector equation:

$$(A + BFC)v_i = \lambda_i v_i \quad (\text{Eq C.5})$$

ORIGINAL PAGE IS
OF POOR QUALITY

where

λ_i ($i = 1, \dots, n$): Set of distinct closed loop eigenvalues

v_i ($i = 1, \dots, n$): corresponding set of closed loop eigenvectors

We can rearrange equation (C.5) to obtain the following expression

$$[\lambda_i I - A]v_i = BFCv_i \quad (\text{Eq C.6})$$

Since the B matrix has full rank of m, it is always possible to partition the B matrix to form $B' = [B_1 \ B_2]$ by reordering the state variables in equation (C.1). B_1 is an $m \times m$ nonsingular submatrix.

With no loss of generality, we can assume that the B matrix has the following partition form

$$B = \begin{bmatrix} B_1 \\ B_2 \end{bmatrix} \quad (\text{Eq C.7})$$

where

B_1 : $m \times m$ nonsingular matrix

B_2 : $(n - m) \times m$ matrix

Consequently, we can express equation (C.6) in the following partitioned form

$$\begin{bmatrix} \lambda_i I_m - A_{11} & -A_{12} \\ -A_{21} & \lambda_i I_{n-m} - A_{22} \end{bmatrix} \begin{bmatrix} z_i \\ w_i \end{bmatrix} = \begin{bmatrix} B_1 \\ B_2 \end{bmatrix} FC \begin{bmatrix} z_i \\ w_i \end{bmatrix} \quad (\text{Eq C.8})$$

where

$$A = \begin{bmatrix} \overset{m}{A_{11}} & \overset{n-m}{A_{12}} \\ \overset{m}{A_{21}} & \overset{n-m}{A_{22}} \end{bmatrix} \begin{matrix} m \\ n-m \end{matrix} \quad (\text{Eq C.9})$$

ORIGINAL PAGE IS
OF POOR QUALITY

$$B = \begin{bmatrix} B_1 \\ B_2 \end{bmatrix} \begin{matrix} m \\ n-m \end{matrix} \quad (\text{Eq C.10})$$

$$v_i = \begin{bmatrix} z_i \\ w_i \end{bmatrix} \begin{matrix} m \\ n-m \end{matrix} \quad (\text{Eq C.11})$$

and where

I_j = the j^{th} order identity matrix

Considering the first matrix equation of (C.8), we readily obtain

$$\begin{bmatrix} \lambda_1 I_m - A_{11} & -A_{12} \end{bmatrix} \begin{bmatrix} z_i \\ w_i \end{bmatrix} = B_1 \text{FC} \begin{bmatrix} z_i \\ w_i \end{bmatrix} \quad (\text{Eq C.12})$$

or equivalently

$$\left[\lambda_i \left[I_m \mid 0 \right] - \left[A_{11} \mid A_{12} \right] \right] \begin{bmatrix} z_i \\ w_i \end{bmatrix} = B_1 \text{FC} \begin{bmatrix} z_i \\ w_i \end{bmatrix} \quad (\text{Eq C.13})$$

Letting

$$A_1 \triangleq \left[A_{11} \mid A_{12} \right] \quad (\text{Eq C.14})$$

then (C.13) can be expressed as:

$$\left[\lambda_i \left[I_m \mid 0 \right] - A_1 \right] \begin{bmatrix} z_i \\ w_i \end{bmatrix} = B_1 \text{FC} \begin{bmatrix} z_i \\ w_i \end{bmatrix} \quad (\text{Eq C.15})$$

Rearranging (C.15) we obtain

$$(A_1 + B_1 FC) \begin{bmatrix} z_i \\ w_i \end{bmatrix} = \lambda_i z_i \quad (\text{Eq C.16})$$

or using (C.11) we get

$$(A_1 + B_1 FC) v_i = \lambda_i z_i \quad (\text{Eq C.17})$$

With the rank of C equal to r, one can assign r closed loop eigenvalues using output feedback (Reference 5). It should be noted that one can assign n closed loop eigenvalues in the full state feedback case where the C matrix is an nth order identity matrix.

Rewriting equation (C.17) to include the complete set of eigenvectors and eigenvalues:

$$(A_1 + B_1 FC) V = Z\Lambda \quad (\text{Eq C.18})$$

where

$$\Lambda = \begin{bmatrix} \lambda_1 & & 0 \\ & \lambda_2 & \\ 0 & & \lambda_r \end{bmatrix} \quad (\text{Eq C.19})$$

$$Z = [z_1 \ z_2 \ \dots \ z_r] \quad (\text{Eq C.20})$$

$$V = [v_1 \ v_2 \ \dots \ v_r] \quad (\text{Eq C.21})$$

Rearranging (C.18) we have

$$FCV = B_1^{-1} (Z\Lambda - A_1 V) \quad (\text{Eq C.22})$$

C and V each have full rank of r; therefore [CV] is nonsingular. From equation (C.22), we can solve for F directly

$$F = B_1^{-1}(ZA - A_1V)(CV)^{-1} \quad (\text{Eq C.23})$$

The inverse of CV will always exist in physical systems with a meaningful sensor implementation.

C.2 Eigenvector Assignment. - In the previous section we have mentioned that the number of assignable closed loop eigenvalues equals the rank of the C matrix. In this section, the significance of closed loop eigenvector assignment in modern flight control theory are discussed.

Consider the time-invariant, closed loop system

$$\dot{x} = (A + BFC)x, \quad x(t_0) = x_0 \quad (\text{Eq C.24})$$

Suppose the matrix [A + BFC] has distinct eigenvalues and eigenvectors denoted by $(\lambda_1, \lambda_2, \dots, \lambda_n)$ and (v_1, v_2, \dots, v_n) , respectively. It can be shown that the solution of (C.24) can be written as

$$x(t) = \sum_{i=1}^n e^{\lambda_i t} v_i (l_i x_0) \quad (\text{Eq C.25})$$

where

$$l_i = i^{\text{th}} \text{ row vector of } T^{-1}$$

and

$$T = [v_1 \ v_2 \ \dots \ v_n]$$

(i.e., T is the modal matrix of (A + BFC)).

This shows that the response of the closed loop system (C.24) is a composition of motions along the closed loop eigenvectors v_i ($i = 1, 2, \dots, n$). It is important to know that the i^{th} mode λ_i is excited by the component of the initial state, x_0 , along its corresponding closed loop eigenvector v_i . Therefore, in flight control system design it is desirable to decouple the motions

by proper choice of the closed loop eigenvectors to improve aircraft handling qualities. For example, in an aircraft lateral axis design problem, we want the roll subsidence mode to show up dominantly on roll rate, but not on yaw rate or sideslip. Similarly, we want the dutch roll mode to show up dominantly on sideslip and yaw rate respectively for the real part and imaginary part of closed loop eigenvectors, but not on the roll rate. In this simplified example, we show a desire to decouple the roll subsidence mode and the dutch roll mode. In the sense that the roll subsidence mode only affects the roll rate while the dutch roll mode only affects the yaw rate and sideslip.

It is well known that (Reference 4,5) we can not completely specify a set of closed loop eigenvectors for our feedback system. But we do have some flexibility in obtaining a set of closed loop eigenvectors such that they will best approximate the set of predescribed or desirable eigenvectors (Reference 6). We will discuss the eigenvector assignment problem for the following two situations:

- (1) Complete specification of desired eigenvectors
- (2) Incomplete specification of desired eigenvectors

C.2.1 Complete specification of desired eigenvector case: The closed loop eigenvalue and eigenvector are defined by the following equation:

$$(A + BFC)v_i = \lambda_i v_i \quad (\text{Eq C.26})$$

where λ_i and v_i are the closed loop eigenvalue and eigenvector, respectively. The above equation can be rewritten in a different form.

$$(\lambda_i I - A)^{-1} B m_i = v_i \quad (\text{Eq C.27})$$

where

$$m_j \triangleq FCv_j \quad (j = 1, 2, \dots, r) \quad (\text{Eq C.28})$$

A closer look at equation (C.27) reveals that the designer has the freedom to arbitrarily select a set of r independent m -vectors ($r = \text{rank } [C]$, $m = \text{rank } [B]$) such that the closed loop control system will have the desired performance characteristics. The only restriction on m_j is that $m_i = m_j^*$ whenever $\lambda_i = \lambda_j^*$. The asterisk indicates the complete conjugate. This condition must be satisfied in order to obtain a realizable feedback matrix.

In order to capitalize on the freedom in m-vector assignment, it is beneficial to select a set of m-vectors $\{m_i\}$ such that they will best approximate the desired eigenvector, v_i^d , with v_i . Therefore, we define a cost function

$$J(m_i) \triangleq \begin{pmatrix} v_i^d - v_i \end{pmatrix}^T \begin{pmatrix} v_i^d - v_i \end{pmatrix} = \begin{pmatrix} v_i^d - L_i m_i \end{pmatrix}^T \begin{pmatrix} v_i^d - L_i m_i \end{pmatrix} \quad (\text{Eq C.29})$$

where

$$L_i \triangleq (\lambda_i I - A)^{-1} B \quad (\text{Eq C.30})$$

and proceed to minimize the cost function with respect to m_i .

$$\frac{d}{dm_i} J(m_i) = \frac{d}{dm_i} \begin{pmatrix} v_i^d - L_i m_i \end{pmatrix}^T \begin{pmatrix} v_i^d - L_i m_i \end{pmatrix} = 2L_i^T (L_i m_i - v_i^d) \quad (\text{Eq C.31})$$

Setting equation (C.31) to zero yields the following

$$m_i = \begin{pmatrix} L_i^T L_i \end{pmatrix}^{-1} L_i^T v_i^d \quad (\text{Eq C.32})$$

Therefore, the least squares method (described by equation (C.32)) is an optimum way for selecting the set of m-vectors of (C.28). The closed loop eigenvector (v_i) obtained from equation (C.27) will best approximate the desired eigenvector (v_i^d) in the least squares sense.

C.2.2 Incomplete specification of desired eigenvector case: In the previous section, we have described an optimum way in selecting the m-vectors for the case where all components of the desired eigenvector are specified.

However, it will generally be true that only few components in the desired eigenvector are actually specified; while the rest can be arbitrary. In this case, we will formulate our problem as follows:

Given: (1) closed loop eigenvalue/eigenvector equation

$$(\lambda_i I - A)^{-1} B m_i = v_i \quad (\text{Eq C.33})$$

and (2) desired closed loop eigenvectors

$$v_i^d = \begin{bmatrix} v_{1i} \\ x \\ v_{3i} \\ x \\ x \\ v_{ni} \end{bmatrix} \quad (\text{Eq C.34})$$

where

v_{ji} = designer specified components

x = unspecified components

Problem: Find m_i such that the actual closed loop eigenvector (i.e., v_i in equation (C.33)) will best approximate the desired eigenvector (v_i^d) in the least squares sense.

To solve this problem, we will introduce a row reordering operator, $\{ \}^{R_i}$. The operation involves simultaneous reordering of the $\{(\lambda_i I - A)^{-1} B\}$ matrix and the v_i^d vector until v_i^d is partitioned into two subvectors. One contains the specified components and the other contains the unspecified components. After the row reordering operation, we have the following matrix representation.

$$\{(\lambda_i I - A)^{-1} B\}^R v_i = \begin{bmatrix} \hat{L}_i \\ \hat{D}_i \end{bmatrix} \quad (\text{Eq C.35})$$

$$\{v_i^d\}^R = \begin{bmatrix} l_i \\ d_i \end{bmatrix} \quad (\text{Eq C.36})$$

where

l_i = contains the specified components of v_i^d

d_i = contains the unspecified components of v_i^d

then

$$\hat{L}_i m_i = l_i \quad (\text{Eq C.37})$$

Using the same minimization procedure described in paragraph (C.2.1), we obtain the following results.

- (1) row dimension of $\hat{L}_i \geq m$

$$m_i = \left(\hat{L}_i^T \hat{L}_i \right)^{-1} \hat{L}_i^T l_i \quad (\text{Eq C.38})$$

- (2) row dimension of $\hat{L}_i = 0$

If the row dimension of \hat{L}_i is zero, it corresponds to the situation that the designer does not care about the mode distribution among output components. Hence, this design procedure is similar to output feedback designs using only pole placement. In this case, the designer must arbitrarily select a set of m -vectors (m_i). The closed loop eigenvectors are computed using equation (C.38); i.e.,

$$v_i = (\lambda_i I - A)^{-1} B m_i \quad (\text{Eq C.39})$$

C.2.3 Feedback gain calculation: Once we have obtained r closed loop eigenvectors, the feedback gain matrix can be calculated from equation (C.23).

APPENDIX D

Pitch Attitude Loop Lag-Lead Circuit

The pitch attitude sensor channel includes a lag-lead circuit to produce a signal component of derived incremental speed. Consequently, the speed increment feedback signal used for phugoid mode control is no longer required.

A block diagram of the lag-lead circuit used in the pitch attitude loop is given in Figure 81. The symbols K_1 and K_2 represent the static parts of the velocity and pitch attitude transfer functions, respectively. The symbols G_1 and G_2 represent the frequency variant parts of the velocity and pitch attitude transfer functions.

The speed and pitch attitude transfer functions can be expressed in the following forms by taking the Laplace transform of the open loop state-space equation (Equation B.1 of Appendix B) and applying Cramers rule.

$$\frac{u}{\delta_{H_C}} = \frac{|N_u|}{|D|} = \frac{K_1 G_1}{D} = \frac{K_1 (\gamma_{u_1} s+1) (\gamma_{u_2} s+1) \dots (\gamma_{u_7} s+1)}{(\gamma_{D_1} s+1) (\gamma_{D_2} s+1) \dots (\gamma_{D_8} s+1)} \quad (\text{Eq. D.1})$$

$$\frac{\theta}{\delta_{H_C}} = \frac{|N_\theta|}{|D|} = \frac{K_2 G_2}{D} = \frac{K_2 (\gamma_{\theta_1} s+1) (\gamma_{\theta_2} s+1) \dots (\gamma_{\theta_7} s+1)}{(\gamma_{D_1} s+1) (\gamma_{D_2} s+1) \dots (\gamma_{D_8} s+1)} \quad (\text{Eq. D.2})$$

where γ denotes a root reciprocal (real or complex).

The γ_{u_i} ($i = 1, 2, \dots, 7$), γ_{θ_i} ($i = 1, 2, \dots, 7$), and γ_{D_i} ($i = 1, 2, \dots, 8$) represent the root reciprocals of the polynomial equations for the velocity, pitch, attitude, and dynamic determinants respectively. The lag-lead circuit (Figure 82) transfer function is:

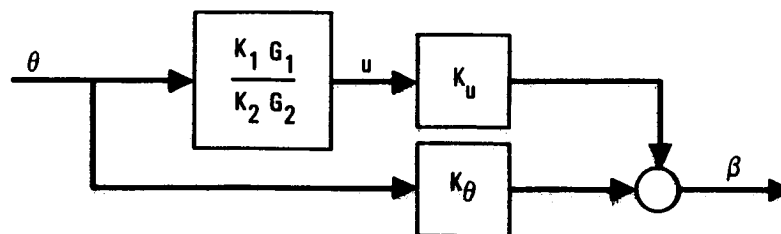


Figure 81. - PACS lag-lead circuit block diagram.

$$\frac{\beta}{\theta} = K_u \frac{K_1 G_1}{K_2 G_2} + K_\theta \quad (\text{Eq. D.3})$$

Substitution of Equations D.1 and D.2 numerators into Equation D.3 provides:

$$\frac{\beta}{\theta} = K_u \frac{K_1 (\gamma_{u_1} s+1) (\gamma_{u_2} s+1) \dots (\gamma_{u_7} s+1)}{K_2 (\gamma_{\theta_1} s+1) (\gamma_{\theta_2} s+1) \dots (\gamma_{\theta_7} s+1)} + K_\theta \quad (\text{Eq. D.4})$$

Writing of Equation D.4 in terms of index notation provides:

$$\frac{\beta}{\theta} = K_u \frac{K_1}{K_2} \frac{\prod_{i=1}^7 (\gamma_{ui} s+1)}{\prod_{j=1}^7 (\gamma_{\theta j} s+1)} + K_\theta \quad (\text{Eq. D.5})$$

The effect of the higher order powers of s are negligible in the phugoid range of frequencies. Thus β/θ can be written as:

$$\frac{\beta}{\theta} = \frac{K_u K_1}{K_2} \cdot \frac{(\gamma_{uPA} + \gamma_{uPB}) s + 1}{(\gamma_{\theta PA} + \gamma_{\theta PB}) s + 1} + K_\theta \quad (\text{Eq. D.6})$$

where the PA and PB subscripts designate the complex or real pair of root reciprocals corresponding to the phugoid mode frequencies. To facilitate writing, the following notation will be adopted.

$$a_1 = \gamma_{uPA}$$

$$b_1 = \gamma_{uPB}$$

$$a_2 = \gamma_{\theta PA}$$

$$b_2 = \gamma_{\theta PB}$$

Equation D.6 can now be written in the following form:

$$\frac{\beta}{\theta} = \frac{K_u K_1}{K_2} \cdot \frac{(a_1 + b_1) s + 1}{(a_2 + b_2) s + 1} + K_\theta \quad (\text{Eq. D.7})$$

ORIGINAL PAGE IS
OF POOR QUALITY

By mathematical manipulation Equation D.7 can be put in the following form:

$$\frac{\beta}{\theta} = \frac{K_u K_1 + K_\theta K_2}{K_2} \left[\frac{1}{(a_2 + b_2) s + 1} \right] \left[\frac{K_u K_1 (a_1 + b_1) + K_\theta K_2 (a_2 + b_2)}{K_u K_1 + K_\theta K_2} s + 1 \right]$$

Let:

$$\frac{K_u K_1 + K_\theta K_2}{K_2} = K_3$$

$$\frac{K_u K_1 (a_1 + b_1) + K_\theta K_2 (a_2 + b_2)}{K_u K_1 + K_\theta K_2} = \tau_1$$

$$a_2 + b_2 = \tau_2$$

Then:

$$\frac{\beta}{\theta} = K_3 \left(\frac{\tau_1 s + 1}{\tau_2 s + 1} \right) = \left(K_3 \frac{\tau_1}{\tau_2} \right) \left[1 + \left(\frac{\tau_2}{\tau_1} - 1 \right) \frac{\frac{1/\tau_2}{s}}{1 + \frac{1/\tau_2}{s}} \right] \quad (\text{Eq. D.8})$$

This equation is now in the form for gain scheduling. The polynomial coefficients for each of the gain-scheduled terms are given in Table 6.

APPENDIX E

Feed-Forward Loop Control Law

The block diagram used for development of the feed-forward control law is shown in Figure 82.

The input to the summing point from the feed-forward loop is:

$$X_I = (1 + C_F K_{FF} G_{FF}) X_C \quad (\text{Eq. E.1})$$

The transfer function for the aircraft with feedback loop closed is:

$$\frac{N_Z}{X_I} = \frac{J' K_A G_A}{1 + J' K_A G_A K_{FB} G_{FB}} \quad (\text{Eq. E.2})$$

Substitution of Equation E.1 into Equation E.2 and setting $X_C = F_C / C_F$ gives:

$$\frac{N_Z}{(1 + C_F K_{FF} G_{FF}) F_C / C_F} = \frac{J' K_A G_A}{1 + J' K_A G_A K_{FB} G_{FB}} \quad (\text{Eq. E.3})$$

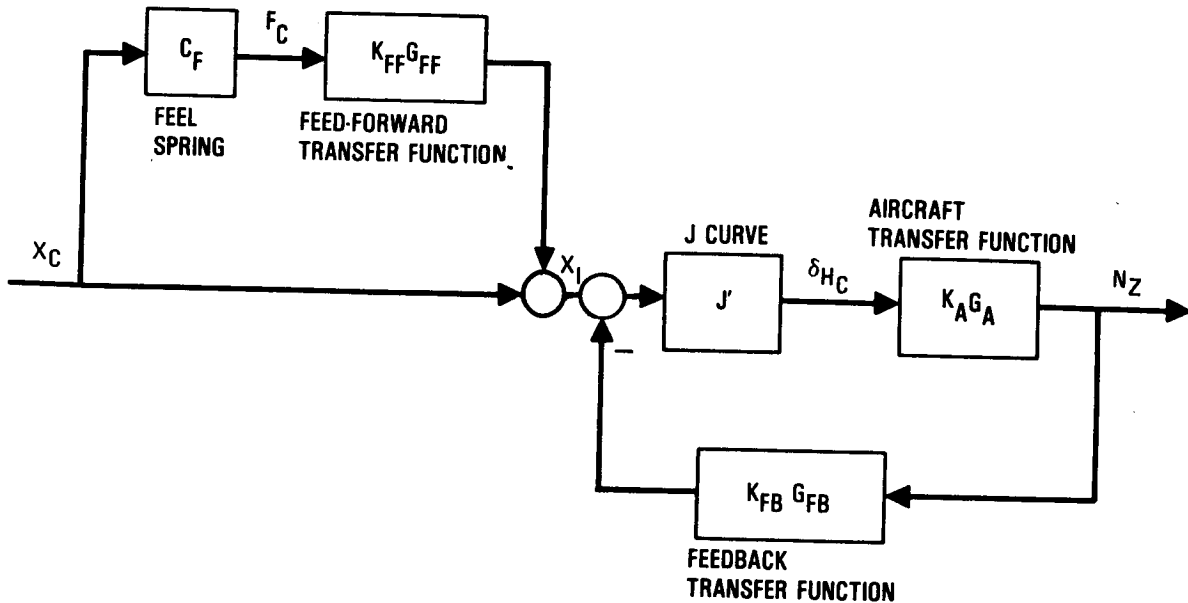


Figure 82. - PACS feed-forward loop block diagram.

ORIGINAL FORM OF
OF POOR QUALITY

Equation E.3 can be solved to obtain the force gradient:

$$\frac{F_C}{N_Z} = \frac{C_F (1 + J' K_A G_A K_{FB} G_{FB})}{K_A J' G_A (1 + C_F K_{FF} G_{FF})} \quad (\text{Eq. E.4})$$

A value for the force gradient that is desired can now be picked from the design criteria of Figure 6 (e.g., a line that is half way between the upper and lower limits). This value is defined as $(F_C/N_Z)_D$ to designate that it is the desired column force gradient.

The problem is to determine the feed-forward gains that will provide the desired column force gradient. Thus Equation E.4 is solved for $K_{FF} G_{FF}$ to give:

$$K_{FF} G_{FF} = -\frac{1}{C_F} + \frac{(1 + J' K_A G_A K_{FB} G_{FB})}{J' K_A G_A (F_C/N_Z)_D} \quad (\text{Eq. E.5})$$

The symbols in Equation E.5 are defined as follows:

C_F = Pitch feel spring rate

J' = J curve derivative

$K_A G_A$ = Aircraft open loop transfer function

$K_{FB} G_{FB}$ = Feedback transfer function based on N_Z signal

$(F_C/N_Z)_D$ = Desired column force gradient

The pitch feel spring rate is a function of stabilizer trim position and Mach number. Figure 50 shows the spring rates for the L-1011 S/N 1001 aircraft.

J' is the derivative of the J curve which is shown in Figure 4.

The method for computing the $K_A G_A$ and $K_{FB} G_{FB}$ transfer functions is illustrated by the block diagram in Figure 83. The value of the $K_A G_A$ transfer function is obtained by solving the baseline aircraft state-space equation B.1 by using Cramer's rule. This gives:

$$K_A G_A = \frac{N_Z}{\delta_{H_C}} = \frac{|N_{N_Z}(s)|}{|D(s)|} \quad (\text{Eq. E.6})$$

ORIGINAL PAGE IS
OF POOR QUALITY

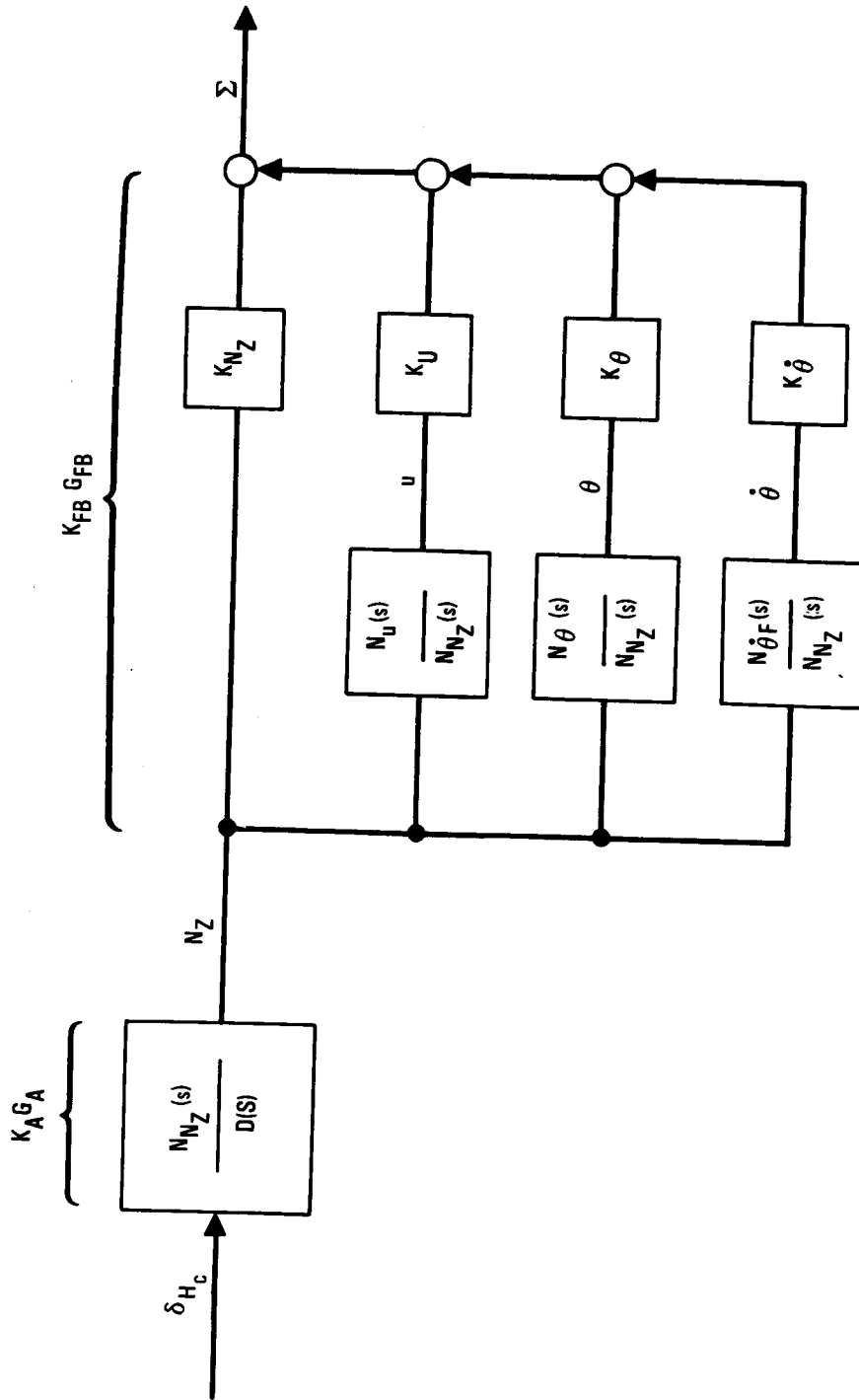


Figure 83. - PACS equivalent feedback gain block diagram for N_Z signal.

The values of the determinants are determined as discussed in Appendix D (e.g., Eq. D.1). Cramer's rule is used to obtain the transfer functions u/δ_{H_C} and θ/δ_{H_C} . These transfer functions are then divided by the N_{N_Z}/δ_{H_C} transfer function to express the respective signal values in terms of the N_Z signal. The $K_{FB}^{G_{FB}}$ transfer function is:

$$K_{FB}^{G_{FB}} = \frac{\Sigma}{N_Z} = \frac{K_{N_Z} N_{N_Z}(s) + K_u N_u(s) + K_\theta N_\theta(s) + K_{\dot{\theta}} N_{\dot{\theta}}(s)}{N_{N_Z}(s)} \quad (\text{Eq. E.7})$$

It can be noted that the transfer function Σ/δ_{H_C} is the same, regardless of which signal is fed back. Now, since the desired column force gradient $(F_C/N_Z)_D$ was picked, all terms of Equation E.5 are known, and the feed-forward transfer function $K_{FF}^{G_{FF}}$ can be computed.

The PACS is not sensitive to the frequency variant part (G_{FF}) of the transfer function. Thus mechanization was achieved by making the following assumptions.

- Only the short-period mode frequency is important.
- The frequency is an average value.
- The damping ratio is equal to one.
- One of the duplicate poles is dropped.

These assumptions allow G_{FF} to be written as:

$$G_{FF} = \frac{1}{\left(\frac{s}{\omega_{SP}} + 1\right)} \quad (\text{Eq. E.8})$$

If $1/\omega_{SP} = \tau_C$, G_{FF} defines the low pass filter in the feed-forward loop shown in Figure 16.

The static part (K_{FF}) of the feed forward control is:

$$K_{FF} = \frac{1}{C_F} \left\{ \left[-1 + \left(\frac{1}{K_L} + 1 \right) \right] \frac{C_F K_{FB}}{(F_C/N_Z)_D} \right\} \quad (\text{Eq. E.9})$$

K_L = total loop gain of closed-loop system

The resulting feed-forward gains are scheduled and plotted in Figure 13.

APPENDIX F

Primary Gain Scheduling

Plots of the compensated feedback gains (e.g., the pitch rate gains in Figure 12) for each flight condition indicate that gain scheduling can be expressed as polynomial functions of dynamic pressure (q) and of horizontal stabilizer trim position (δ_{HT}).

The feedback gains to be scheduled were:

$$K_{\dot{\theta}} \sim \text{degrees } \delta_{Hc} / \text{degree per second } \dot{\theta}$$

$$K_{NZ} \sim \text{degrees } \delta_{Hc} / g \Delta N_z$$

$$1/\tau_2 \sim \text{sec}^{-1}$$

$$\left(\frac{\tau_2}{\tau_1} - 1 \right) \sim \text{dimensionless}$$

$$K_3 \frac{\tau_1}{\tau_2} \sim \text{degrees } \delta_{Hc} / \text{degree } \theta$$

The feed-forward gain to be scheduled was:

$$K_{FF} \sim \text{in/lbs}$$

A comparison of the least-mean-square values determined the order of the polynomial to be used. The second order polynomial given in Equation F.1 was found to provide a satisfactory curve fit.

$$K = a + bq + cq^2 + d\delta_{HT} + e\delta_{HT}^2 \quad (\text{Eq. F.1})$$

Pseudo-inverse matrix operations were used to determine the coefficients of the least-square fit for the complete flight envelope gain values. Thus, a set of simultaneous equations relating the set of points $\{p\}$ to the set of coefficients $\{c\}$ can be written in terms of a matrix equation.

$$[P] \{c\} = \{p\} \quad (\text{Eq. F.2})$$

If the polynomial matrix [P] is not a square matrix, it has no inverse matrix with which to solve the coefficient vector {c}. However, if its dimensions are m x n with n > m, then by premultiplying both sides of the equation by the P matrix transpose [P]^T as shown in Equation F.3, the P^TP matrix is a square matrix with m x m dimensions.

$$[P]^T [P] \{c\} = [P]^T \{p\} \quad (\text{Eq. F.3})$$

Thus, the equation can not be solved explicitly for a coefficient vector.

$$\{c\} = [P^T P]^{-1} [P]^T \{p\} \quad (\text{Eq. F.4})$$

[P^TP]⁻¹ [P]^T is the pseudo-inverse matrix of P. Equation F.4 yields a set of numbers {c} which represent the least-square fit for the set {p}.

An expression of a set of equations such as Equation F.1 in the matrix form of Equation F.2 provides Equation F.5.

$$\begin{bmatrix}
 1 & q_1 & q_1^2 & \delta_{HT_1} & \delta_{HT_1}^2 \\
 1 & q_2 & q_2^2 & \delta_{HT_2} & \delta_{HT_2}^2 \\
 - & - & - & - & - \\
 - & - & - & - & - \\
 1 & q_n & q_n^2 & \delta_{HT_n} & \delta_{HT_n}^2
 \end{bmatrix}
 \begin{bmatrix}
 a \\
 b \\
 c \\
 d \\
 e
 \end{bmatrix}
 =
 \begin{bmatrix}
 p_1 \\
 p_2 \\
 - \\
 - \\
 p_n
 \end{bmatrix}
 \quad (\text{Eq. F.5})$$

By using the values of required gains that have been computed (e.g., K₀ of Table 4) for the column-matrix elements (p₁, p₂...p_n) and the corresponding δ_{HT} and q values of Table 5, the values of the polynomial coefficients (a, b, ... e) can be computed. The results of the computation are given in Table 6.

APPENDIX G

Secondary Gain Scheduling

Secondary gain scheduling is used to compensate for:

- Pitch-up at high-Mach/high-g flight conditions
- Outboard aileron symmetric effects when the AACS is activated

The pitch-up phenomena is caused by stalling of the wing tips at high-Mach/high-g flight conditions. Thus, the lift aerodynamic center is shifted forward relative to a fixed c.g. location and the static stability margin is reduced.

The AACS operates the outboard ailerons in a symmetric mode in response to normal acceleration of the aircraft c.g. and wing tips. For high speed flight conditions (flaps-up), the outboard ailerons are up biased approximately 2 degrees and for the low speed flight conditions (flaps-down) the ailerons are up biased approximately 10 degrees. The response of the ailerons to normal acceleration provides a pitching moment that is equivalent to reducing the static stability margin by about 5 percent.

The reduced static stability due to pitch up and active AACS are similar to reducing the stability margin by moving the c.g. aft. Therefore, the scheduled feed-forward and feedback primary gain schedules (such as Figures 15 and 14) can be used to provide the required pitch control for pitch-up and AACS operation conditions by modifying the value of δ_{HT} by an increment $\Delta\delta_{HT}^*$. This modified value has been designated δ_{HT}^* .

A block diagram of the secondary gain controller is given in Figure 84. Inputs to the controller are:

- Angle of attack (α)
- Bank angle (ϕ)
- Mach number
- AACS/Flap conditions

The equation for δ_{HT}^* can be written from the diagram to be

$$\delta_{HT}^* = \delta_{HT} + K_m \delta_\alpha + C_\phi \delta_{HT}^2 (1 - \cos \phi) + \delta_{AACS} \quad (\text{Eq. G.1})$$

This is the δ_{HT}^* value shown for secondary gain scheduling in Figure 16.

GAIN CONTROLLER

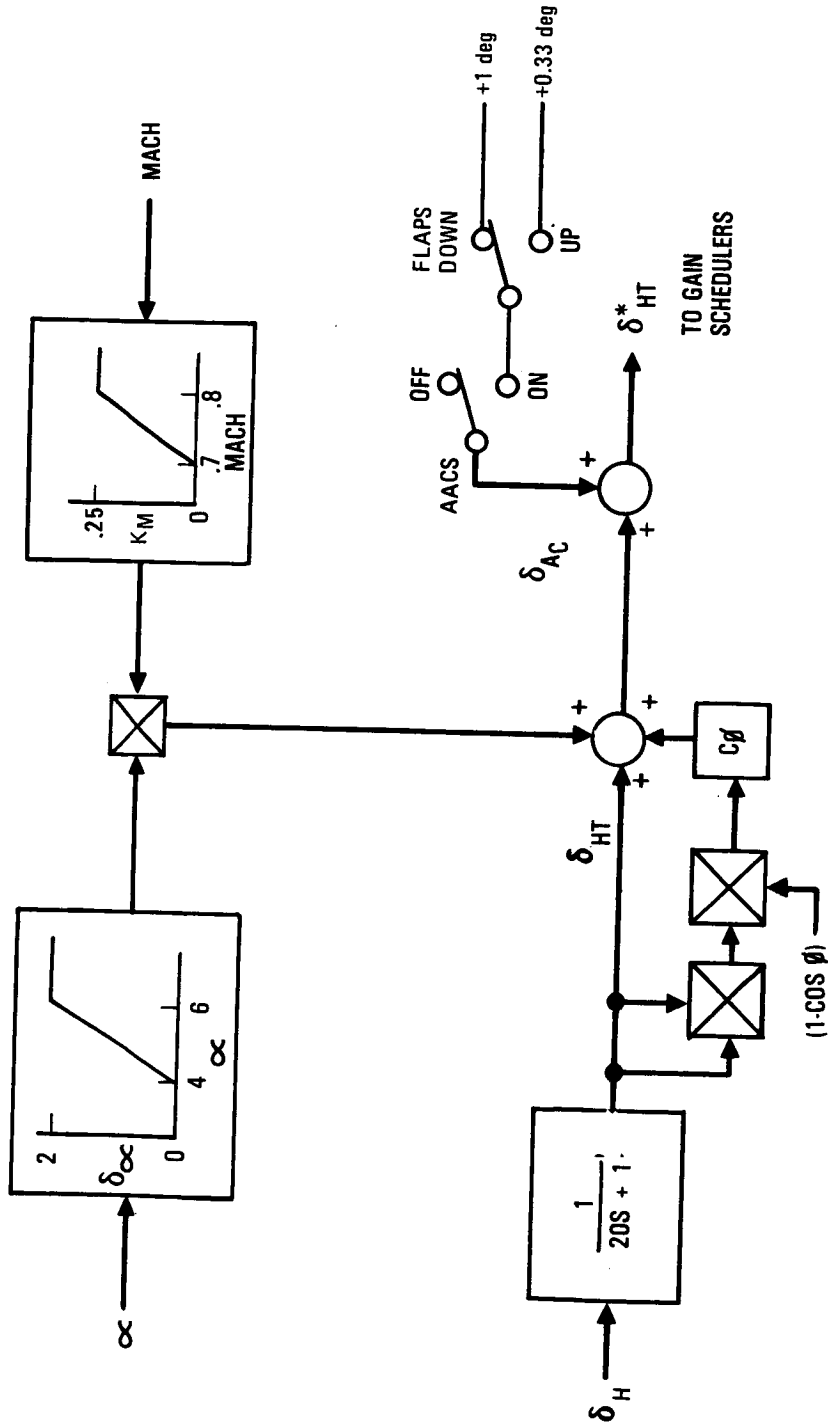


Figure 84. - PACS secondary gain controller.

APPENDIX H

Pitch Attitude Loop Synchronizer Circuit

The pitch synchronizer has two modes of operation: fixed or controlled. These operational modes are shown in Figure 85. The fixed mode provides a reference attitude (θ_R) equal to the aircraft trim attitude (θ_T). Thus, if a control column force changes the attitude of the aircraft, the sensed attitude (θ_S) will be compared with θ_R to provide an error signal (θ_E). Thus, when the control force is reduced to zero the aircraft attitude will return to θ_T . The controlled mode causes the reference attitude signal to track the sensed attitude signal during a maneuver. Then, at the instant when the control column force is reduced to zero, the reference attitude is set equal to the aircraft controlled attitude (θ_C). Any sensed attitude changes will result in an error signal which will cause the aircraft to return to the controlled attitude.

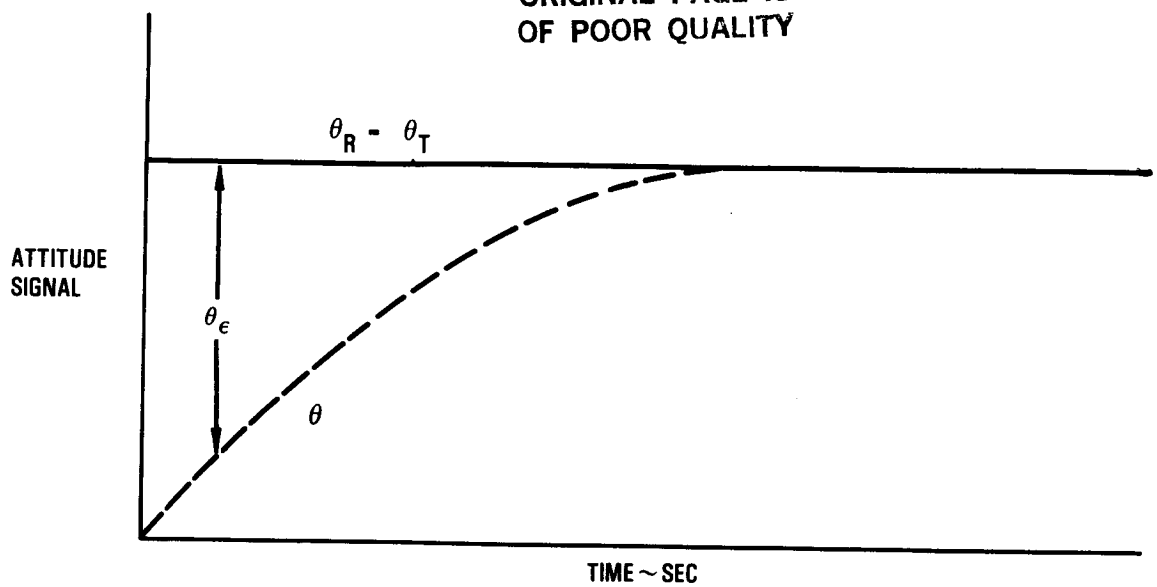
Figure 86 represents a schematic diagram of the pitch synchronizer circuit. Symbols used in the figure are defined as follows.

- C - Pilot optional control switch state (0 or 1)
- F - Applied column force switch state (0 or 1)
- K_C - Controlled reference integrator gain
- K_T - Trim reference integrator gain
- S_1 - Trim switch
- S_2 - Pilot-optional-control switch
- S_3 - Controlled reference tracking switch
- S_4 - Integrator-closed-feedback switch
- S_5 - Trim reference tracking switch
- T - Horizontal stabilizer trim button switch state (0 or 1)

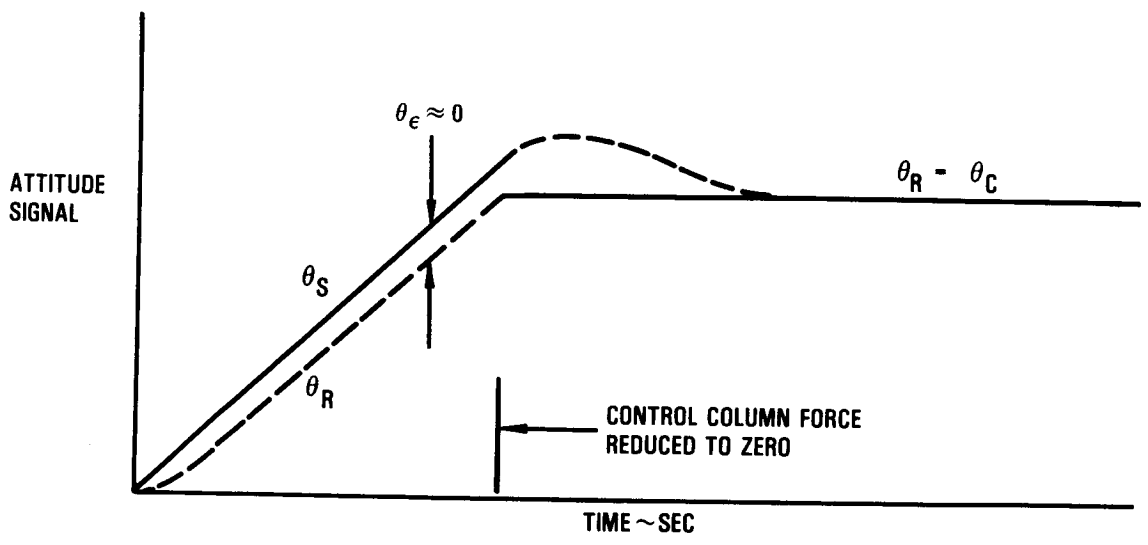
The circuit logic operation is determined by Boolean Algebra methods. The switches in the circuit are controlled by one or more of the following three inputs.

- Pilot optional control $\sim C$
- Trim setting $\sim T$
- Column force $\sim F$

ORIGINAL PAGE IS
OF POOR QUALITY



a. FIXED MODE



b. CONTROLLED MODE

Figure 85. - PACS pitch synchronizer operation modes.

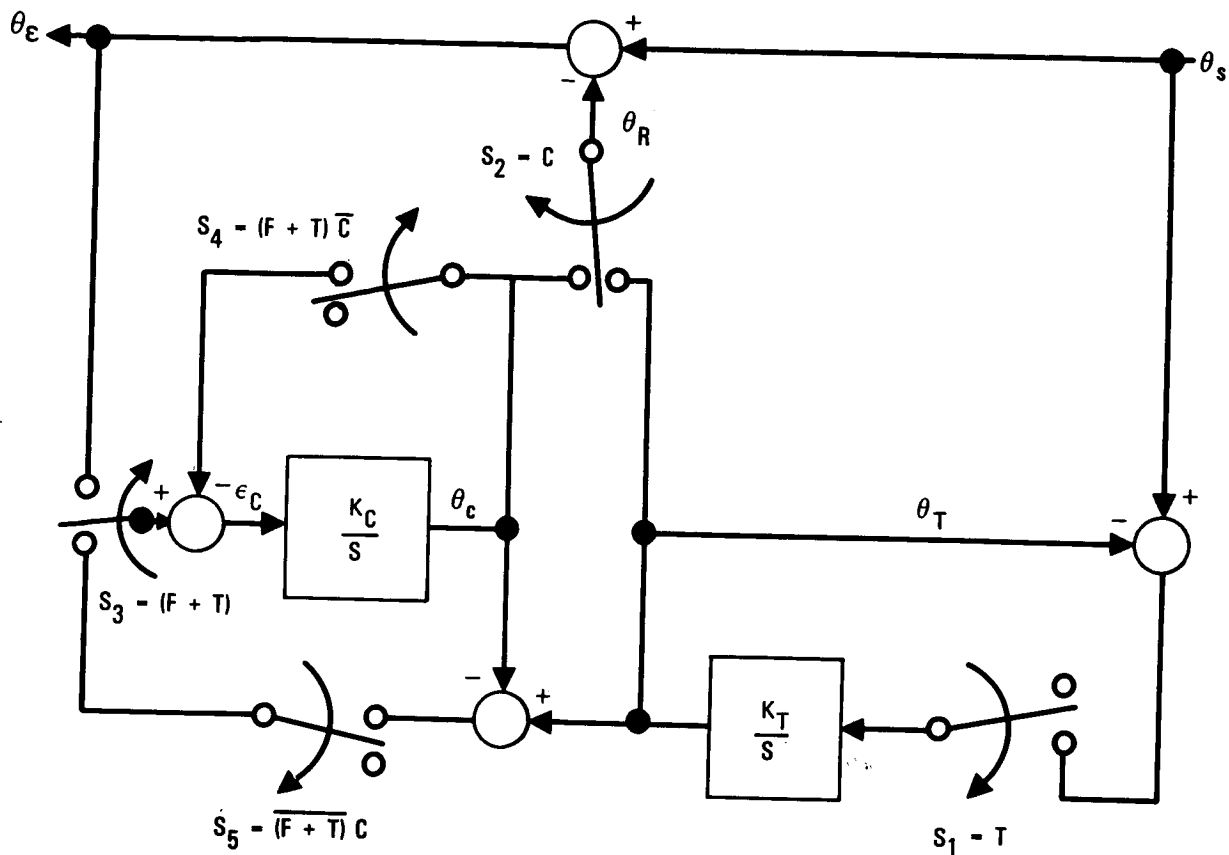


Figure 86. - PACS pitch attitude loop synchronizer circuit.

Each input has two conditions (on or off). Thus, logic theory requires that a system with three inputs which are controlled by two conditions have 8 different input states (2^3) as shown in Table 16. A 1 in the table indicates the signal is applied and a 0 indicates that a signal is not applied.

The switches in Figure 86 are normally open (O) or closed in the direction of the arrow (C) as determined by the Boolean Algebra equations shown for each switch. The Boolean terminology used is:

x = signal is applied

\bar{x} = signal is not applied

$x + y$ = signal x or signal y is applied

$\overline{x + y}$ = neither signal x nor signal y is applied

xy = signal x and signal y are applied

$x\bar{y}$ = signal x is applied and signal y is not applied

$\bar{x}y$ = signal x is not applied and signal y is applied.

ORIGINAL PAGE IS
OF POOR QUALITY

The last two columns of Table 17 show that for circuit conditions 1 and 2 the reference attitude is equal to the trim attitude, for circuit condition 3 the reference attitude is equal to the controlled attitude, and for the other conditions the reference attitude is tracking the sensed attitude signal.

TABLE 17. - PACS PITCH SYNCHRONIZER INPUT STATES


CIRCUIT CONDITION NUMBER	F	T	C
1	0	0	0
2	1	0	0
3	0	0	1
4	0	1	0
5	0	1	1
6	1	0	1
7	1	1	0
8	1	1	1

TABLE 18. - PACS PITCH SYNCHRONIZER SWITCH POSITIONS AND ATTITUDE REFERENCE

CIRCUIT CONDITION NUMBER	S ₁	S ₂	S ₃	S ₄	S ₅	PITCH ATTITUDE REF. (θ_R)	CONTROL CONDITION
1	0	0	0	0	0	θ_T	HOLD
2	0	0	C	C	0		
3	0	C	0	0	C		
4	C	0	C	C	0	θ_S	TRACKING
5	C	C	C	0	0		
6	0	C	C	0	0		
7	C	0	C	C	0		
8	C	C	C	0	0		

REFERENCES

1. Guinn, W.A., "Development and Flight Evaluation of an Augmented Stability Active Controls Concept," NASA CR 165951, September 1, 1982.
2. Urie, D.M., "Accelerated Development and Flight Evaluation of Active Controls Concepts for Subsonic Transport Aircraft - Volume II - Aft C.G. Simulation and Analysis," NASA CR 159098, September 1979.
3. Rising, J.J., "Development of a Reduced Area Horizontal Tail for a Wide Body Jet Aircraft," NASA CR-172278, February 1, 1984.
4. Moore, B.C., "On the Flexibility Offered by State Feedback in Multivariable Systems Beyond Closed Loop Eigenvalue Assignment," IEEE Transactions on Automatic Control, October 1976, pp. 689-692.
5. Srinathkumar, S. "Eigenvalue/Eigenvector Assignment Using Output Feedback," IEEE Transactions on Automatic Control, Vol. AC-23, No. 1, February 1978, pp. 79-81.
6. Harvey, C.A. and Stein G., "Quadratic Weights for Asymptotic Regulator Properties," IEEE Transactions on Automatic Control, Vol. AC-23, No. 3, June 1978, pp. 378-387.

1. Report No. NASA CR-172277		2. Government Accession No.		3. Recipient's Catalog No.	
4. Title and Subtitle Development of an Advanced Pitch Active Control System for a Wide Body Jet Aircraft				5. Report Date February 1, 1984	
				6. Performing Organization Code	
7. Author(s) Wiley A. Guinn, Jerry J. Rising, and Walt J. Davis				8. Performing Organization Report No. LR 30644	
9. Performing Organization Name and Address Lockheed California Company Burbank, California 91520				10. Work Unit No.	
				11. Contract or Grant No. NAS1-15326	
12. Sponsoring Agency Name and Address National Aeronautics and Space Administration Washington, DC 20546				13. Type of Report and Period Covered Contractor Report	
				14. Sponsoring Agency Code	
15. Supplementary Notes Langley technical monitor: Dennis W. Bartlett, Final Report					
16. Abstract An advanced PACS control law was developed for a commercial wide-body transport (Lockheed L-1011) by using modern control theory. Validity of the control law was demonstrated by piloted flight simulation tests on the NASA Langley visual motion simulator. The PACS design objective was to develop a PACS that would provide good flying qualities to negative 10 percent static stability margins that were equivalent to those of the baseline aircraft at a 15 percent static stability margin which is normal for the L-1011. Also, the PACS was to compensate for high-Mach/high-g instabilities that degrade flying qualities during upset recoveries and maneuvers. The piloted flight simulation tests showed that the PACS met the design objectives. The simulation demonstrated good flying qualities to negative 20 percent static stability margins for hold, cruise and high-speed flight conditions. Analysis and wind tunnel tests performed on other Lockheed programs indicate that the PACS could be used on an advanced transport configuration to provide a 4 percent fuel savings which results from reduced trim drag by flying at negative static stability margins.					
17. Key Words (Suggested by Author(s)) Active Control System, Control System, Pitch Control, Longitudinal Control, Aircraft Fuel Savings			18. Distribution Statement 		
19. Security Classif. (of this report) Unclassified		20. Security Classif. (of this page) Unclassified		21. No. of Pages 172	22. Price*